Master's thesis

NTNU
Norwegian University of Science and Technology
Faculty of Medicine and Health Sciences
Department of Clinical and Molecular Medicine

Jon Olav Malvik

HR MAS NMR based metabolic profiling of colorectal tumor progression organoids

Identification of metabolic biomarkers for tumor progression and response to chemotherapy

Master's thesis in Pharmacy
Supervisor: Siver Andreas Moestue
December 2020

NTNU
Norwegian University of Science and Technology

Jon Olav Malvik

HR MAS NMR based metabolic profiling of colorectal tumor progression organoids

Identification of metabolic biomarkers for tumor progression and response to chemotherapy

Master's thesis in Pharmacy
Supervisor: Siver Andreas Moestue
December 2020

Norwegian University of Science and Technology
Faculty of Medicine and Health Sciences
Department of Clinical and Molecular Medicine

NTNU
Norwegian University of
Science and Technology

Abstract

Colorectal cancer (CRC) is the second most deadly cancer type in Norway. This is partly due to asymptomatic disease development which often causes patients to seek medical attention in late stages of CRC. Fast diagnosis, staging and evaluation of response to pharmacological treatment is therefore important, particularly in patients with metastatic disease. By todays standard, 4-6 weeks are needed to evaluate treatment response which is often to late. There is a need for novel diagnostic tools in the management of CRC patients.

Cancer cells display metabolic reprogramming in their natural form and when exposed to chemotherapeutic agents. It is therefore hypothesized that metabolic responses to treatment occurs faster than changes in tumor volume. This implies that treatment response can be evaluated after a few days instead of 4-6 weeks.

In this study we utilized tumor progression organoids where the four most common genetic mutations *APC*, *KRAS*, *P53* and *SMAD4* in CRC have been sequentially introduced using CRISPR/CAS9. The tumor progression organoids (TPO) were treated with oxaliplatin (OxPt), 5-fluorouracil (5-FU), Sn-38 (the active metabolite of irinotecan) and a combination of these drugs, for 48 and 96hr. Untreated controls were collected at 0hr, 48hr and 96hr. The goal was to describe reprogramming during transformation from normal to malignant organoids, and to identify metabolic biomarkers for treatment response by ^{1}H and ^{31}P high resolution magic angle spinning.

The results indicate that phosphocholine (Pcho), total choline-containing compounds (tCCC) and myo-inositol (myo-in) decreases with accumulating mutations compared to wild-type organoids. We observed a strong trend of increasing lactate with increasing mutations, but the trend was not significant. Lactate decreases with all treatments regardless of mutations and response status. Pcho and tCCC show a treatment dependency, with increasing levels when organoids are treated with OxPt, 5-FU or a combination of these drugs. However, Pcho and tCCC were unable to discriminate between responding and non-responding organoids. Organoids responding to treatment with Sn-38 showed a decrease in Pcho and tCCC levels regardless of mutations, but non-responders were observed to have a unchanged or higher amount. These metabolites could therefore potentially serve as biomarkers for response to irinotecan treatment. Alanine was observed to decrease in organoids treated with Sn-38 and 5-FU, but could not distinguish between responders from non-responders in Sn-38 treatment. Myo-inositol decreased in organoids treated with OxPt and Sn-38 at 48hr or 96hr in response to treatment. Myo-inositol discriminated between responders and non-responders where unchanged or elevated amount correlated with non-responders.

In summary, it was found that the levels of choline-containing metabolites, phosphocholine and myo-inositol decreased during malignant transformation, while a strong inverse trend was observed for lactate. Lactate displayed potential as an universal biomarker for response to therapy. Myo-inositol was found to decrease in response to Sn-38 and OxPt treatment and to discriminate between responding and non-responding organoids.

Sammendrag

Kolorektal kreft er den nest dødeligste krefttypen i Norge. Dette er delvis på grunn av et asymptomatisk sykdomsforløp som ofte forårsaker at pasienter søker medisinsk hjelp sent i sykdommen. Rask diagnose, staging og evaluering av respons til farmakologisk behandling er derfor viktig, spesielt i pasienter med metastatisk sykdom. Dagens standard er 4-6 uker for å evaluere respons på behandling som ofte er for sent. Det er derfor behov for nye diagnostiske verktøy i behandlingen av kolorektal kreft pasienter.

Kreftceller utviser metabolsk reprogrammering i sin naturlige form og når de blir utsatt for cytostatika. Det er derfor trodd at metabolske responser oppstår raskere enn forandringer i tumor volum. Dette impliserer at behandlingsrespons kan evalueres etter noen dager istedenfor 4-6 uker.

I denne studien bruker vi tumor progresserende organoider hvor de fire mest vanlige genetiske mutasjonene *APC*, *KRAS*, *P53* og *SMAD4* i kolorektal kreft har blitt sekvensielt introdusert ved bruk av CRISPR/CAS9. TPOene er behandlet med oksaliplatin (OxPt), 5-fluoruracil (5-FU), Sn-38 (aktive metabolitten av irinotecan) og kombinasjonen av disse legemidlene i 48t og 96t. Ubehandlede organoider ble skaffet på tidspunkt 0t, 48t, og 96t. Målet var å beskrive metabolsk reprogrammering under transformasjon fra normale til maligne organoider, og identifisere metabolske biomarkører for behandlingsrespons ved bruk av ^{1}H og ^{31}P HR MAS NMR.

Resultatene indikerer at fosfokolin (Pcho), totalt kolin-inneholdende forbindelser (tCCC) og myo-inositol (myo-in) reduseres ved akkumulerte mutasjoner sammenlignet med vill-type organoider. En sterk trend av økende laktat med antall mutasjoner ble observert, men ble funnet til å ikke være signifikant. Laktat reduseres i alle behandlingene uansett mutasjoner og responsstatus. Pcho og tCCC viser behandlingsavhengighet, hvor et økende nivå er observert i organoider behandlet med 5-FU, OxPt og kombinasjonen av disse behandlingene. Pcho og tCCC skilte derimot ikke mellom responderende og ikke-responderende organoider. Responderende organoider behandlet med Sn-38 hadde reduserte mengder Pcho og tCCC uavhengig av mutasjoner, mens ikke-responderende organoider hadde uendret eller høyere nivåer av Pcho og tCCC. Disse metabolittene kan derfor potensielt brukes som biomarkører ved irinotecan behandling. Mengden alanine var redusert i organoider behandlet med Sn-38 og 5-FU, men var ikke i stand til å diskriminere mellom respons og ikke-respons i Sn-38 behandlede organoider. Mengden myo-inositol reduserte i organoider behandlet med OxPt og Sn-38 ved 48t eller 96t. Mengden myo-inositol skilte mellom responsstatus i organoider behandlet med OxPt og Sn-38 ved at ikke-responderende organoider hadde uendret eller høyere nivåer.

Oppsummert ble det funnet at mengden kolin-inneholdende metabolitter og myo-inositol reduserte under malign transformasjon, mens en sterk invertert trend ble observert for laktat. Laktat vises som den potensielt beste universale biomarkøren for behandlingsrespons. Myo-inositol mengden ble observert til å redusere ved Sn-38 og OxPt behandling, og til å diskriminere mellom responderende og ikke-responderende organoider.

Forord

Takk til Siver Moestue som hovedveiler for god hjelp underveis. Takk til Maria Tunset Grinde som biveileder med all hjelp på laboratoriet og analyse av data. Trygve Andreassen for hjelp av HR MAS NMR, og alle på MR cancer group, NTNU. Takk til Wybe van der Kemp for dyrkning, behandling og responstesting av organoidene.

Contents

Abbreviations/symbols

1H	^{1}Hydrogen
2D	Two-dimentional
3D	Three-dimentional
5-FU	5-fluorouracil
6-PG	6-phosphogluconolactone
^{18}F-FDG	^{18}F-fluorodeoxyglucose
31P	^{31}Phosphorus
AKT	Protein kinase B
Ala	Alanine
ANOVA	Analysis of variance
APC	Adenomatous poyposis coli
ATP	Adenosine triphosphate
AUC	Area under the curve
c-Fos	Cellular oncogene fos
c-Myc	Cellular myelocytomatosis oncogene
CDK	Cyclin-dependent kinase
CDP-choline	Cytidine 5-diphosphocholine
CDP-ethanoleamine	Cytidine diphosphate ethanoleamine
CHK-α	Choline kinase alpha
Cho	choline
CIN	Chromosomal instability
Combi	Combinational treatment
CRC	Colorectal cancer
CRISPR/CAS9	Clustered regularly interspaced short palindromic repeats/CRISPR associated protein 9
CT	Computed tomography
DNA	Deoxyribonucleic acid
ECM	Extracellular matrix
EMT	Epithelial-mesenchymal transition
ER	Estrogen receptor
ERK	Extracellular-signal-regulated kinase
FID	Free induction decay
G6P	Glucose-6-phosphate
G6PDH	Glucose-6-phosphate dehydrogenase
GDP	Guanosine diphosphate
GLUT	Glucose transporter
GPC	Glycerophosphocholine
GTP	Guanosine triphosphate
GTPase	Guanosine triphosphate kinase
HIF1	Hypoxia-inducible factor 1
HR	High resolution
Hr	hour
HSQC	Heteronuclear single quantum correlation
InsP6	Inositol hexaphosphate
KRAS	Kirsten rat sarcoma
Lac	Lactate
MAS	Magic angle spinning

MDM2	Mouse double minute 2 homolog
MEK	Mitogen-activated protein kinase kinase
MIN	Microsatellite instability
MMR	Mismatch repair system
MR	Magnetic resonance
MRS	Magnetic resonance spectroscopy
MS	Mass spectrometry
mTor	Mammalian target of rapamycin
NADPH	Nicotinamine adenine dinucleotide phosphate
NMR	Nuclear magnetic resonance
NOESY	Noesygppr1d
NR	Non-responding
O1	Frequency of water
OxPt	Oxaliplatin
P	Pulse
P53	Cellular tumor antigen p53
PC	Principal component
PCA	Principal component analysis
Pcho	phosphocholine
PDK1	Phosphoinositide-dependent kinase-1
PE	Phosphoethanolamine
PET	Positron emission tomography
PFK-1	Phosphofructokinase 1
PI3K	Phosphoinositide 3-kinase
PIP	Phosphatidylinositol-phosphate
PKM2	Pyruvate kinase M2
ppm	Part per million
Ptdcho	phosphatidylcholine
Ptdeth	phosphatidylethanolamine
R	response
RAF	Rapidly accelerated fibrosarcoma
RAS	Rat sarcoma
RECIST	Response evaluation criteria in solid tumors
RTK	Receptor tyrosin kinase
SAC	Spindle assembly checkpoint
SMAD4	Mothers against decapentaplegic homolog 4
Sn-38	Active metabolite of irinotecan
SNR	Signal to noise ratio
T	Tesla
tCCC	Total choline containing compounds
TGF-β	Transforming growth factor beta
TIGAR	P53-inducible glycolysis and apoptosis regulator
TNM	Tumor, Nodes and metastases
TPO	Tumor progression organoids
TPO0	Tumor progression organoids wild type
TPO2a	Tumor progression organoids APC-KRAS
TPO2b	Tumor progression organoids APC-P53
TPO3	Tumor progression organoids APC-KRAS-P53
TPO4	Tumor progression organoids APC-KRAS-P53-SMAD4
WAF1	Cycline-dependent kinase inhibitor

Wnt	Wingless-related integration site

1 Introduction

Colorectal cancer (CRC) is the 4th most common cancer in Norway with 3068 new cases in 2018, but is the second most deadly form of cancer relative to death toll of 1763. The incidence of colorectal cancer is slightly higher for men than women (1). A clinical challenge in CRC is the asymptomatic disease development which often causes patients to seek medical help to late. It is estimated that 14% to 18% of patients seeking medical help for the first time is at an metastatic stage, and 10% to 25% develop metastases at the time of resection of the primary colorectal tumor (2). Metastases frequently occur in the liver because of the natural link between these two organs, the portal vein. The high incidence of metastases in CRC limits the efficacy of todays curative treatment which depends on surgical resection. If rescection is not an option, chemotherapy is the preferred option to which patients may or may not respond. To date, the only certain way to measure treatment response from chemotherapy is to utilize imaging diagnostic to see if the tumor is in remission. Assessment of tumor volume according to RECIST is the current goldstandard for diagnosing tumor remission, however the drawback is the time used to measure this, often weeks of precious time lost if the patient is non-responsive. The need for better treatment alternatives and reliable biomarkers in CRC response assessment is still unmet.

The malicious growth and proliferation of cancer cells partly depend on metabolic reprogramming due to the increased rate of biomass productions. The metabolic abnormalties can be used diagnostically, both for the detection of tumor and for phenotyping/risk assessment. In principal, metabolic information may have predictive value and can therefore be used to make informed decisions on choice of chemotherapy. Furthermore, it has been suggested that metabolic responses to chemotherapy occur earlier than anatomical changes, and it may be possible to drastically cut down the time used to detect chemotherapy response. It is therefore of interest to identify metabolic biomarkers that can help doctors asses the right chemotherapy regimen, and make the right decision to wether keep the chemotherapy regimen, or switch to another if the patient is non-responsive.

To date we know of many metabolites which is altered in the hallmark of cancer, for example lactate, cholines and glutamate. The increased production of lactate in cancer cells is known as the Warburg effect, which allow cancer cells to form energy in form of Adenosine triphosphate (ATP) even in the presence of oxygen (3). Choline metabolism has been subject to extensive researched the past decades to determine if it can be used as a biomarker to either predict chemotherapy response or tumor progression. However one universal conclusion wether the concentration of Cholines increases or decreases in respect to chemotherapy response have not yet been made. In respect to these observation many have theorized that the alteration seen in metabolism for CRC originate in gene mutation (4, 5). To date little is known how oncogenic activation and/or tumor suppressor gene mutations, and the vast combination of these seen in cancer cells, affects metabolic processes. Furthermore, little is known how to use metabolic data, for example cholines, to predict response of a given chemotherapy regimen or

tumor progression. Further research on the subject is required and it is thought to give great clinical value for cancer patients.

In this study we utilize tumor progression organoids (TPO) which has been genetically modified by CRISPR/CAS9 technology where the four most common genetic mutations, *APC*, *KRAS*, *P53* and *SMAD4*, found in CRC. The TPO's have been treated with either 5-fluorouracil (5-FU), oxaliplatin (OxPt) or the active metabolite of irinotecan (SN-38) and the combination of these. The purpose of this is to analyze the effect of accumulating mutations on the TPO's metabolic characteristics and to study metabolic responses to chemotherapy. To determine metabolite levels in the TPO's we utilized ^{1}H and ^{31}P high resolution magic angle spinning nuclear magnetic resonance spectroscopy (HR-MAS NMR).

2 Background

2.1 Cancer

Cancer is not a specific disease but a common term used for different diseases where the organism lose control over cell proliferation. Every cell and tissue in the organism that have a nucleus can develop cancer. This uncontrolled cellular growth often cause cancer cells to invade normal surrounding tissue, or to colonize other organs (known as metastasis). This invasion of cancerous cells, without treatment, will inevitably lead to harmful effects of the organism.

The transformation of a healthy cell to a cancer cell is a gradual process, and often take years to finish. This process involves mutations in spesific genes known as oncogenes, tumor suppressor genes and/or caretaker genes. These genes play an important role in cell inhibition, growth, DNA-repair and survival. The need to have mutations in multiple set of genes in order to develop cancer have termed this disease as "a series of unfortunate incidents" or " a game of chance".

The characteristics of a cancer cell in term of uncontrolled cellular growth is known as hallmark of cancer. The hallmarks are characteristics a cancer cell must aquire to be a well-functioned cancer cell which include sustaining proliferative signaling, resisting cell death, activating invasion and metastasis, evading growth suppressors, deregulating cellular energetics and avoiding immune destruction to name a few (6).

Cancer research have improved our ability to treat cancer patients over the past decades with new chemotherapy and improvement in diagnostics. However it is estimated that 9,6 million people died from cancer in 2018 globally (7). This numbers leaves us with unmet needs of more advanced, faster and better tools in diagnostics and chemotherapy treatment.

2.2 Colorectal cancer

CRC is a common term used for cancer which has its origin in the colon or rectum. In 2018 it is estimated that 1,8 million new cases of CRC occurred and 862 thousand patients died of CRC (7). The incidence of CRC is higher for males, and the mortality rate is slightly higher for males than females while the incidence of CRC increases with increased age (8). The 5-year survival rate is highly dependent upon disease stage at the time point of diagnosis, and ranges from about 90% when detected at an early stage to about 10% when detected in a late metastatic state (9).

CRC is often divided into 3 categories based on genetic predisposition. The first category is sporadic CRC which occurs with no genetic predisposition and evolves based on random mutation over the time of years and accounts for around 70% of the CRC cases. It usually starts with a benign polyp or adenoma and over years will eventually evolve into a malignant adenocarcinom due to gene mutation and epigenetic alterations.
The second category is termed familial CRC and is the least understood. People who are close relative to CRC patients have two to six fold increase of developing CRC with unknown reasons (10). The third category is inherited CRC where mutated genes crucial for normal cell proliferation is passed down to future generations making them more susceptible to develop CRC. One example of such a disease is familial adenomateous polyposis which is caused by a mutation in the *APC* gene. The APC gene is a tumor suppressor gene which prevents uncontrolled cellular growth. Without the function of this gene we observe the characteristics of polyps formed in familial adenomateous polyposis in the intestine which predispose this patient group of developing CRC. The chance of them developing CRC in their lifespan is almost 100% if untreated (10, 11). With further addition of *KRAS* mutation, the epithelium is characterized by larger polyps and mild dysplasia. The accumulated loss of tumor suppressor gene *P53* characterize the epithelium as high-grade dysplasia/carcinoma in situ. Lastly, addition of *SMAD4* mutation transforms the cell to invasive adenocarcinoma (12).

2.2.1 Diagnosis and treatment in colorectal cancer

All patiens over the age of 40 will be examined for CRC if one or more of the following criteria is met; blood from the intestines with unknown origin, findings of polyps or tumor and/or change in a stable bowel pattern for more than 4 weeks. From 2019 a national screening program in Norway started, and everyone over 55 years should be offered intestinal screening for the detection of CRC by the usage of immunochemical fecal occult blood test (13).

Primary diagnostic for detecting colorectal cancer is colonoscopy/rectoscopy with biopsy. The biopsy is used to determine the diagnosis, staging and histology of the tumor. CT-colography has seen an increase in usage over the last years. It is seen as equally good method as colonoscopy for detecting lesions greater than 10mm. Lesions smaller than 10mm the accuracy of CT-colography falls, and colonoscopy is preffered. After diagnosis, staging according to the TNM system is indicated. For colon cancer; CT thorax, abdomen and pelvis is recommended, while for rectal cancer; MR, transrectal ultrasound and CT thorax, abdomen and pelvis (13).

For detection and diagnosis of liver metastases, a usual occurrence of CRC, CT and MR with liverspesific contrast agents is used. Liver biopsy is an alternative if the diagnosis after imaging is not certain.

TNM status is a international classification system used to describe the extent of spread of cancer. T describes the degree of spread of the primary tumor with a number ranging from 0 to 4. 0 means no tumor and 4 means higly invasive tumor. N describes the degree of spread to lymph nodes with a number ranging from 0 to 3. 0 means no spread and 3 means that the tumor has spread to numerous and distant lymph nodes. M describes the presence of metastases or not, where 0 is no metastasis and 1 means detected metastases (14).

The treatment for colon cancer is highly dependent upon TNM classification, the patient age and ability to withstand treatment. It usually consists of surgery, radiation and drug treatment. Surgical resection is first-in line treatment of primary tumors where the invasion is not widespread to critical organs and/or nerves which makes it inoperable. After surgical treatment the patient should start adjuvant chemotherapy which consists of combination treatment with Kapecitabin and oxaliplatin or 5-FU, OxPt and folinate for 6 months. For patients over 70 years old the adjuvant treatment consists of either kapecitabin or 5-FU and OxPt (13).

The usual treatment for rectal cancer consists of preoperative radiation in combination with kapecitabin or 5-FU and folinate dependent on T stadium and the size of the tumor before rectal resection. Adjuvant chemotherapy is not indicated after preoperative radiation and chemotherapy. If locally relapse of rectal cancer, surgery is indicated in combination with radiation. A common problem for CRC patients are liver metastases and the only curable treatment is liver resection. However, in many of the cases the tumor metastases is to widespread or invasive to remove surgically. For patients with potentially resectable livermetastases it is indicated neoadjuvant treatment of 5-FU and OxPt, or irinotecan until the metastatic tumor is resectable (13).

For patients with incurable CRC the focus is on palliative and life-prolonging treatment and to maintain life quality. This includes radiation, strong pain-killers and various chemotherapeutic agents to reduce tumor volume and symptoms of hemmorhage and pain (13).

2.2.2 Pathophysiology

The most common type of CRC is adenocarcinoma which mean cancerous eptihelial cells which offsprings from glands. It should be noted that other forms of CRC exists, but are much rarer. The adenoma-carcinoma sequence model purposed by Vogelstein and colleaugues in 1990 explains how a adenoma will eventually evolve into a carcinoma through a series of accumulated mutations (12). Through activation of oncogenes and/or inactivation of tumor suppressor genes, cells gradually acquire properties that allow them to form a neoplasm, the so-called hallmarks of cancer (6). Mutations occur randomly throughout our life span, but can also arise due to spesific mechanisms of genomic instability in CRC; chromosomal instability (CIN) and microsatellite instability (MIN).

CIN is a process where the euploid number of chromosomes becomes aneuploid meaning an abnormal number of chromosomes in a cell. This phenomenon occurs because of mis-segregation of the duplicated chromosomes in the mitosis. There are many mechanisms of how this happends. In the metaphase, the chromosomes are connected via the kinetochore to microtubule to a centrosome, each in different directions. Normally the microtubule will pull the chromosomes apart and separate them, and then cleave the cell in the anaphase. However, if the chromosomes are orientated the wrong way in space, the microtubule is not properly attached or one centrosome is attached to both chromosomes it will result in a odd number of chromosomes in one cell leading to aneuploidity. Cells have mechanisms in hand to cope with such errors as cyklin-dependent kinases and the spindle assembly checkpoint (SAC). In order for this mechanism to work properly it requires full function of many genes and proteins. One known mutation which inhibits the effect of SAC and cyklin-dependent kinases is the *APC* mutation (often mutated in CRC) which causes checkpoint defects and aneuploidy. It should be noted that there are many genes, proteins and carcinogens which are mutated or cause mutation that can effect CIN including the important *P53* gene. The consequences of CIN is an increase in chromosomal translocation and abnormalties leading to alteration of oncogenes and tumor suppressor genes further increasing the carcinogenesis and heterogenesis seen in CRC (15).

Microsatellites are regions in the DNA with repetitive motifs of various individual length. They are often located in non-coding regions of the DNA but also in regulatory and coding regions. During DNA replication short errors can occur like insertions (addition of a nucleotide base) and deletions (nucleotide base left out). These errors are usually corrected for by the DNA mismatch repair (MMR). However in about 15% of the CRC cases we observe that the MMR gene is inactivated due to mutations causing a defective MMR system. This will lead to a higher mutation rate therefore increasing the activation of oncogenes, knocking out tumor suppressor genes and promotes carcinogenesis (16).

2.2.3 *APC*, *KRAS*, *P53* and *SMAD4* mutations in colorectal cancer

These four genes are the most commonly found mutated genes in CRC patients and plays an important role in the tumorigenesis. The *P53* gene is found to be mutated in up to 75%, *KRAS* in 25%-60%, *APC* in 20%-48% and *SMAD4* in approximately 30% of the CRC patient population (10, 17).

The *P53* gene also known as *tumor suppressor P53*, *TRP53* and *phosphoprotein P53*, is a tumor suppressor gene located at chromosome 17 with two alleles in humans. The *P53* gene is activated to produce P53 protein in response to DNA damage (such as UV radiation, mutagens, genotoxins) or increased oxidative stress. The P53 protein activates a long cascade of downstream cell signaling, but most notably the activation of *WAF1* gene encoding P21 protein. The P21 protein binds to cyclin dependent kinases such as CDK4/CDK6, CDK2 and CDK1 preventing G1/S transition in the cell cycle. Once the

damaged cell is under arrest, P53 protein activates DNA repair genes. If the DNA damage is beyond repair the P53 protein will either induce apoptosis or cellular senescence (permanent form of cell-cycle arrest). Mouse double minute 2 homolog (MDM2) is a protein that binds P53 protein causing degradation and therefore regulation of P53 protein. P53 protein activates the transcription of MDM2 protein and regulates itself in a negative feedback loop. If both alleles of the *P53* gene are damaged in some way, the loss of cell cycle arrest, apoptosis and senescence will eventually lead to cancerous cell development. The important role of the *P53* gene in the cell cycle has therefore dubbed it the guardian of the genome (18).

The *KRAS* gene encode for guanosine triphosphatase (GTPase), an enzyme that converts guanosine triphosphate (GTP) to guanosine diphosphate (GDP). The GTPase activates when an extracellular growth factor ligand binds to a receptor tyrosin kinase (RTK). Through a series of phosphorylations, eventually replacing GTPase/GDP complex in its inactivated state with GTP. The GTPase/GTP complex can further activate RAF/MEK/ERK and PI3k/PDK1/Akt pathways through phosphorylation and other proteins (19). ERK from the RAF/MEK/ERK pathway, when activated, can translocate to the nucleus and activate numerous transcription factors. The most notably transcription factors are C-myc and C-fos. C-myc and C-fos stimulates cell proliferation by upregulating cyclins and downregulates P21, but also regulates differentiation, cell growth and apoptosis (20). The activation of Akt from the PI3K/PDK1/Akt pathway excerts many functions through a vast network of complex signaling in the cell. Most notably, Akt inhibits activation of cell death genes and promote cell survival, angiogenesis and glucose metabolism (21). A mutation in the *KRAS* gene will result in a amino acid change in the GTPase. The effect of this may alter the activity of the GTPase in the form of reduced ability to hydrolyze GTP to GDP or locking the conformational active position indefinite or for a longer periode of time, thus increasing the downstream signaling. *KRAS* mutation in cancer is therefore associated with increased proliferation, angiogenesis, cell survival, glucose metabolism and evading apoptosis by the described mechanisms (22).

The *APC* gene encode for the APC protein which is a tumor suppressor gene important for the regulation of cell growth. The *APC* and *KRAS* gene is usually the first two genes to be mutated in CRC forming dysplasia or early adenoma given by its name adenomatous polyposis coli (APC). The APC protein is a regulator in the Wnt signaling pathway, it forms a complex with other proteins that enable degradation of β-catenin. β-catenin is a transcription factor which will upregulate C-myc and CDK1, drivers in cell proliferation, apoptosis and cell-cycle progression. The APC protein exerts a stabilizing function on microtubuli and mitotic spindle in the metaphase of mitosis, ensuring correct cleaving in the anaphase with the corresponding chromosomes. Studies have shown that a mutated *APC* gene cause defective formation of mitotic spindle therefore contributing to CIN and tumor progression. A mutated *APC* gene also increases cell survival by deaccelerating apoptosis through the caspase pathway (signaling pathway which mediates apoptosis), where caspase 2 is unable to cleave the APC protein for accelerating the apoptotic signal (23, 24).

The SMAD4 protein is an important mediator in the TGF-β (transforming growth factor) signaling pathway which mediates extracellular signaling to the nucleus. Upon ligand binding to the receptor, kinases will phosphorylate SMAD2/3 and form a complex with

SMAD4. The SMAD2/3/4 complex can translocate itself to the nucleus and activate transcription of genes key to inducing cell cycle arrest and apoptosis and is therefore a tumor suppressor gene. TGF-β signaling activates transcription of p15 and p21, and downregulates its inhibitor C-myc. P21 and p15 inhibits CDK4 while p15 also activates p27 which inhibits CDK2, key drivers for the transition from G1 to the S phase in the cell cycle. Mutations in *SMAD4* can lead to loss of stability in the SMAD2/3/4 complex, restricting cell signaling in the TGF-β pathway leading to loss of control in the cell cycle (25). The TGF-β pathway is regulated by the APC protein complex from the Wnt pathway, by ERK through inhibition of SMAD4 from the RAF/MEK/ERK pathway and mTor from the PI3k/PDK1/Akt pathway, highlighting the complexity and crosstalk of cell signaling pathways (17).

It is believed that these four genes plays an important role in CRC tumorigenesis. The adenoma-carcinoma sequence propose that CRC tumorigenesis starts with mutation in *APC* gene, followed by defective *KRAS*, *P53* and *SMAD4* (12). These four genes are described as the foundation for transforming a normal cell to colorectal cancer.

2.3 Metabolism in cancer

Metabolism is all the chemical reactions that occur in an organism in order to maintain cell growth, proliferation and survival. Metabolism is a common term used for two distinct processes, namely catabolism and anabolism. Catabolism is the process where large molecules breaks down to smaller molecules, yielding energy in the process. Anabolism is the process where smaller molecules are used as building blocks to synthezise larger molecules and use energy in the process. This neatly balanced and regulated process between catabolism, the need for energy, and anabolism, the need to use energy, is often distorted in cancer. With the malicious growth and proliferation tendency of cancer, a lot of energy in the form of ATP is required, but also building blocks such as nucleotides, amino acids and proteins to synthezise larger structures and produce biomass.

Cancer cells typically reside in a harsh environment and are able to grow and proliferate despite conditions such as hypoxia, acidic pH and variable access to nutrients. Metabolic reprogramming is one of the adaptions cancer cells have made in order to cope with these challenges. Metabolic pathways that we often observe is reprogrammed is glycolysis, Glutamin, lipid and pentose phosphate metabolism to name a few which is directly coupled to genetic mutations in oncogenes (26). Oncogene signaling important in CRC pathogenesis and tumor development such as *APC, KRAS and P53* also contributes to rewiring cell metabolism besides exerting its effects on proliferation and control over the cell cycle (27). The rewiring of metabolism in order to survive and proliferate have made it a characteristic trait of cancer and is recognized by hanahan & Weinberg as one of the hallmarks of cancer (6).

2.3.1 Glucose metabolism in cancer

Cancer cells display a significant deviation in glucose metabolism compared with normal cells. Even in normoxia conditions, cancer cells typically produce large amounts of lactate through aerobic glycolysis,a phenomenon known as the Warburg effect. The metabolism of one molecule of glukose yields 2 ATP molecules through lactate production, but the process of oxidative phosphorylation yields 36 ATP molecules. Why a cancer cell would favour less over more energy is uncertain, however it is speculated that cancer cells metabolize nutrients in the interest of proliferation and not necessary ATP (3). *KRAS* gene has been traditionally connected to downstream cell signaling for proliferation, also have a effect on rewiring glucose metabolism. Elevation of glycolysis and upregulation of the GLUT1 transporter, further fueling glycolysis, has been connected to oncogenic KRAS mutation contributing to the Warburg effect (28) (figure 2.3.1.0). Another contributor to glucose metabolism in cancer is the *P53* tumor suppressor gene. The *P53* gene usually exerts direct inhibition on transcription and thereby expression of GLUT1 and GLUT4, and indirectly on GLUT3. *P53* also induces TP53-inducible glycolysis and apoptosis regulator (TIGAR). TIGAR is an enzyme that exerts many functions, but in glycolysis fructose-2-bisphosphate is an allosteric activator of phosphofructokinase-1 (PFK-1). PFK-1 is an important enzyme in the glycolysis faciliating the convertion of fructose-6-phosphate to fructose 1,6-bisphosphate and is being referred to as the gate-keeper of glycolysis. TIGAR reverts fructose-2-bisphosphate back to fructose-1-phosphate, thereby removing the allosteric activator of PFK-1 and slowing down the glycolysis. In *P53* mutational cancer we observe the loss of these functions and therefore an increase in glycolysis and enhanced glucose uptake (26).

The glucose transport is often upregulated generating a higher influx of glucose. The excess glucose is used to fuel glycolysis, but also pentose phosphate pathway (PPP). PPP produces ribose-5-phosphate, an important building block in the nucleotide biosynthesis used during cell proliferation and growth to synthesize new DNA. The PPP is a parallell glucose pathway to the glycolysis and is divided into the oxidative and non-oxidative branch. The oxidative branch is a major contributor to the production of NADPH, a reducing agent crucial for dealing with oxidative stress and reactive oxygen species and therefore cell survival, but also plays an important part in the synthesis of fatty acids. The non-oxidative branch converts the glucose back to its original state continuing the PPP cycle or for the usage in glycolysis (29). The first enzymatic step of the process is the conversion of glucose to glucose-6-phosphate (G6P). G6P can either be used in the glycolysis or in the PPP. In the PPP, G6P is converted to 6-phosphogluconolactone (6-PG) by the enzyme glucose-6-phosphate dehydrogenase (G6PDH) in the oxidative branch. This process continues through various enzymatic steps yielding ribose-5-phosphate and the continued production of ribonucleotides. The conversion of G6P to 6-PG via G6PDH is the key controller of PPP glucose flux (30). The transcriptional p53 exerts the ability to block G6PDH and therefore controlling the synthesis of NADPH and ribonucleotides. The mutational version of *P53* seems to lose the ability to inhibit G6PDH contributing to increased proliferation and cancer cell survival (31). Ying H. and colleagues (32) demonstrated that oncogenic *KRAS* mutation in pancreatic cancer mouse model upregulated transcriptional genes encoding enzymes in the non-oxidative branch of PPP therefore stimulating ribonucleotide production.

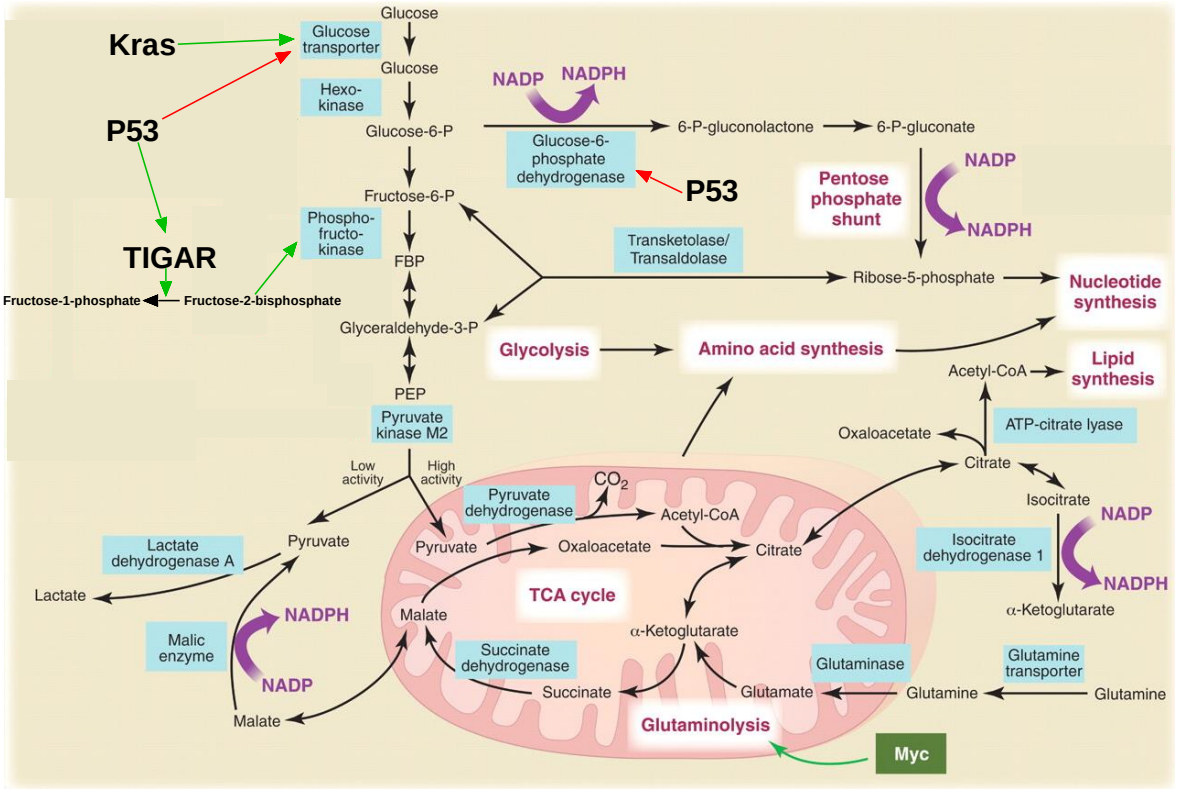

Figure 2.3.1.0 show parts of the glycolysis, pentose phosphate pathway and the citric acid cycle (TCA). Green arrows indicate activation, red arrows indicate inhibition. FBP; fructose-1-6-bisphosphate, P; phosphate. Borrowed from Vander Heiden, M.G with modifications (3).

2.3.2 Choline metabolism in cancer

The synthesis of choline is a part of the lipid biosynthesis for the production of phospholipids incorporated in the cell membrane. The synthesis of cholines is branched into two distinct pathways, the cytidine diphosphate ethanolamine (CDP-ethanolamine) and cytidine 5-diphosphocholine (CDP-choline) (figure 2.3.2.0). The CDP-ethanoleamine branch yields phosphatidylethanolamine (PtdEth) and phosphatidylserine through various enzymatic steps from its precursor ethanolamine, both end products ready to be incorporated in the cell membrane. The CDP-choline branch utilizes free choline (cho) taken up by the cell. The choline is phosphorylated by choline kinase yielding phosphocholine (Pcho). Pcho is further processed to CDP-choline and eventually to phosphatidylcholine (Ptdcho) which is the endproduct to be incorporated in the cell membrane. Ptdcho can be catabolized back to choline either directly by phospholipase b

or indirectly phospholipase A2 and lysophospholipase giving the intermediate glycerophosphocholine (GPC). GPC is catabolized to choline by glycerophosphodiesterase, thus continuing the kennedy pathway cycle. The Kennedy pathway is responsible for greater than 50% of the phospholipids incorporated in the cell membrane and therefore plays a crucial part in growth and proliferation of cells (33). Ptdcho can also be metabolized by phospholipase C and D, yielding second messengers such as Diacylglycerol, lysophosphatidylcholine and arachidonic acid which can be further metabolized to other signaling molecules including mitogens (33).

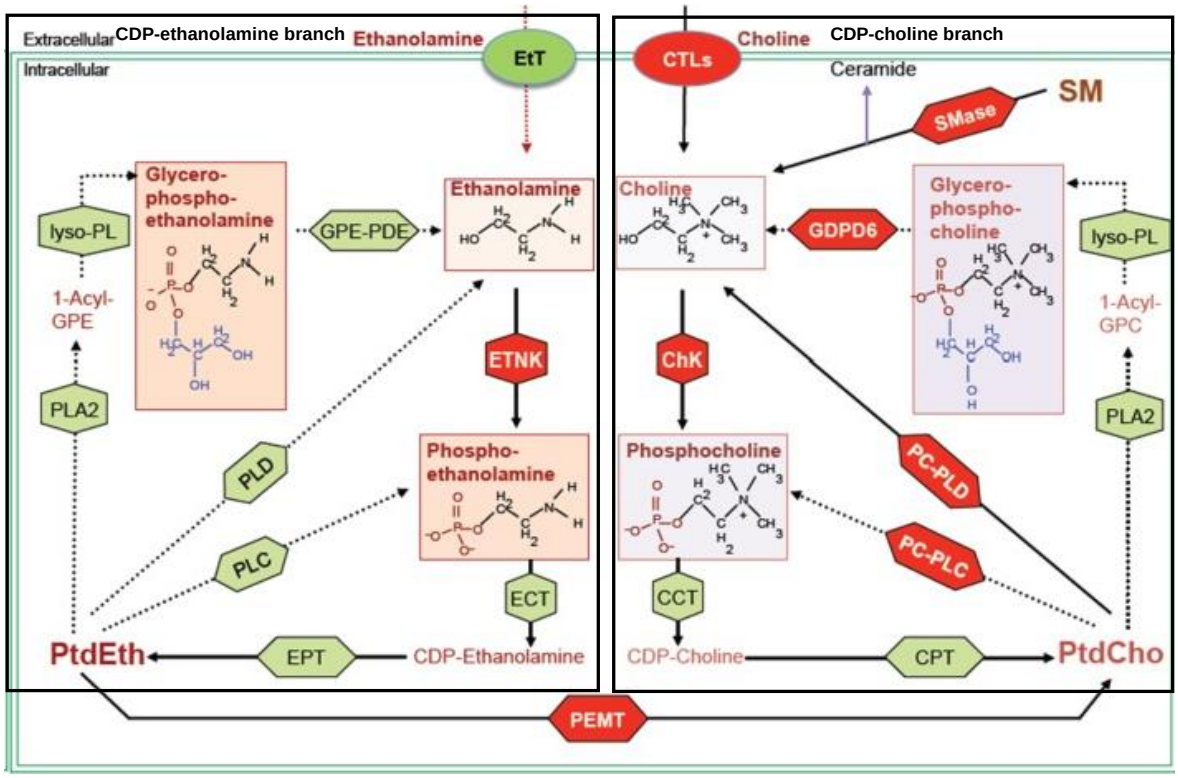

Figure 2.3.2.0 the kennedypathway divided in the CDP-ethanolamine and CDP-choline branch. 1-acyl-GPE; 1-acyl-glycerophosphoethanoleamine, 1-acyl-GPC; 1-acyl-glycerophosphocholine, PtdCho; phosphatidylcholine, PtdEth; phosphatidylethanolamine, SM; Sphingomyelin, CCT; phosphocholine cytidyltransferase, ChK; choline kinase, CPT; diacylglycerol cholinephosphotransferase, CTL; choline transporter-like protein, EtT; ethanolamine transporter, ECT; phosphoethanolamine cytidyltransferase, EPT; diacylglycerol ethanolaminephosphotransferase, ETNK; ethanolamine kinase, GPE-PDE; glycerophosphoethanolamin phosphodiesterase, GDPD6; glycerophosphodiester phosphodiesterase domain containing 6, lyso-PL; lysophospholipase, PEMT; phosphatidylethanolamine N-methyltransferase, PLA2; phospholipase A2, PLC; phospholipase C, PLD; phospholipase D. borrowed from Cheng M. with modifications (34).

The abnormalities seen in the choline metabolism pathway is due to an enzymatic overexpression. The enzymes that we usually observe as overexpressed is choline kinase-α (CHK-α) and phospholipase A2 thus increasing the levels of Pcho and GPC respectively. The microenvironment in solid tumors such as vascularization, hypoxia and acidosis has shown a decrease in expression of CHK-α in prostate and breast cancer xenografts compared to the same non-xenografts cancer cell lines, concequently lowering the concentrations of Pcho and total cholins demonstrated by Mori N. and colleagues (35). Oncogenic activation of *KRAS* causes induction of CHK-α through downstream PI3K

signaling. The transcription factor C-myc, often upregulated through oncogenic signaling, also induces CHK-α, and a 3-fold increase in Pcho has been observed in serum C-myc spiked fibroblast cells (36). Other oncogenic signaling that control CHK-α includes RAF and ERK either directly or through transcription factors (37). One notably study by Glunde K. and colleagues observed that prostate cancer cell line and prostate xenografts under hypoxia expressed increased levels of Pcho and total cholines by induction of CHK-α. The underlying mechanism was observed to be increased hypoxia-inducible factor 1 (HIF1), a transcription factor expressed during hypoxia to promote cell survival, that bound to the promotor region of CHK-α and upregulated transcription (38). Adressing the somewhat opposite findings between Mori N. and Glunde K. highlights missing links in the litterature in the field of choline metabolism, however this doesn't mean CHK-α isnt of clinical value. CHK-α is thought to have prognostic values where it is observed that overexpression of CHK-α is associated with more malignant tumors in ER-negative breast cancer (39). Based on the clinical value CHK-α presents, a novel CHK-α inhibitor has been developed and tested in xenografts bearing mice. The inhibitory effect of this compund has shown to arrest cancer cells in the cell cycle and mediate apoptosis, thus a reduction in tumor volume (40).

It has also been reported upregulation of choline transporter protein in breast, lung and colon cancer with uncertain mechanisms (41). Moestue and colleagues demonstrated that higher levels of GPC than Pcho was associated with more aggressive breast cancer due to difference in gene expression (42). The underlying mechanisms for the gene expression might be partly explained by oncogenic *RAS* activation which again can activate PI3K and RAF/MEK/ERK. PI3k, RAF and RAS can either increase or decrease enzymatic activity of phosphocholine kinase and RAS and ERK can influence phospholipase A2. It should be noted that these signaling pathways also stimulate enzymatic overexpression in an indirect manner through increased gene transcription (37). It has also been shown that activation of the oncogenic *P53* gene causes an increase in total choline levels in colon cancer cell cultures, but the underlying mechanism for this action is unknown (43).

By the usage of high resolution magnetic resonance spectroscopy it has been detected abnormal levels of choline metabolism in cancer cells. Increased levels of Pcho, GPC and cho have been detected in numerous cancer types (37), but also reports of decreased choline containing compund levels in cancer cells making it ambiguous (5). These inconsistencies have led to the use of Pcho/GPC ratio as a biomarker for tumor progression (34).

2.4 Analytical techniques for studying cancer metabolism

The study of cancer metabolism has led to the usage of many types of anlytical instruments to quantify and identify metabolites thought to be important for tumor development and prognosis. However the complexity of the metabolic factory within a cell creates many challenges. The vast amount of different metabolites, their relative difference in abundancy, different concentration in different compartments and some metabolites have close similarities in chemical structure. The difficulties arises in the

analytical instrumentations because of overlapping peaks, thus hardening the task of identification and quantification in tissue.

Mass spectroscopy (MS) is described as one of the two major workhorse in modern metabolomics. The molecules are fragmented in the ion source, accelerated out and separated based on the relationship between the ions mass and charge. This information is used to produce a mass specter where the amount of ions (intensity) is plotted against their given mass in a histogram manner (44). MS can be combined with gas cromatography and high performance liquid cromatography as a separation technique, has a high sensitivity and low detection limit and is able to quantify metabolites by using a isotope labeled internal standards. The relative high sensitivity enables us to see even small changes in metabolites that other analytical tools can not discover, making MS a prefferd method for targeted analysis of metabolomics. However the drawbacks are quite clear in untargeted analysis of metabolomics. The high sensitivity often cause detection of thousands of metabolites making quantification and identification difficult. Furthermore, contaminants within the sample can change the ionization efficiency of metabolites making the reproducibility poor. This problem creates the need for extensive sample preparation compared to other methods such as magnetic ressonance spectroscopy (MRS) (45).

The other workhorse in modern metabolomics is magnetic ressonance spectroscopy which utilize the active spin moment of atoms to detect signals. Atoms that exhibit spin must have unpaired neutrons and protons such as proton ^{1}H, flouride ^{19}F and phosphorus ^{31}P. Other important atoms in biochemistry such as carbon ^{12}C, oxygen ^{16}O and nitrogen ^{14}N have paired number of protons and neutrons and is therefore not visible in MRS. However their corresponding isotopes carbon ^{13}C, oxygen ^{17}O and nitrogen ^{15}N do display nuclear spin and can be measured by MRS (46). The intensity of the peak corresponds to the amount of atoms that give rise to the signal and therefore MRS can be used for relative quantification. MRS is highly reproducible and can analyze intact tissue and liquids with minimal sample preparation, and detect great variety of metabolites making it a suitable method for untargeted analysis of metabolomics. The recent development in high magnetic field strength such as 3T and 7T MR scanners have enabled us better signal to noise ratio (SNR) in-vivo MRS for detection of metabolites in clinical purposes. However the SNR and spectral resolution is still poor compared to ex-vivo because of lower magnetic field strength and dipol-dipol interactions which limits observable metabolites (47). The major concern with MRS is the low sensitivity and the acquisition time needed to achieve a decent signal. The low sensitivity also lowers the ability to detect metabolites in low abundancy and might not be the best choice of instrumentation in targeted analysis of metabolomics (45).

2.4.1 Nuclear magnetic resonance and T1-relaxation

Nuclei's with a odd number of protons and neutrons such as ^{1}H and ^{31}P, posess a physical intrinsic property known as spin. Nuclei's with spin also exerts a magnetic dipole moment μ according to the equation $\mu=I*\gamma$, where I is the quantum number and γ is the

gyromagnetic ratio which varies between different nuclei's. The orientation of the spin in normal condition is random, but under a strong magnetic field the spin will either be alligned parallel or anti-parallel in respect to the magnetic field. The distribution of the different spins are described via the Boltzmann distribution where the population of spins that is parallel to the magnetic field is slightly higher than for spins that are anti-parallel to the magnetic field. How many different orientation a given atom can possess is decided by its quantum number. For protons which have a quantum number of ½ , the number of orientations it can possess will be (2x ½ + 1) =2 i.e parallel or anti-parallel in respect to the magnetic field. The two different spin orientations also differ in the term of energy level where the anti-parallel spin is of higher energy. The difference in energy between the two spin states is given by $\Delta E = \frac{h\gamma}{2\pi} * B_0$ where h is plancks constant, y is the given gyromagnetic ratio and B_0 is the strength of the applied magnetic field.

A nuclei in a applied magnetic field precess at a certain rate, termed larmorfrequency, which is proportional to the magnetic field. By applying electromagnetic radiation with the same frequency as the nuclei's larmorfrequency the magnetic vector will tip out of the +z plane towards the xy plane depending on the duration of time of the applied electromagnetic radiation. This means that nuclei's of lower lower energy level (parallel to the magnetic field) will shift towards a higher energy level (anti-parallel to the magnetic field). When the applied radiation stops, the nuclei's will return to equilibrium given by the Boltzmann distribution through a process known as T1-relaxation, emitting energy in the process. The emitted energy and the frequency where it occurs is detected by the NMR coil and give rise to a NMR spectrum (48).

2.4.2 T2-Relaxation and free induction decay

When the net magnetization is tiped out of equilibrium by electromagnetic radiation from the +z plane towards the xy plane, the nuclei's will be in phase coherence meaning they will have the same orientation and rotates in the same velocity and precess around the xy plane giving rise to the signal detected in NMR. When the electromagnetic radiation ceases, immediatley following the nuclei's will start to lose phase coherence in the xy plane and/or the magnetic vector will realign itself back to the applied magnetic field. The time it takes for these two gradual processes to occur are termed T2-relaxation time and T1-relaxation time respectively. Both mechanisms lead to the exponential decay of the sinus wave signal observed in NMR termed the free induction decay (FID). The FID measures intensity of the signal over time. By replacing the time-domain with a frequency domain, through a process known as fourier transform, we obtain a NMR spectrum with intensity in the y-axis and frequency in parts per million in the x-axis known as chemical shifts (48, 49).

2.4.3 Identification by MRS

If all nuclei's of the same element would resonate at the same frequency we would observe one peak in the MRS spectre, however that is not the case. The frequency needed to achieve resonance for a given nuclei in a molecule is dependent by the magnetic field felt by the nuclei. The felt magnetic field is often slighty different between nuclei's in the same molecule because of different neighbouring atoms. The biggest mechanism that contributes to this effect is called chemical shielding and is due to the electron cloud surrounding a molecule. Electrons are charged particles in motion and therefore induces its own magnetic field. The electron magnetic field will interact with the actual magnetic field felt by a given nuclei making it resonate at a lower frequency therefore a change in chemical shift is observed. Since the distribution of the electron cloud in a molecule is given by its contents of functional groups, nuclei's neighbouring electronwithdrawing groups have a tendency to be downfield while nuclei's neighbouring electrondonating groups show upfield tendency. Thus making the effect of chemical shielding a usefull tool in identification of a molecule by MRS (49).

Another interaction between nuclei's are J-coupling (also termed spin-spin splitting and scalar coupling). This effect occurs when nuclei A is close to nuclei X (usually 2-3 bonds apart from each other with deviations because of spatial orientations). Nuclei X have its own induced magnetic field that can either be alligned parallel or antiparallel to the applied magneticfield. If nuclei X is alligned parallel with the applied magnetic field, then the magnetic field felt by nuclei A will be bigger therefore making it resonate at a slightly higher frequency. In contrast, if nuclei X's magnetic field is alligned antiparallel to the applied magnetic field, the magnetic field felt by nuclei A will be lower than the applied magnetic field and therefore resonate at a slightly lower frequency. The phenomenon of J-coupling are mediated by electrons through bonds where the spin of nuclei X perturbs the shared electrons which in turn perturbs the spin of nuclei A. if there is only one nuclei affecting nuclei A, we will observe nuclei A as a doublett, if there is two nuclei's affecting nuclei A, we will observe it as a triplett and so forth. J-coupling is always mutual between nuclei's and is a crucial indirect interaction for structure determination and identification (46, 48).

The heteronuclear single quantum correlation (HSQC) experiment is a valuable technique for identifying heteroatoms that is directly bonded to protons. By applying various pulse sequences to the proton and heteroatom channel, we are able to detect the signals from the contributors in two dimensions. The 2D-spectra reveal the chemical shift of the proton and the heteroatom where they are directly bonded to each other in the form of a peak in between them. This information can be used to determine the structure of molecules and secure identification in complex biological tissue that contains many different metabolites and overlapping peaks (50, 51).

2.4.4 HR MAS MRS

As described in section 2.4.3 identification by NMR, magnetic interactions between atoms in a molecule cause the atoms to ressonate at a different frequency. J-coupling and chemical shielding is isotropic interactions meaning that the magnitude of the interaction is not dependent upon molecular orientation. However interactions that are dependent on the molecular orientation in respect to the magnetic field, termed anisotropic interactions, is not observed in liquid MRS because molecules orient and rotate freely due to brownian motion which evens the anisotropic interactions (52). In solid state and semi-solid state (such as tissue) MRS, the molecules are locked in position, restricting brownian motions and therefore anisotropic interactions can not be ignored. The restricted motion cause the same molecule to be locked in every possible orientation it can pocess and will therefore affect the frequency over a wide range a given nuclei will resonate at, generating a broad peak and poor resolution. The anisotropic interactions contributing to this effect are chemical shift anisotropy, dipolar couplings and quadrupolar coupling for nuclei's with a quantum spin number unequal 0 (i.e ½, 1, $^5/_2$ etc.). The chemical shift anisotropy is based on asymmetrical distribution of the electron cloud around a molecule, thus depends on the orientation of the molecule in respect to the magnetic field. The dipolar coupling is the nuclei's ability to exert its own magnetic field. The exerted magnetic field can perturb the applied magnetic field experienced by surrounding nuclei's through space, and is highly orientation dependent in respect to the applied magnetic field. The quadrupolar interaction is only present for nuclei with spin greater than ½ (^{14}N I=1, ^{17}O I=$^5/_2$). The quadrupolar moment of a nuclei can couple to the electric field gradient and cause line broadning (53).

The anisotropic interactions in solid state MRS can be dealt with because it follows a angular dependency between the applied magnetic field and the distance between two interacting nuclei's given by the equation $3\cos^2(\Theta) - 1$ where Θ is the angle. When the sample is spun rapidly around its own axis with an angle of 54,7° in respect to the applied magnetic field the equation yields 0, and high resolution spectrums are obtained in solid state MRS thus mimicking brownian motions observed in liquid MRS (52, 54, 55).

2.5 Model systems in cancer research

Cell cultures has been the main driver for cancer research throughout history and still is to this date. They can be cultured from donors (primary cell lines) or obatined from bio banks. The primary cell lines often contain several cell types and the isolation of the correct cell type is important, but may cause difficulties. The short life span of primary cell lines have also been an issue. The alternative is to use an immortalized cell line from a bio bank which contains models for various cancer types.

The utilization of cell cultures have made it possible to understand biology, mechanism for diseases and drugs, morphology, gene functions and more. The extensive use of cell cultures is partly due to the low maintenance cost and the ability to perfom functional tests (56). However, cell cultures have disadvantages as they are not structured as natural tissue or tumors and also do not replicate the microenvironment in terms of cellular heterogeneity or levels of nutrients and signaling molecules. This makes the cell cultures differ in terms of morphology, proliferation and signal transduction compared to in-vivo settings. These issues have led to the development of organoids for more accurate replication of the in-vivo environment (57). In order to model cancer in vivo, animal models can be used. Such models can be spntaneous, chemically induced or

based on allo- or xenograft tissue transplantation. However, animal models are labor-intensive to establish and maintain, and may be difficult to perform mechanistic studies in them.

2.5.1 Organoids

The term organoid has not been uniformly defined, but can be described as a 3 dimentional in vitro cellular modeling system derived from stem cells capable of self-sustaining and self-organizing, and show similar organ functionality and structures as the parent tissue. The 3D modelling system resembles the condition of organization and cellular relationship as observed in-vivo therefore making it a more accurate model in cell signaling networks than traditional cell culture models (58).

Despite the progress of organoids, they do have limitations. Compared to animal models, organoids are only an approximation of the physiology of the human body. This is reflected in the inability of the organoids to pocess a functional immune system, nervous system and vascular system. This makes organoids less efficient as a model system where complex physiological mechanisms between multiple organs are in play (59).

Organoids can be cultured from cells such as embroynic stem cells, pluripotent stem cells, adult stem cells (somatic stem cells) and cancer cells to name a few, and can replicate numerous organs such as lung, stomach, liver, small intestine and colon. The cells can be derived from human adult tissue and human embrynoic progenitors, but also from mice (60).

Organoids has been used as modelling systems for human development biology, human disease progression, personalized medicine, preclinical disease drug screening and cancer modeling (59). The usage of organoids gives a wide range in utilization between different fields of research and is thought to make great contributions in the years to come.

2.5.2 Organoids in cancer research

The ability of organoids to replicate the parent organ has given new insight in cancer biology, and a new modelling system in cancer research. Tumor organoids in fields of pancreas, liver, lung, bladder, prostate, breast, intestinal and colon has been established with interesting results. CRC organoids show similarites with the primary tumor in

differentiation, histology and mutational landscape. It has also been recently shown that with knockout of the DNA mismatch repair system in a healthy human colon organoid by CRISPR/CAS9 technology, led to increased DNA mutation through replicative errors with similarities as tumorigenesis observed in cancer patients (61). Drost J. with colleagues demonstrated that CRC organoids cultured from healthy human colon tissue genetically modified by CRISPR/CAS9 by knocking out a set of important genes normally found mutated in CRC patients, was able to replicate the tumorigenesis of CRC observed in patients. It was also observed that with the loss of *APC* and *P53* gene, the CRC organoid developed chromosomal instability and aneuplodity, a great contributor in the development of CRC. This research demonstrated the close similarities of tumor organoids versus in-vivo conditions, but also driver oncogenes behind CIN (62). The genetic variation between the original tumor and the corresponding cultured organoid was found to have little variance and therefore showed a proof-of-concept for the usage of tumor organoids as a model system (63).

Studies suggest that cell signaling in tumor organoids is altered compared to traditional 2D cell cultures. The reason behind this change is unknown, but observations implies that modifications in the regulation of genes encoding cell signaling plays a part. The presence of extracellular matrix (ECM) in organoids reduces the sensitivy of chemotherapy where this effect was not observed in 2D cell cultured in identical ECM (64). This highlights some of the differences found between traditional 2D cell cultures and organoids.

3 Materials and methods

3.1 Organoid culture

Organoids for HR MAS analysis were grown and tested for response by collaborator Wybe J.M. Van der Kemp, UMC Utrecht, Netherlands. The organoids were established from healthy human colon tissue as described by Sato and colleagues (65) and genetically modified by Drost and colleagues (62). Organoids were cultured for five days on expansion medium in 6 well plates in ~20 ul matrigel droplets (~10 droplets per well) from multiple cell fragment organoids obtained by trypsinizing large organoids. After five days, the organoids were replated (diluted) and grown for five days on differentiation medium (see supplementary material)

3.1.1 Preparation of samples for NMR analysis

Organoid drug treatment was done on day five of differentiation medium culturing. Organoids were harvested at three time points (0, 48 and 96 hrs). The samples at 0 hrs are untreated control samples, whereas both untreated control organoids and chemotherapy treated organoids were harvested at 48 and 96 hrs. For control samples,

two wells were harvested and pooled per NMR sample. For treated organoids, three wells were harvested and pooled per NMR sample (1 sample for extraction 1H NMR and 1 sample for HR MAS NMR with a total of 22 samples). Drug treatment was done with SN-38, oxaliplatin and 5-FU and a combination therapy consisting of these drugs. The experimental setup is presented in table 3.2.1

Organoid harvesting was done on ice with ice cold normal saline in falcon centrifuge tubes. To remove culture medium solution residue, the obtained organoid pellet was three times resuspended in 10 ml normal saline. After these washing steps the organoid pellets were snap frozen in falcon tubes by immersion in liquid nitrogen.

3.2 Assessing treatment response of organoids

Treatment response was assessed by extraction 1H NMR by determining the total sum of all metabolites extracted from the organoids (data not shown), unless otherwise mentioned. With an equal organoid density for control and treated organoids at the start of an experiment, the total metabolite concentration is proportional to the organoid biomass in the wells at the end of the experiment. No metabolites measured, for the treated organoids, would mean total response, while equal metabolite content for controls and treated at 96 hours of treatment would mean no response at all.

A summary of treatment response to single and combination therapy with chemotherapeutic agents is presented in Table 3.2.0. Response (R) was defined as less than 5% biomass (i.e. total metabolite content as determined by 1H NMR) increase for treated organoids after 96 hrs as compared to 0 hrs control, and at least 20% less biomass than the 96 hrs control.

Section 3.1, 3.1.1 and 3.2 were carried out at UMC Utrecht by collaborator Wybe J.M. Van der kemp, Netherlands.

Table 3.2.0 Organoid response to treatment of oxaliplatin (OxPt), fluorouracil (5-FU),the active metabolite of irinotecan (SN-38) and the combination of these after 96 hours of treatment. R:response; NR: non-response; empty: not available.

	Oxaliplatin (OxPt) [uM]			**Fluorouracil (5-FU) [uM]**					**Irinotecan (SN-38) [uM]**					**Combination therapy (OxPt/5-FU/SN-38) [uM]**		
	50	100	150	25	50	75	100	200	0,25	0,5	1	1,5	2	50/50/0,5	50/50/1	75/75/1
TPO0 Wild type																
TPO1 *KRAS*																
TPO2 *APC-KRAS*	R	R	R	R			R	R	R		R		R			R
TPO2 *APC-P53*		NR		R	R		R		NR		NR		R	R		
TPO3 *APC-KRAS-P53*		R		R	R	R			R	R		R			R	
TPO4 *APC-KRAS-P53-SMAD4*		NR		R	R	R			R	R	R			R		

Table 3.2.1 Overview of Oxaliplatin (OxPt), Fluorouracil (5-FU) and the active metabolite of irinotecan (SN-38) concentrations, and the combination of these used to treat the organoids after 48 hours and 96 hours. Untreated control samples were harvested at timeframe 0, 48 and 96 hours for each organoid type. R: Response indicates that treated organoid is sensitive to chemotherapeutic agents; NR: non-response indicates no response to chemotherapy; "-": not determined.

Organoid Type, mutations and number of samples (N)	**Time point [t]**	**Oxaliplatin (OxPt) [uM]**	**Fluorouracil (5-FU) [uM]**	**Irinotecan (SN-38) [uM]**	**Combination treatment (OxPt/5-FU/SN-38) [uM]**	**Number of harvested untreated control organoids**
TPO0 Wild type (N=11)	0	-	-	-	-	1
	48	100-	100 R	1 R	75/75/1 R	1
	96					1
TPO1 *APC* (N=0)	Not analyzed	Not analyzed	Not analyzed	Not analyzed	Not analyzed	Not analyzed
TPO2 *APC-KRAS* (N=11)	0	-	-	-	-	1
	48	100 R	100 R	1 R	75/75/1 R	1
	96					1
TPO2 *APC-P53* (N=11)	0	-	-	-	-	1
	48	100 NR	50 R	1 NR	50/50/0,5 R	1
	96					1
TPO3 *APC-KRAS-P53* (N=11)	0	-	-	-	-	1
	48	100 R	75 R	1,5 R	50/50/1 R	1
	96					1
TPO4 *APC-KRAS-P53-SMAD4* (N=11)	0	-	-	-	-	1
	48	100 NR	75 R	0,5 R	50/50/0,5 R	1
	96					1

3.3 HR MAS NMR analysis

3.3.1 Sample preparation

The TPO's was shipped to Trondheim, Norway from Utrecht, Netherlands on liquid nitrogen, and then stored in -80°C freezer until analysis. The work station was cooled down in the -80°C freezer and the organoids were thawed for 5 minutes. A 30 uL disposable HR MAS insert was filled with 5 uL 25 nM sodium formate in D_2O. Any excess liquid was removed from the sample tube. A pipette led to the middle of the organoid pellet was used to transfer 25 uL organoid to the disposable HR MAS insert. The disposable HR MAS insert was closed using a taper and screw cap before the disposable HR MAS insert were inserted in 80 uL HR MAS rotor closed with a spinning cap.

3.3.2 HR MAS NMR

HR MAS NMR spectra were obtained on a Bruker Avance III spectrometer (600 MHz, 14,1 Tesla) equipped with a $^{1}H/^{13}C/^{31}P/^{2}H$ MAS probe (Bruker, Biospin GmbH, germany). Temperature calibrations were performed once a week and the magic angle of 54,7° was measured once daily in accordance to the laboratory's quality control program.

Prepared samples were put manually in the HR MAS probe with temperature set to 278,15 K with a spin rate of 5000 Hz. Tuning and matching were done manually to ensure right frequency of ^{1}H and ^{31}P channels. Locking of the magnetfield to D_2O was done to ensure stability of the magnetfield during acquisition. Shimming was performed manually in a 1D NOESY (bruker: noesygppr1d) with 4 scans. Automatic phasing, and manually phasing was performed if necessary. The shape and width of the formate peak at approximately 8,4 ppm was evaluated and considered acceptable if the full width half maximum of the peak was under 1 Hz with little to no asymmetric distribution, otherwise shimming was performed manually by acquiring spectra in real time (GS mode, Bruker) until criteria met. Pulsecalibration was performed manually to determine the optimum pulse value for each sample in a zg (bruker: zg) experiment. The P1 value was considered optimal when the signal of P1x4 value is equal to zero at 360° pulse. For water supression, the frequency of water (O1 value) were determined manually in a zgpr (bruker: zgpr) experiment where a optimal O1 value corresponds to a low signal intensity of water at approximately 5 ppm with the observed best p1 value for each sample from the pulsecalibration. The acquisition of 1H spectra was perfomed in a 1D NOESY (bruker: noesygppr1d) experiment with the O1 and P1 values determined for each sample. The 2D ^{1}H and ^{31}P were aquired by proton decoupling HSQC (bruker: hsqcetgpprsisp2.2) experiment with the O1 and P1 values determined for each sample, and 1D ^{31}P spectra were aquired by a proton decoupling zgpg (bruker: zgpg) experiment with P3 and P4 determined for each sample (equals P1 and P1x2 for proton pulse respectively). For further information on acquisition parameters see table 3.3.2.0.

Table 3.3.2.0 Overview of NMR acquisition parameters. D1;delay

Method	**1D ^{1}H-NMR-spectroscopy**	**1D ^{31}P-NMR-spectroscopy**	**2D ^{1}H-^{31}P-NMR-spectroscopy**	
			F1	**F2**
Pulseprogram (bruker)	Noesygppr1d	zgpg	Hsqcetgpprsisp2.2	
Temperature [k]	278,15	278,15	278,15	
Number of scans (NS)	256	256	128	
Acquisition time (AQ) [sec]	2.74	0,446	0,003	0,106
Repetition time (D1+AQ) [sec]	3,74	5,446	1,003	1,106
Total acquisition time [min]	64	23	37	
Size of FID (TD)	98304	65536	32	2048
Number of dummy scans (DS)	4	0	16	
Spectral width (SW) [ppm]	29,9	302,7	22	16
Receiver gain (RG)	40,3	203	203	

3.4 Identification of metabolites

The metabolites were identified by using Chenomx NMR suite 8.6 (Chenomx Inc., Canada). By loading a representative specter, chenomx searches for compounds based on number of peaks and ppm from its library. The peaks can be fitted manually to the loaded specter for matching. Where feasible, human metabolome database (hmdb.ca) was used as a reference. 2D HSQC (^{1}H/^{31}P) spectra were used to secure identification of Pcho, GPC, PE and glycerophosphoethanolamine (GPE).

3.5 Data processing

After acquisition, the spectra were fourier transformed and line broadened 0,3 Hz and 1 Hz (-1D ^{1}H NOESY and 1D ^{31}P zgpg respectively), and phased in 0. and 1. Order.

Furthermore, alanine was calibrated to 1,48 ppm for 1D ^{1}H NOESY spectra (topspin 4.0.9, bruker biospin GmbH, Germany). 1D ^{1}H NOESY spectra were further preprocessed using Matlab R2020a (the Mathworks, Inc., USA). The spectra were aligned using the formate peak at approximately 8,45 ppm as reference, using the icoshift algorithm (66). Icoshift uses the spectrum which correlates best with other spectra as a reference, and splits other spectra into intervalls that are individually aligned and optimized. Baseline correction was made to set baseline to zero by asymmetric least squares method which estimates a baseline and substracts it from the spectra (67).

Before PCA analysis, the spectra were mean normalized by dividing each variable in a specter by its mean. Contaminants (e.g methanol, ethanol and dimethylsulfoxide), water region, formate and noisy regions were removed from the spectra leaving metabolite containing regions of 0,8 ppm-4,5 ppm and 5,4 ppm-8,7 ppm. These metabolite containing regions were used for multivariate modeling.

3.6 Multivariate comparison of spectra

Principal component analysis (PCA) was used to assess metabolic differences between TPO's using PLS_Toolbox R8.8.1 (Eigenvector research, USA). 51x14149 variables from matlab was preprocessed by mean centering in PLS_Toolbox. Cross-validation method used is leave-one-out. The output was score plot with corresponding loading profiles.

3.7 Quantification of selected metabolites

The spectra were baseline corrected manually using topspin 4.0.9 and peaks in the metabolite containing regions of 0,8 ppm to 1,1373 ppm, 1,2375 ppm to 2,7230 ppm, 2,750 to 3,3067 ppm, 3,49 ppm to 4,60 ppm, 5,86 ppm to 8,39 ppm were integrated using topspin 4.0.9. The area under the curve (AUC) of formate was intergrated from 8,431 ppm to 8,46 ppm. The AUC of formate was divided by the total AUC of the respectively spectre times thousand to normalize the spectra. Furthermore, Chenomx NMR suite 8.6 (Chenomx Inc., Canada) was used to quantify the spectra by inputting the calculated formate AUC as the chemical shape indicator with sample pH set to 7,35 ± 0,1 with no processing. The spectra were sent to chenomx processor and the chemical shape indicator formate were calibrated to fit the formate peak at approximately 8,45 ppm. The spectra were sent back to chenomx profiler for manually fitting of metabolites were the height of the peak corresponds to a relative quantification of the metabolite. Lactate, alanine, total choline containing compounds (tCCC, Pcho+GPC+Cho+PE) and myo-inositol which has well-defined peaks were quantified using another method. Alanine, lactate, tCCC and myo-inositol using the intervalls 1,465 ppm to 1,493 ppm and 1,317 ppm to 1,349 ppm, 3,2050 ppm to 3,25 ppm, and 3,517 ppm to 3,557 ppm respectively were integrated using topspin. The AUC of alanine, lactate, tCCC and myo-inositol was divided by the total AUC of the given specter times hundred, and alanine, lactate, tCCC and myo-inositol are therefore presented as percentage contribution relative to the total AUC in each spectrum.

3.8 Statistical analysis of untreated control TPO's

The mean untreated TPO2a (*APCKRAS*), TPO2b (*APCP53*), TPO3 and TPO4 were compared to validate statistically significant difference from mean untreated TPO0. This was done by utilizing a one way ANOVA followed by holm-bonferroni corrected two samples t-test assuming equal variances in excel 2016 (Microsoft inc., USA). This was performed both for the results of quantification and the PC1 score from PCA of untreated organoids.

3.9 Excluded samples

The combinational treatment samples including TPO0 48hr and 96hr, and TPO2a 96hr has been excluded for further analysis because of lack of organoid cells. These TPO's has most likely underwent cell death to such an extend that there was no or little organoid cells left to conduct further analysis with HR MAS NMR.

TPO2b 0hr ctrl was excluded for further analysis because the specter did not resemble TPO2b 48hr and 96hr control nor the other control spectra, see figure 3.9.0 for further details.

The amount of lactate in TPO3 96hr combi could not be quantified because of poorly defined peaks. The reason is large amount of lipids from 1,26 ppm to 1,36 ppm relative to the intensity of the lactate peak as shown in figure 3.9.1

The quantification of TPO2a 48hr combi was made difficult with lack of intensity of the metabolites as shown in figure 3.9.2 and is therefore not quantified.

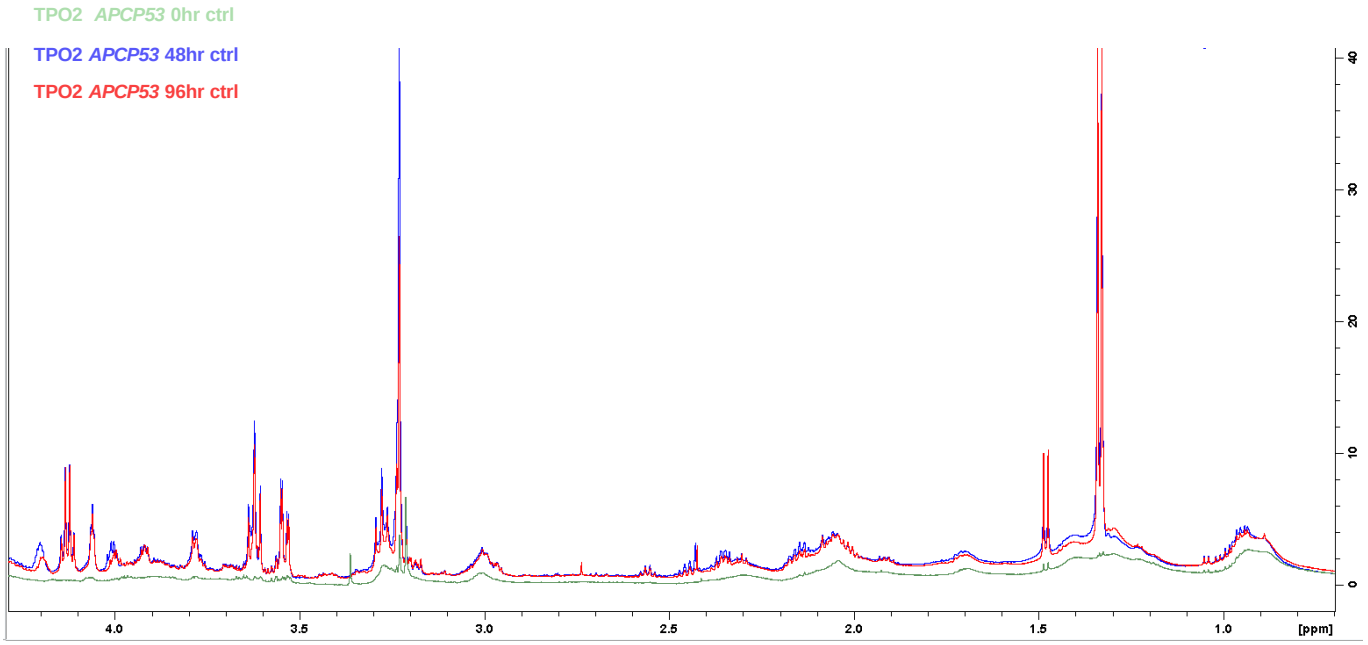

Figure 3.9.0 Raw spectra of untreated TPO2 *APCP53* 0hr, 48hr and 96hr in green, blue and red respectively.

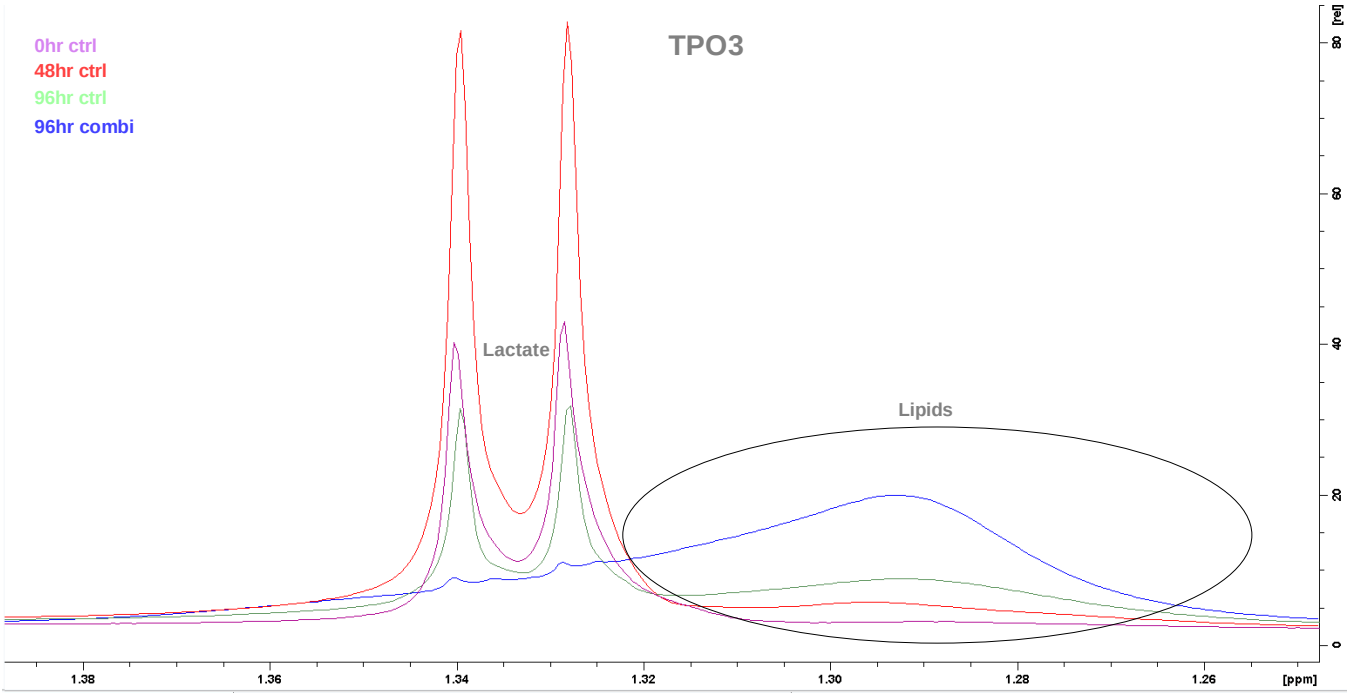

Figure 3.9.1 Raw spectra of untreated TPO3 0hr, 48hr, 96hr and 96hr combi treated organoid in yellow, red, green and blue respectively.

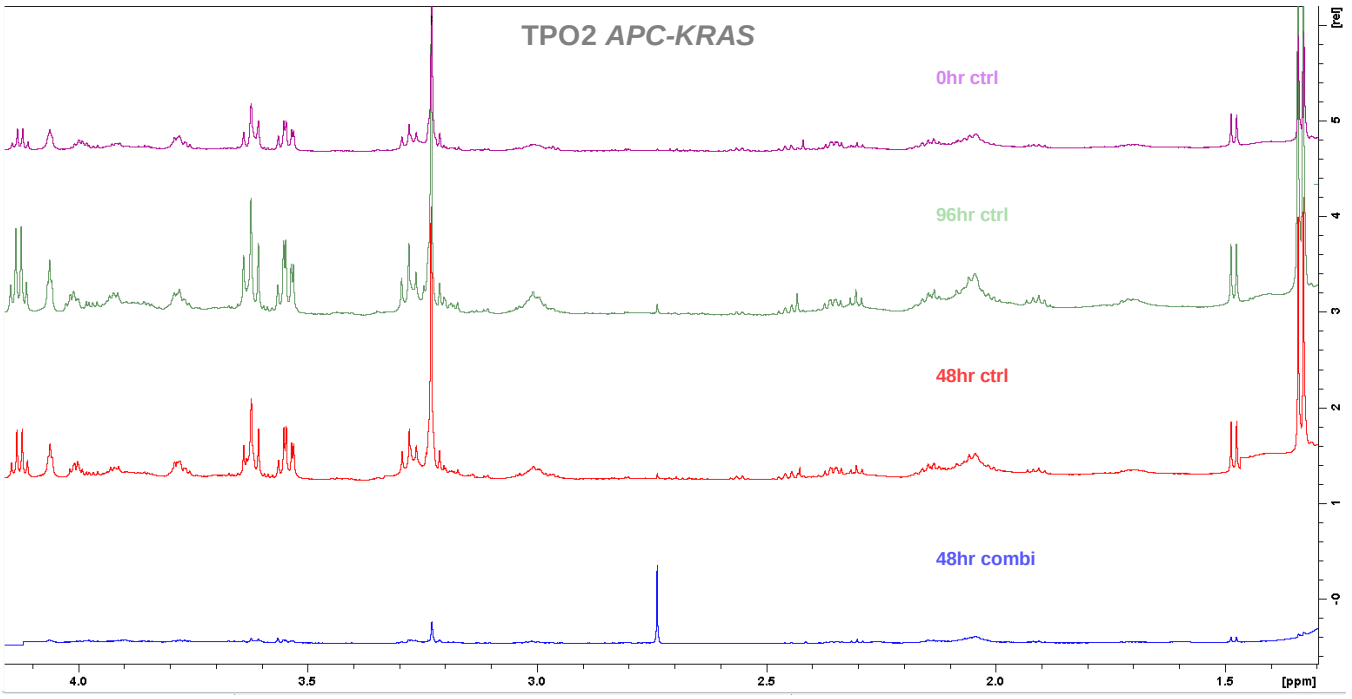

Figure 3.9.2 Raw spectra of untreated TPO2 *APC-KRAS* 0hr, 96hr, 48hr and 48hr combi treated organoid in purple, green, red and blue respectively.

4.0 Results

A total of 51 samples were available for analysis after exclusion of spectra that were considered unsuitable for analysis (see section 3.9). From the 1H and 31P spectra, 16 intracellular metabolites were identified in the TPO's. Assignments are shown in figure 4.0 with corresponding chemical shift values presented in table 4.0

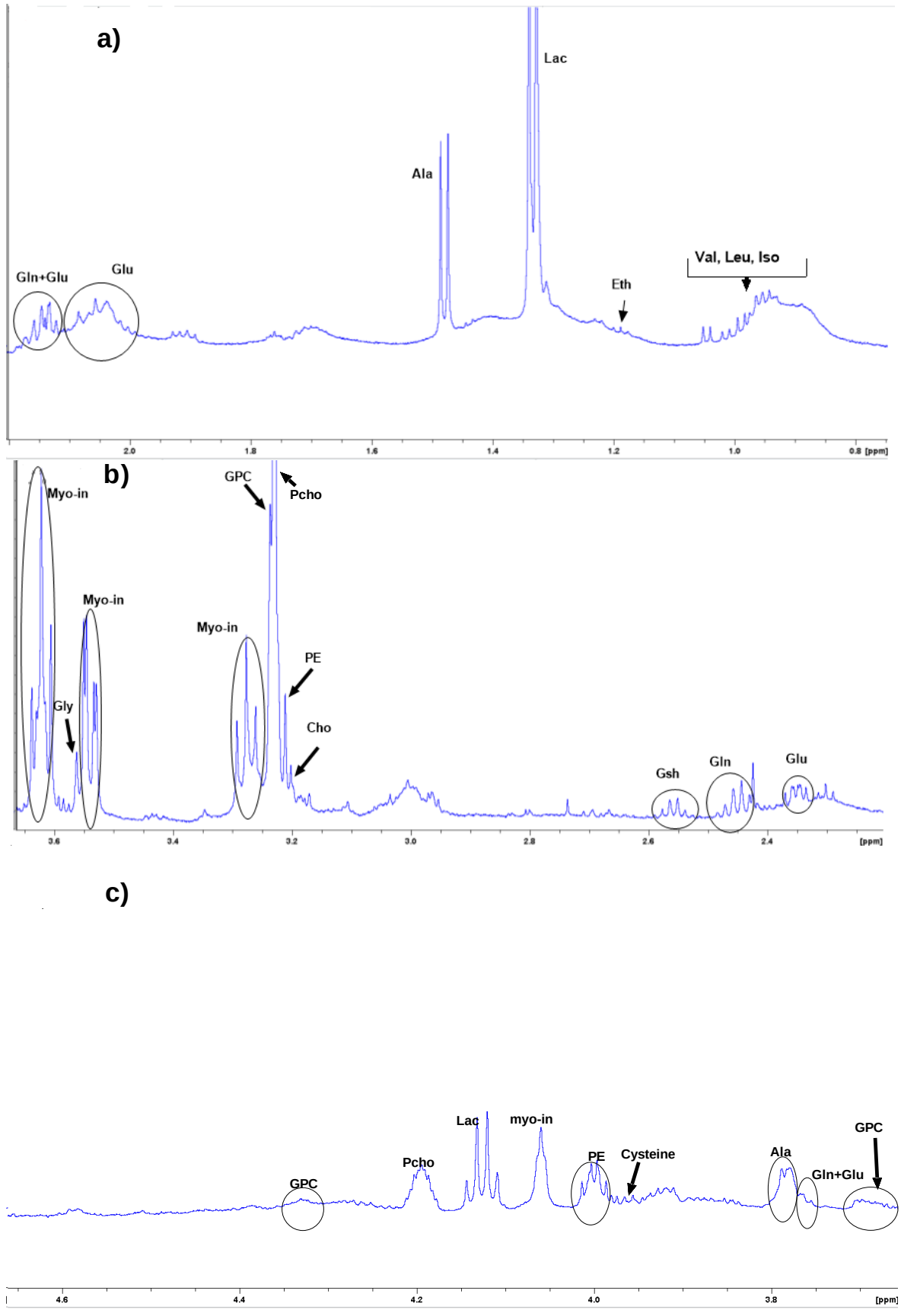
a)
Lac
Ala
Gln+Glu
Glu
Eth
Val, Leu, Iso
2.0
1.8
1.6
1.4
1.2
1.0
0.8 [ppm]
b)
Myo-in
GPC
Pcho
Myo-in
Myo-in
PE
Gly
Cho
Gsh
Gln
Glu
3.6
3.4
3.2
3.0
2.8
2.6
2.4
[ppm]
c)
GPC
Pcho
Lac
myo-in
PE
Cysteine
Ala
Gln+Glu
GPC
4.6
4.4
4.2
4.0
3.8
[ppm]

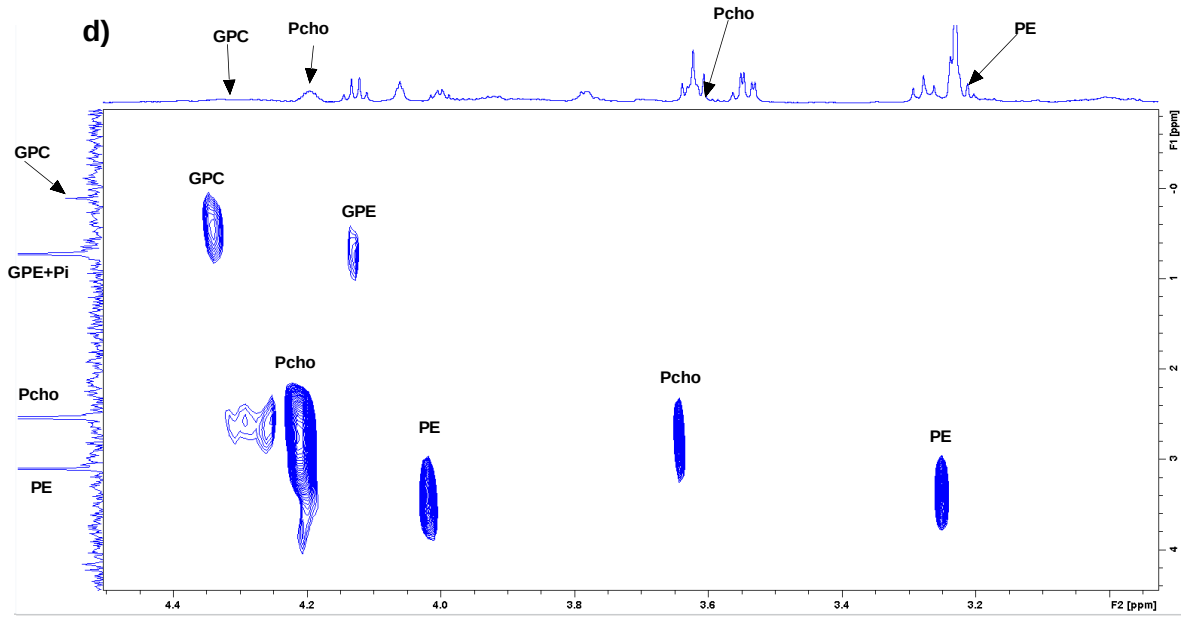

Figure 4.0 a),b) and c) showcase a representative ^{1}H noesygppr1d spectrum with identified metabolites. D) showcase a representative $^{1}H/^{31}P$ hsqcetgprsisp2.2 specter.

Table 4.0 Supplement to figure 4.0 showing abbreviations, number of observable peaks and their respective ppm values in ^{1}H and ^{31}P spectra for identified metabolites. "–" = not determinable number of observed peaks. Empty: not available.

Abbrevation	**Metabolite**	**Number of observable peaks (^{1}H)**	**Chemical shift [ppm]**	
			^{1}H	^{31}P
Iso	Isoleucine	3 2	0,95 1,02	
Leu	Leucine	3	0,97	
Val	Valine	2 2	0,98 1,05	
Eth	Ethanole	3	1,19	
Lac	Lactate	2 4	1,33 4,12	
Ala	Alanine	2 4	1,48 3,79	
Glu	Glutamate	6 10 8 4	2,04 2,12 2,34 3,75	
Gln	Glutamine	6 7 2	2,14 2,44 3,76	
Gsh	Glutathione	8	2,56	
Cho	Choline	1	3,21	
PE	Phosphoethanoleamine	1 6	3,22 4,0	2,81
Pcho	Phosphocholine	1 3 9	3,23 3,61 4,20	2,24
GPC	Glycerophosphocholine	1 - -	3,24 3,66 4,32	0,12
GPE	glycerophosphoethanolamine	-	-	1,38
Myo-in	Myo-inositol	3 4 3 3	3,28 3,54 3,62 4,06	
Gly	Glycine	1	3,56	
Cys	Cysteine	3	3,94	

4.1 Metabolic characteristics of untreated TPO's

Comparing raw spectra from untreated TPO's (Figure 4.1.0 a, b, c and d), several metabolic differences were observed. The lactate level appeared to increase with the number of mutations except for untreated 96hr TPO3 (b)). The opposite was observed for phosphocholine (b)), tCCC (c)) and myo-in (d)), where decreasing levels were observed with increasing number of mutations. PCA of spectra from untreated TPO's (all time points) show that PC1 explained 68,89% of the variation seen between the samples. TPO3 and TPO4 controls had a negative PC1 score, while both TPO2's and TPO0 had positive scores. From the loading profiles, it was observed that TPO4 and TPO3 contains more lactate and less Pcho and myo-inositol than both TPO2's, and especially TPO0 (Figure 4.1.1). The average PC1 score of TPO4, TPO3 and TPO2b (*APC-P53*) is -216,6, -148,8 and 51,4 respectively which is significantly different from mean TPO0 PC1 score of 230,5 ($p \leq 0,05$). Based on visual inspection of spectra and the loading profile of PC1, selected metabolites were quantified. Here, it was found a strong trend of increasing amount of lactate with increasing number of mutations, especially comparing mean TPO0 with mean TPO4 (not significant, P=0,0136) as shown in figure 4.1.2 a). Pcho b), tCCC c) and myo-in d) show the opposite trend of lac with decreasing amounts with increasing number of mutations. The mean of TPO2a (*APC-KRAS*), TPO2b, TPO3 and TPO4 is significantly different both in Pcho and tCCC from the mean of TPO0 ($p \leq 0,05$), while the mean of TPO3 and TPO4 is significantly different from the mean of TPO0 in myo-in ($p \leq 0,05$).

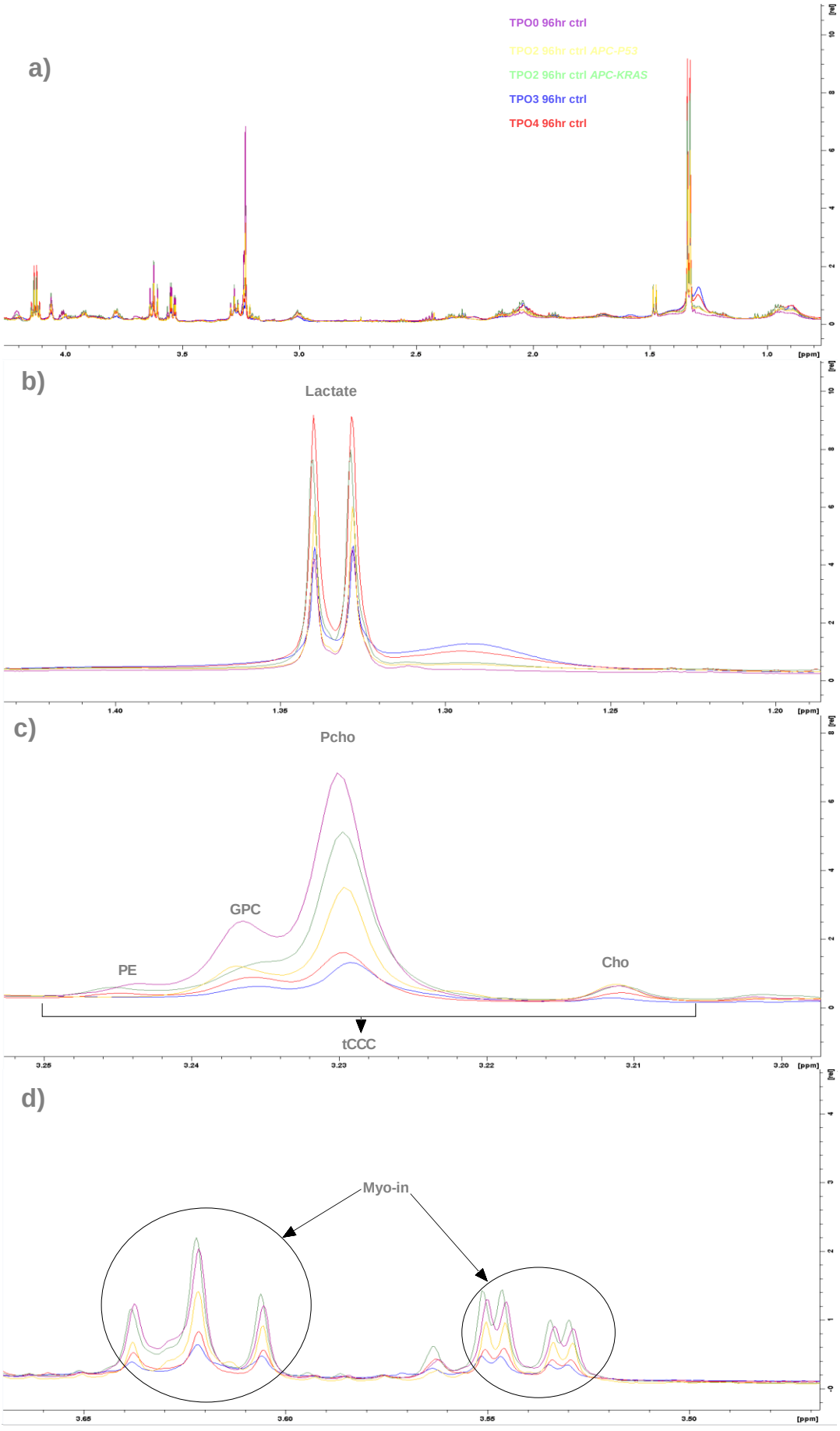
a)
TPO0 96hr ctrl
TPO2 96hr ctrl APC-P53
TPO2 96hr ctrl APC-KRAS
TPO3 96hr ctrl
TPO4 96hr ctrl
b)
Lactate
c)
Pcho
GPC
PE
Cho
tCCC
d)
Myo-in

Figure 4.1.0 Raw spectra of untreated TPO0, TPO2b, TPO2a, TPO3 and TPO4 96hr ctrl indicated with purple, yellow, green, blue and red lines respectively. The metabolic containing regions is shown in a) and metabolites lactate b), Cho; choline, PE; phosphoethanolamine, Pcho; phosphocholine, GPC; glycerophosphocholine, tCCC; total choline containing compounds c) and Myo-in; myo-inositol d) is highlighted.

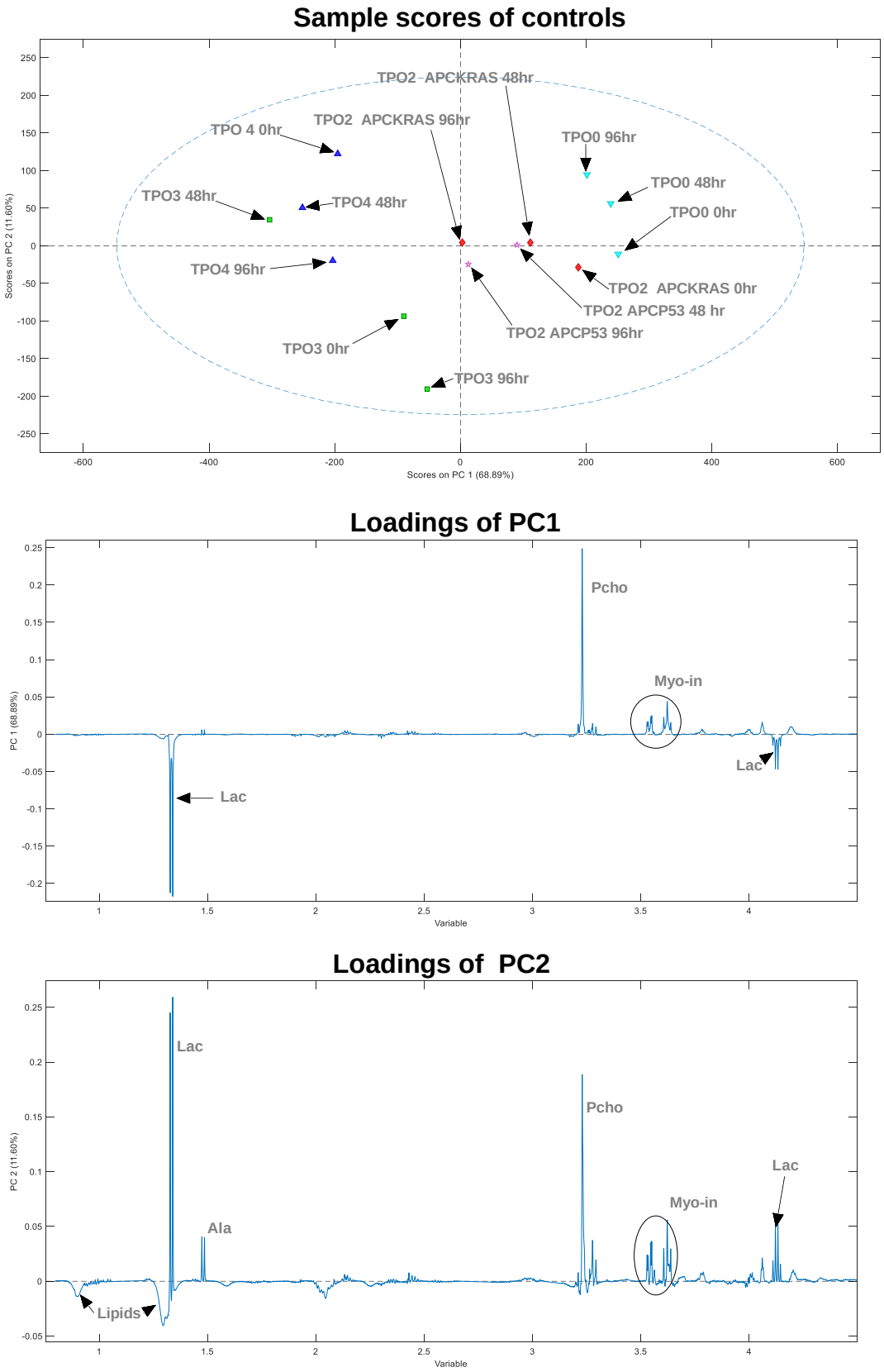

Figure 4.1.1 Principal component analysis (PCA) of untreated organoids with sample scores for PC1 (68,89%) and PC2 (11,60%) and corresponding loading plots for PC1 and PC2.

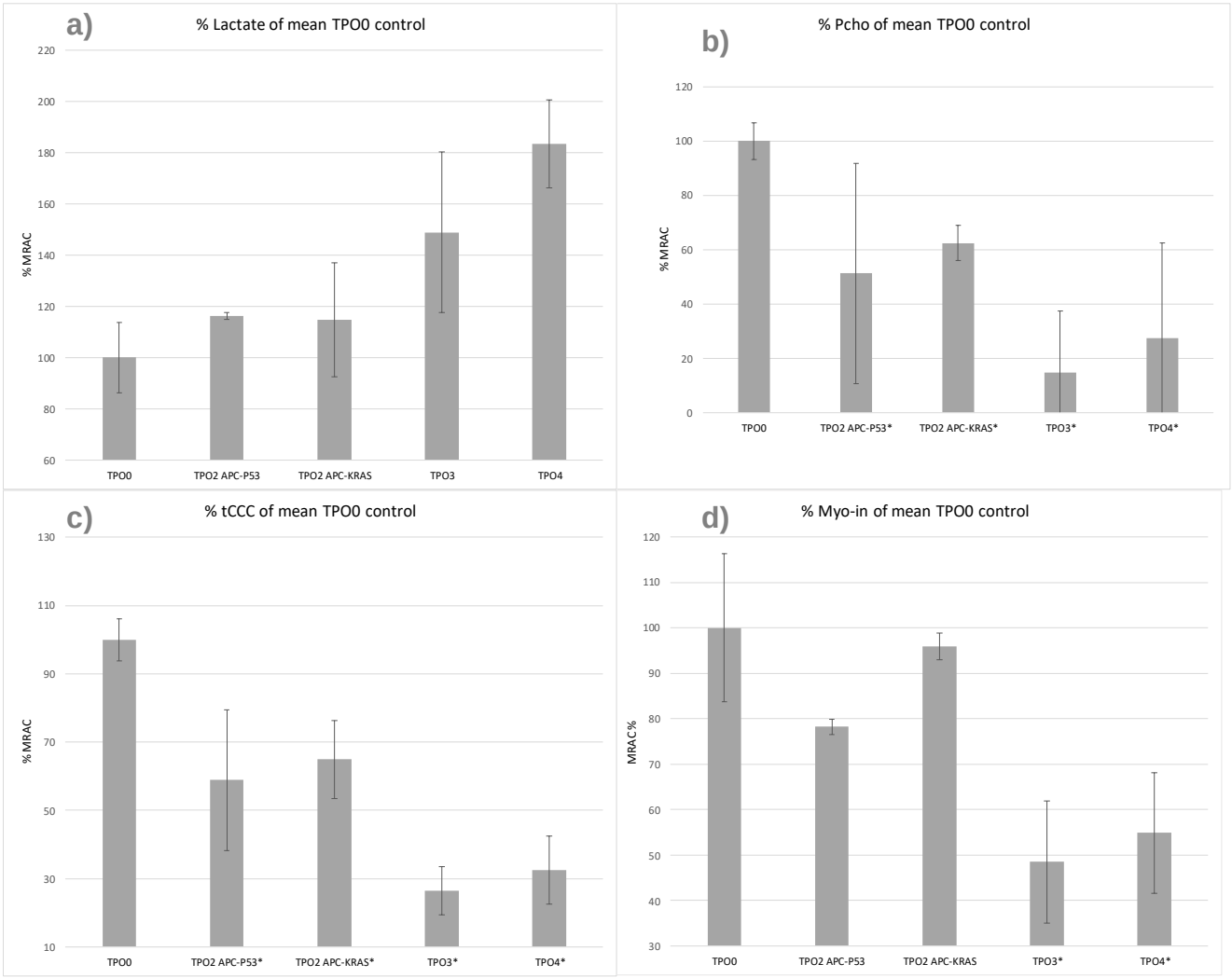

Figure 4.1.2 Content of selected metabolites in untreated organoids. Metabolites levels are presented as area under the curve relative to mean TPO0 (MRAC %). a) lactate, b) phosphocholine, c) percent total choline containing compounds and d) myo inositol. Error bars = standard deviation. * marks significant compared to mean TPO0 ($p \leq 0{,}05$).

4.2 Metabolic response to therapy, TPO0

As shown in figure 4.2.1 the untreated organoids clusters around the score point of 0 in PC1 explaining 55,36% of the variance seen in intracellular metabolites. Untreated organoids divides between a score of 20 and 140 in the PC2 direction accounting for 18,27% of the variation. This indicates that untreated organoids contains approximately the average amount of Pcho, GPC, ala and myo-in compared to the other treated organoids in the PC1 direction. In the PC2 direction, the control samples contains more lac, ala and myo-in where 96hr ctrl contains the most. Both Sn-38 samples show little variance with a low PC1 score indicating less amount of Pcho, GPC and myo-in, and approximately a score difference of 60 in the PC2 direction indicating that 96hr Sn-38 contains less lac and ala. The OxPt treated organoids, 96hr OxPt have a score of approximately 0 in the PC1 direction and 48hr OxPt with a score of around 90 showing the least cluster tendency of the untreated and treated organoids. The 5-FU treated organoids clusters with a high PC1 score and a PC2 score sligthly below 0 indicating high amount of Myo-in GPC and Pcho, and slightly lower lactate levels.

Results from quantification shown in figure 4.2.2 a) indicates that all treatments corresponds with a lower lactate level compared to their respective control for each timepoint. Pcho and tCCC (b) and c)) indicates increasing amount to responding 5-FU treatment, whereas responding Sn-38 treatment indicates lower amount of the same content. Responding OxPt treatment seems not to follow a trend where the 48hr OxPt corresponds to a lower amount of Pcho and tCCC than their respective control, while 96hr OxPt corresponds with a larger amount. Myo-in shown in figure 4.2.1 d) show a slight increase in the 5-FU treated ogranoids and a decrease in 48hr Sn-38 and OxPt treated organoids. Organoids treated with Sn-38 and OxPt at the 96hr timepoint is unchanged and approximately 12% increase in myo-in respectively. The amount of Alanine e) indicates a lower level for all treated organoids except 96hr OxPt which is considered unchanged.

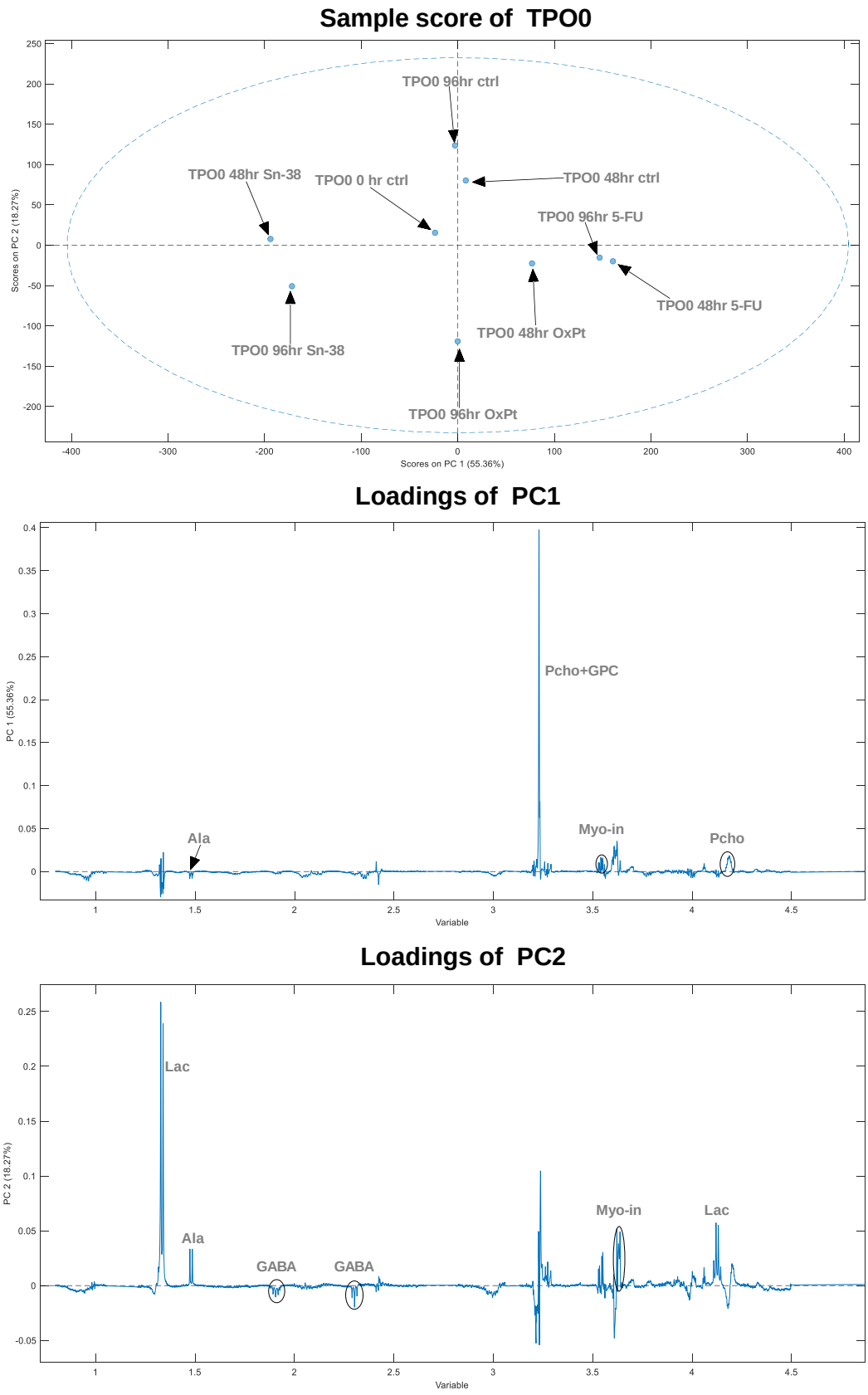

Figure 4.2.1 Principal component analysis (PCA) of all TPO0 wild type samples (excluding TPO0 48hr and 96hr combi). The sample score show PC1 (55,36%) on the x-axis with the corresponding loadings of PC1 and PC2 (18,27%) on the y-axis with the corresponding loadings of PC2.

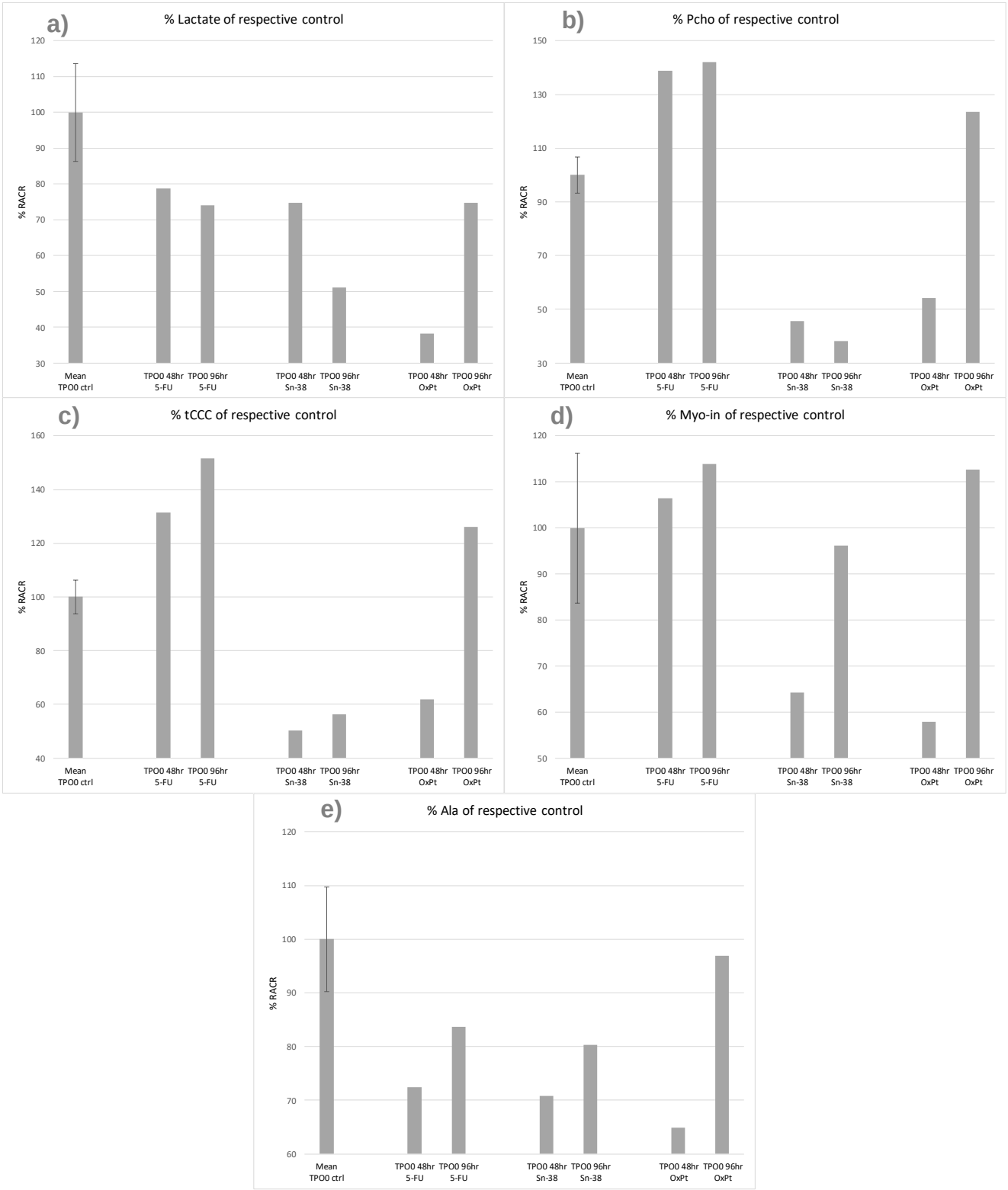

Figure 4.2.2 Metabolite content (relative area under the curve in untreated control) for organoids treated with 5-fluorouracil, oxaliplatin and Sn-38 a) lactate, b) phosphocholine, c) total choline containing compounds, d) myo inositol and e) alanine. Mean TPO0 ctrl includes 0hr, 48hr and 96hr ctrl. Error bars = standard deviation.

4.3 Metabolic response to therapy, TPO2 *APC-P53*

PCA of spectra from treated and untreated TPO2b organoids indicates that PC1 accounts for 70,6% of the observed variance in the metabolic profiles. Untreated organoids score low in PC1 (Figure 4.3.1). The loading profile indicates that untreated organoids contains more lactate and alanine, and less Pcho compared to treated organoids. The PC2 score (12,37% of total variance) indicates that untreated organoids (PC2 score around 30) contain less lipids and more lac, ala, Pcho and GPC. TPO2b was defined as non-responsive to Sn-38. Organoids treated with Sn-38 display relatively similar PC1 score. Interestingly, spectra from Sn-38 treated samples cluster closest to untreated controls on the PC1 axis. The non-responding OxPt treated organoids have a positive PC1 score indicating less lactate and alanine, and more Pcho compared to untreated organoids.

Quantification of metabolites contributing to the PC1 loading profile (figure 4.3.2) indicates that lactate a) decreases for all treatments at all timepoints for both responders and non-responders. The non-responding Sn-38 treatment does not seem to decrease as much as the responding treatments 5-FU and combi, however the non-responding OxPt treated organoids decreases more than responding combi treatment. Pcho b) and tCCC c) indicates increasing levels for 5-FU and combination treated organoids (responders), but also Sn-38 and OxPt treated organoids (non-responders). Combination treated organoids (96hr) and 5-FU treated organoids (96hr) have the largest increase of Pcho and tCCC. The amount of myo-in d) seems to increase across all treatments independent of responders and non-responders except for 48hr OxPt. The amount of ala e) indicates a lower amount for all treatments at all timepoints. The level of ala is lower for the 96hr timepoint for the responding organoids treated with 5-FU and Combi than non-responding organoids treated with Sn-38 and OxPt.

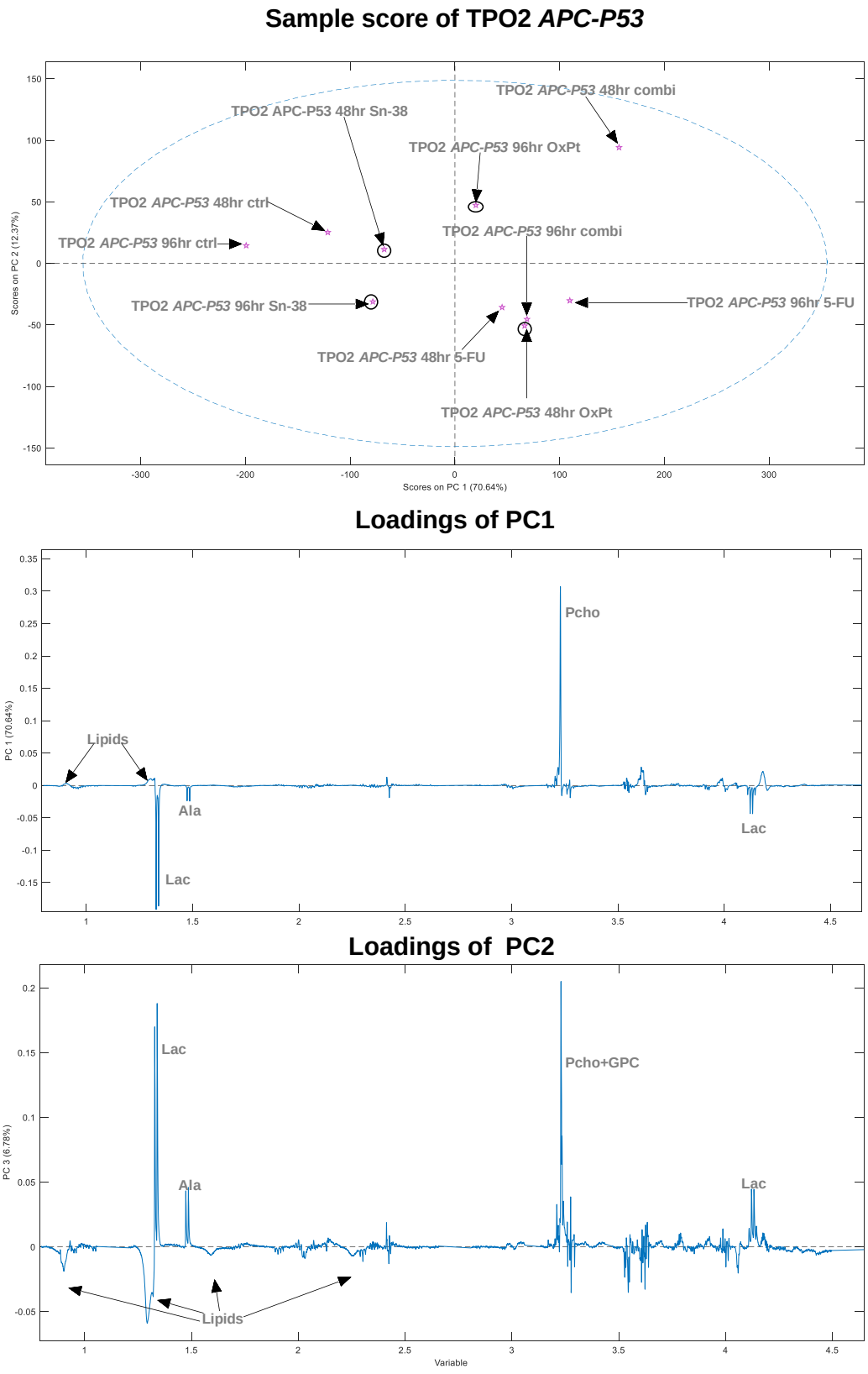

Figure 4.3.1 Principal component analysis (PCA) of all TPO2 *APCP53* samples (excluding 0hr ctrl). The sample score show PC1 (70,64%) on the x-axis with the corresponding loadings of PC1 and PC2 (12,37%) on the y-axis with the corresponding loadings of PC2. Circle in the sample score indicates non-responding samples to treatment.

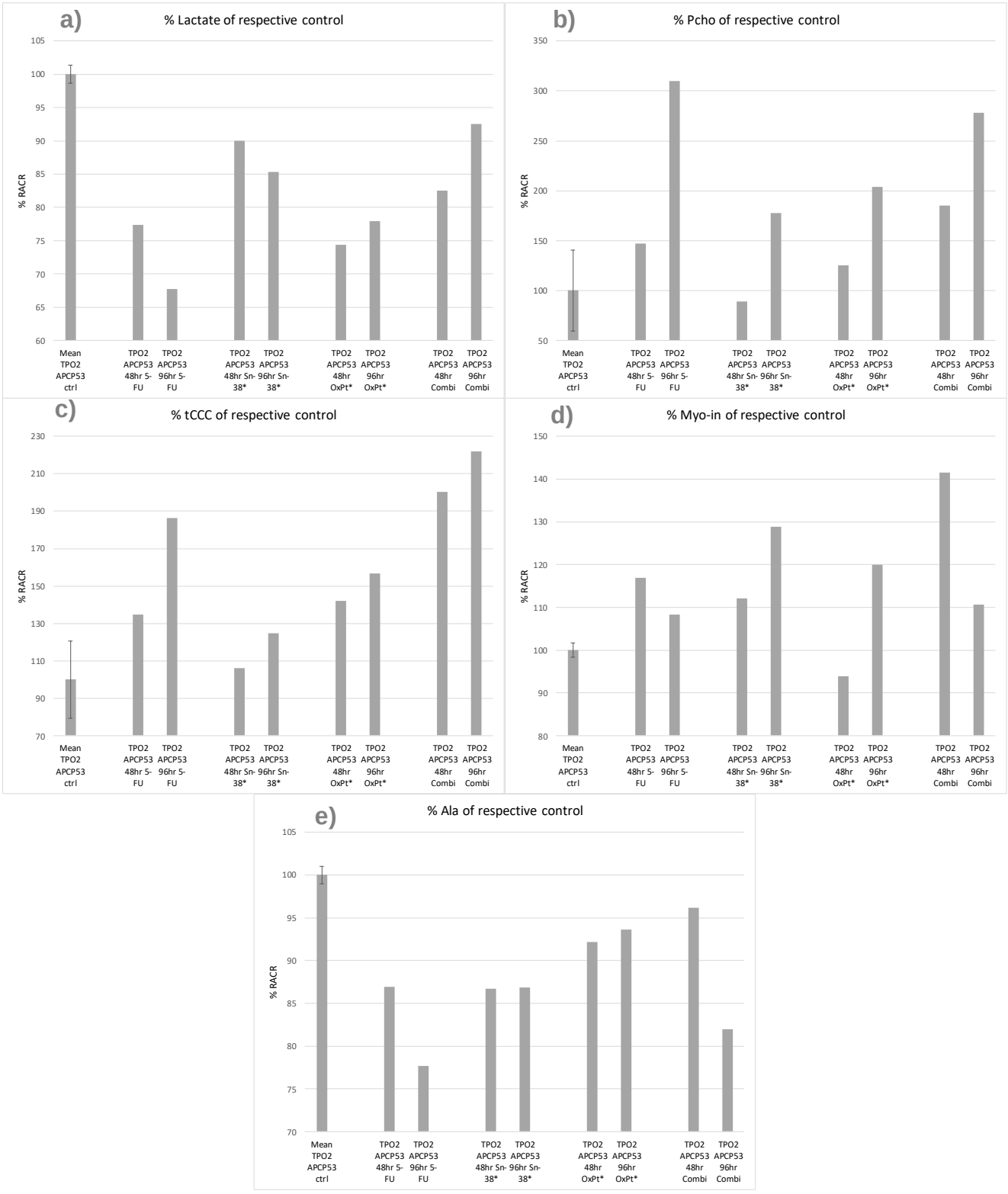

Figure 4.3.2 Metabolite content (relative area under the curve in untreated control) for organoids treated with 5-fluorouracil, oxaliplatin and Sn-38 a) lactate, b) phosphocholine, c) total choline containing compounds, d) myo inositol and e) alanine. Mean TPO2b ctrl includes 48hr and 96hr ctrl. Error bars = standard deviation. * marks organoids that are non-responding to treatments.

4.4 Metabolic response to therapy, TPO2 *APC-KRAS*

The untreated organoids score low in PC1 and PC2 with score intervalls of -20 to -130 and 50 to 120 respectviely (figure 4.4.1). The low PC1 score indicates from loadings that the untreated organoids contains more lac and ala, and less Pcho compared to the treated organoids that has a higher PC1 score (49,41% of the variance). The PC2 score (35,64% of the variance) indicates that the untreated organoids contains more lac, ala, pcho and myo compared to the lipid levels of all treated organoids. Sn-38 treated organoids with a negative PC1 score, indicates high lactate levels and low Pcho and their center around the PC2 axis indicates average levels of lac, ala, pcho and myo-in compared to lipid levels. The 48hr combi treated organoid with a score of -100 on PC1 and -230 on the PC2, indicates large amounts of lipids compared to other metabolites in the PC2 direction. Both 5-FU treated organoids have a positive PC1 score and a negative PC2 score indicating large amount of Pcho compared to lactate and an increase in lipid levels. Both OxPt treated organoids are close in proximity in PC1 score of approximately 170 and PC2 score of around 20. The high PC1 score corresponds to an increase in Pcho and a decrease in lactate and ala.

Quantification of selected metabolites show an overall decrease of lactate across all treatments except for 48hr Sn-38 treated organoid (figure 4.4.2), where the largest decrease is observed at the 96hr timepoint for all treatments. Pcho b) and tCCC c) levels increase with treatments of 5-FU and OxPt, however this observation is stronger with Pcho than tCCC for OxPt treated organoid at 48hr. Pcho and tCCC seems to decrease in organoids treated with Sn-38. Myo-in d) trends towards an overall decrease ranging from 93% to 72%, except 96hr Sn-38 treated organoid with an increase of 108%. All treatments at all timepoints show a decrease of ala e).

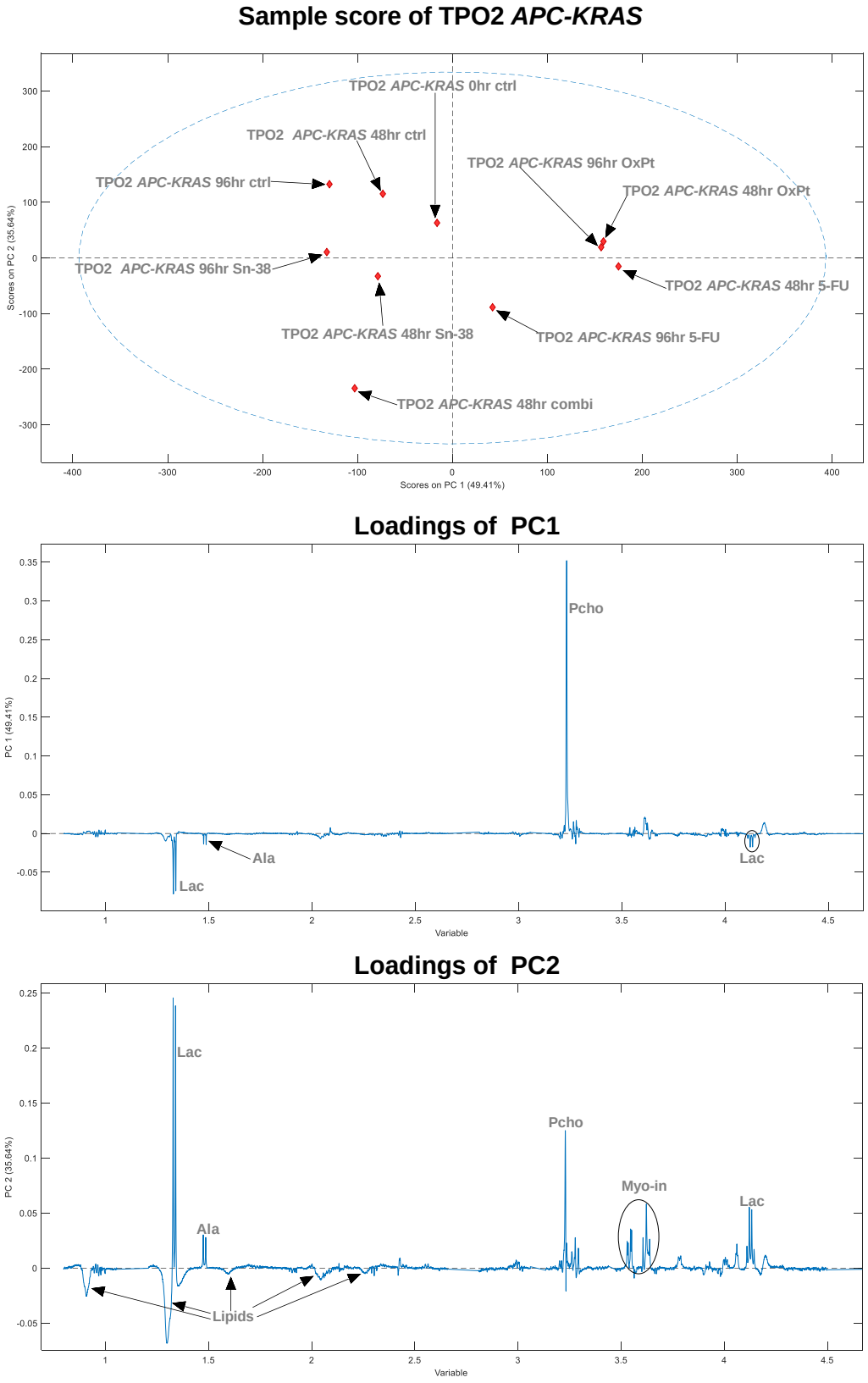

Figure 4.4.1 Principal component analysis (PCA) of TPO2 *APCKRAS* samples (excluding 96hr combi). The sample score show PC1 (49,41%) on the x-axis with the corresponding loadings of PC1 and PC2 (35,64%) on the y-axis with the corresponding loadings of PC2.

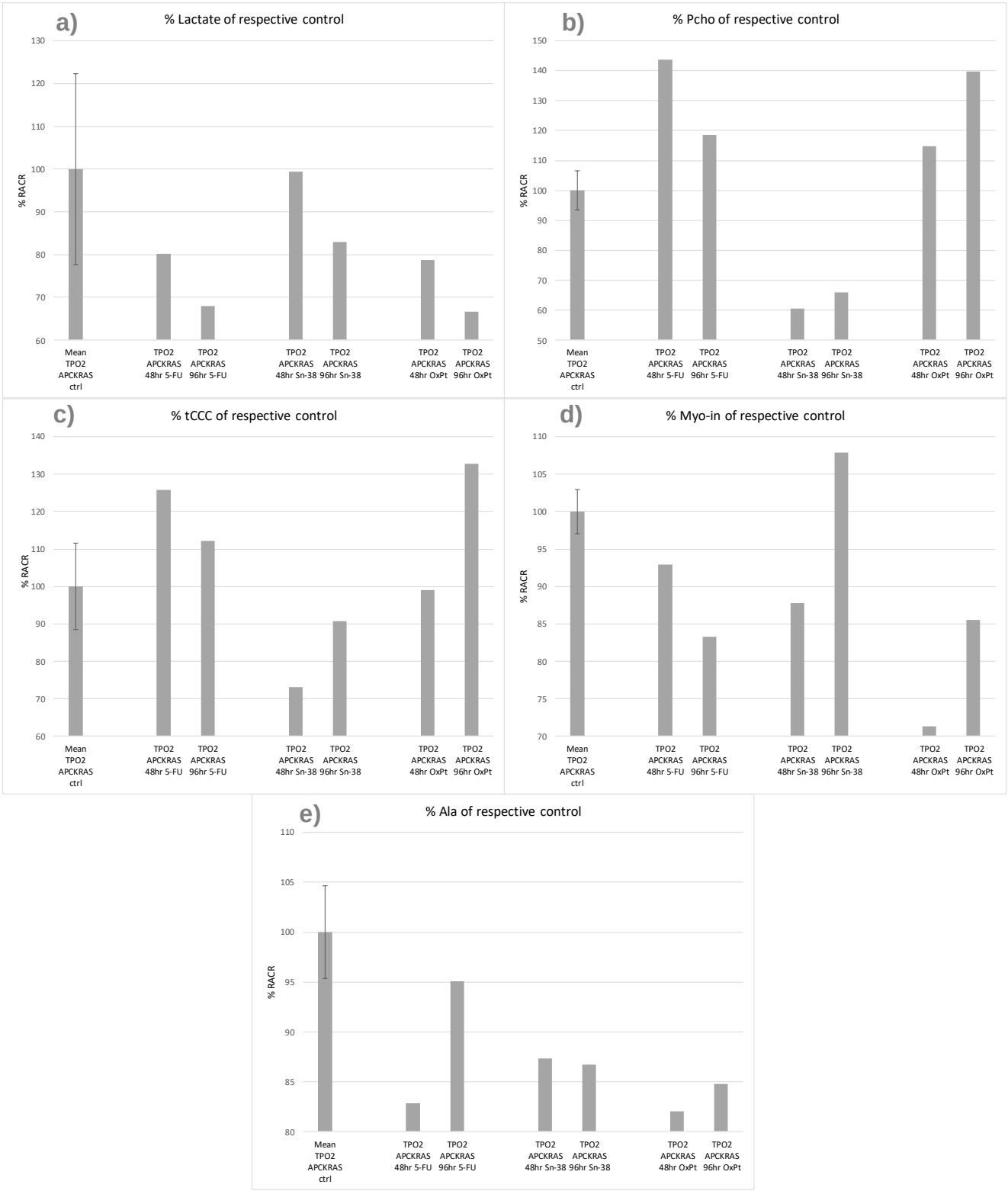

Figure 4.4.2 Metabolite content (relative area under the curve in untreated control) for organoids treated with 5-fluorouracil, oxaliplatin and Sn-38 a) lactate, b) phosphocholine, c) total choline containing compounds, d) myo inositol and e) alanine. Mean TPO2 *APCKRAS* ctrl includes 0hr, 48hr and 96hr ctrl. Error bars = standard deviation.

4.5 Metabolic response to therapy, TPO3 *APC-KRAS-P53*

The untreated organoids seems to have a wider spread in the PC1 (79,01% of the variance) and PC2 (12,09% of the variance) direction in regards to 48hr ctrl. 0hr and 96hr ctrl organoids with a variance in PC1 score of approximately 150, and clusters at the same score in PC2 direction. The 48hr ctrl organoid sample score is approximately 180 above 0hr ctrl in both PC1 and PC2 direction. From the loadings, this indicates that untreated organoids especially 48hr ctrl contains more lac, Pcho, GPC and myo-in compared to lipids in the PC1 directions. 0hr and 96hr untreated organoids contains

average amount of lipids, lac, GPC, Pcho and myo-in compared to the rest of the organoids in the PC2 direction, where 48hr ctrl indicates lager amount of lipids and lac. The OxPt treated organoids have a score spread of approximately 200 in the PC1 direction. This indicates less lactate, Pcho and GPC levels and more lipids for 96hr OxPt compared to 48hr OxPt treated organoids. The 5-FU treated organoids have a score spread of approximately 280, where 96hr 5-FU is associated with a lower PC1 score and show lower metabolic content compared to lipid levels. Combi and Sn-38 treated organoids show a negative score in PC1 where the amount of lipids is large compared to the amount of metabolic content. This trend is stronger for both 96hr combi and Sn-38 treated organoids.

Quantification of TPO3 indicates that lactate a) seems to decrease across all treated organoids except for 96hr Sn-38 where an increase of 120% is observed (figure 4.5.2). Pcho b) and tCCC) increases across all treatments except for 48hr Sn-38 which is approximately the same as 48hr control. However, at the 96hr timepoint a decrease is observed. 48hr OxPt treated organoid contains an extreme value of Pcho with an increase of 638%. An increase of myo-in d) at timepoint 48hr for 5-FU, OxPt and Combi treated organoids is observed. However, at timepoint 96hr, a decrease is observed for all treatments ranging from 88% to 68%. The amount of ala e) decreases at the 48hr timepoint for 5-FU treatd organoid and is approximately the same at timepoint 96hr. Sn-38 treatment is observed to give an overall decrease with the largest offset at 96hr. OxPt treated organoids indicates a slight increase in ala, where combi treated organoids are unchanged.

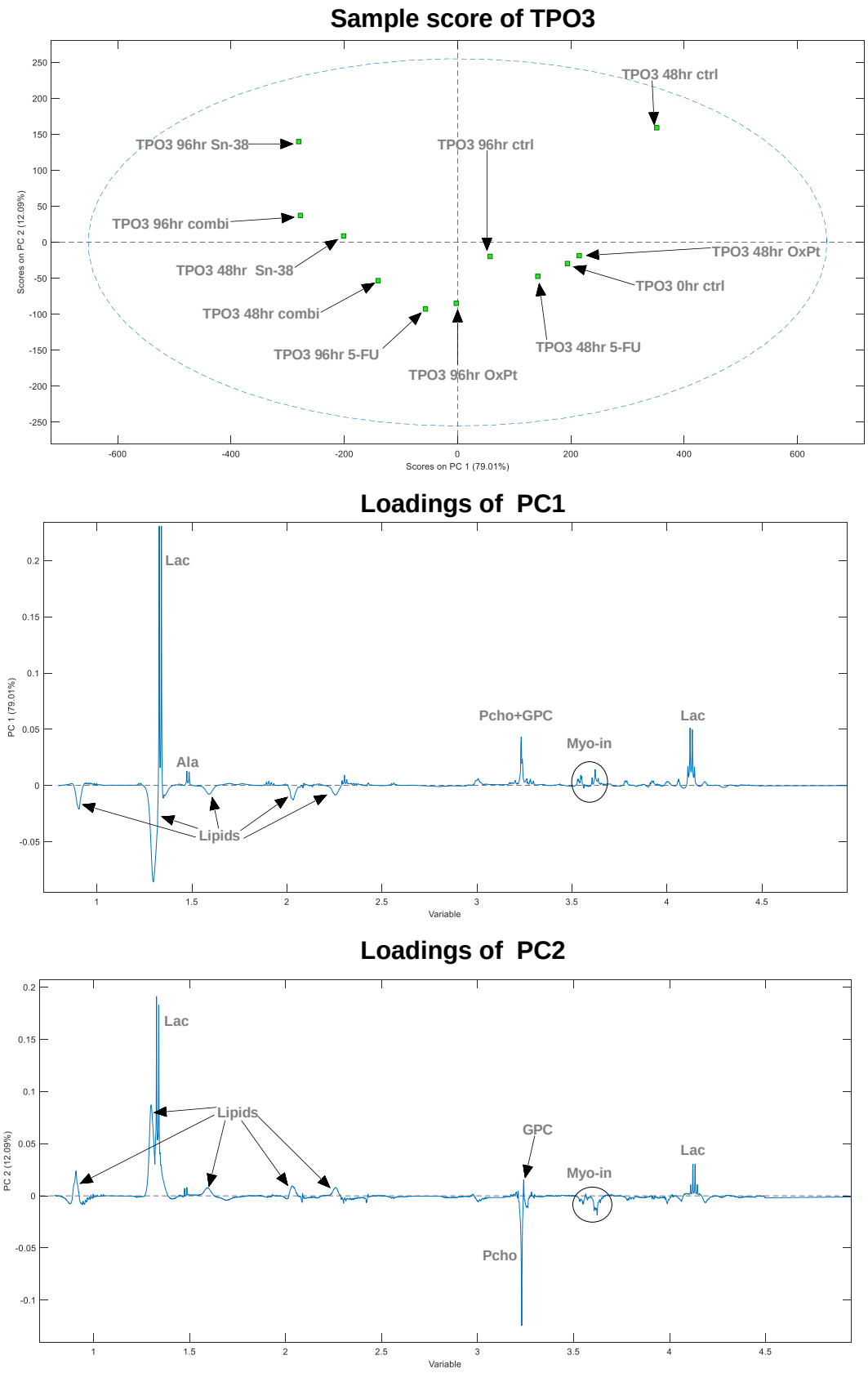

Figure 4.5.1 PCA of TPO3 *APC-KRAS-P53* samples.
The sample score show PC1 (79,01%) on the x-axis with the corresponding loadings of PC1, and PC2 (12,09%) on the y-axis with the corresponding loadings of PC2.

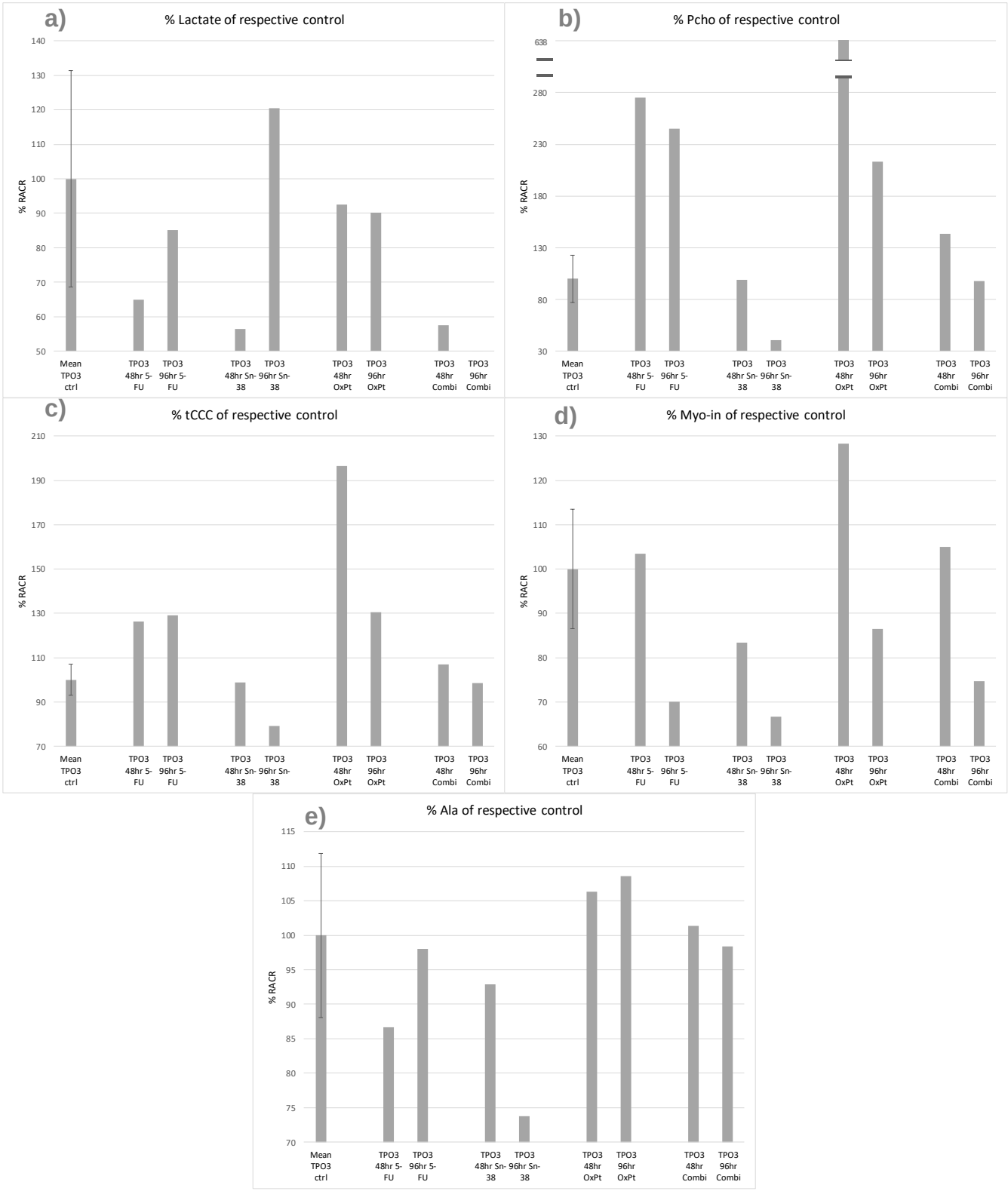

Figure 4.5.2 Metabolite content (relative area under the curve in untreated control) for organoids treated with 5-fluorouracil, oxaliplatin and Sn-38 a) lactate, b) phosphocholine, c) total choline containing compounds, d) myo inositol and e) alanine. Mean TPO3 ctrl includes 0hr, 48hr and 96hr ctrl. Error bars = standard deviation.

4.6 Metabolic response to therapy, TPO4 *APC-KRAS-P53-SMAD4*

The spread of untreated organoids in the sample score ranges from 20 to 100 in PC1 (74,32% of variance) indicating high levels of lac, ala, GPC and Myo-in from the loadings (figure 4.6.1). The tendency for TPO4 sample score is that the 48hr timepoints for each treated organoids is correlated with a positive PC1 score except for 48hr combi, and at the 96hr timepoint, a negative PC1 score is observed. This tendency is also observed for the 96hr OxPt treated organoid (non-responding). Howevr, the negative score of 96hr OxPt treated organoid is higher than the other treated organoids at the 96hr timepoint. This observation indicates a decrease of lactate and an increase of lipids from 48hr to 96hr timepoint for the treated organoids. 96hr combi treated organoid show the lowest score of -200, followed by 96hr Sn-38 and 96hr 5-FU with a score of -180 and -170 respectively.

Quantification of metabolites contributing to the PC1 loading profile (figure 4.6.2) indicates that lac a) decreases for all treated organoids, however this tendency is not as strong for OxPt treated organoids at both timepoints (non-responders). The amount of Pcho b) and tCCC c) indicates an increase for 5-FU, OxPt and combi treated organoids, while a decrease is observed for the Sn-38 treated organoids. Myo-in d) is unchanged or higher at the 48hr timepoint for the treatments 5-FU, Sn-38 and OxPt where a decrease is observed at the 96hr timepoint for the same treatments. However, the opposite is observed for the combi treated organoids. Ala e) indicates unchanged amounts for both timepoints for OxPt (non-responders), 96hr 5-FU and 96hr combi-treated organoids. A decrease is observed for both timepoints for Sn-38, 48hr 5-FU, both timepoints for Sn-38 and 48hr combi-treated organoids.

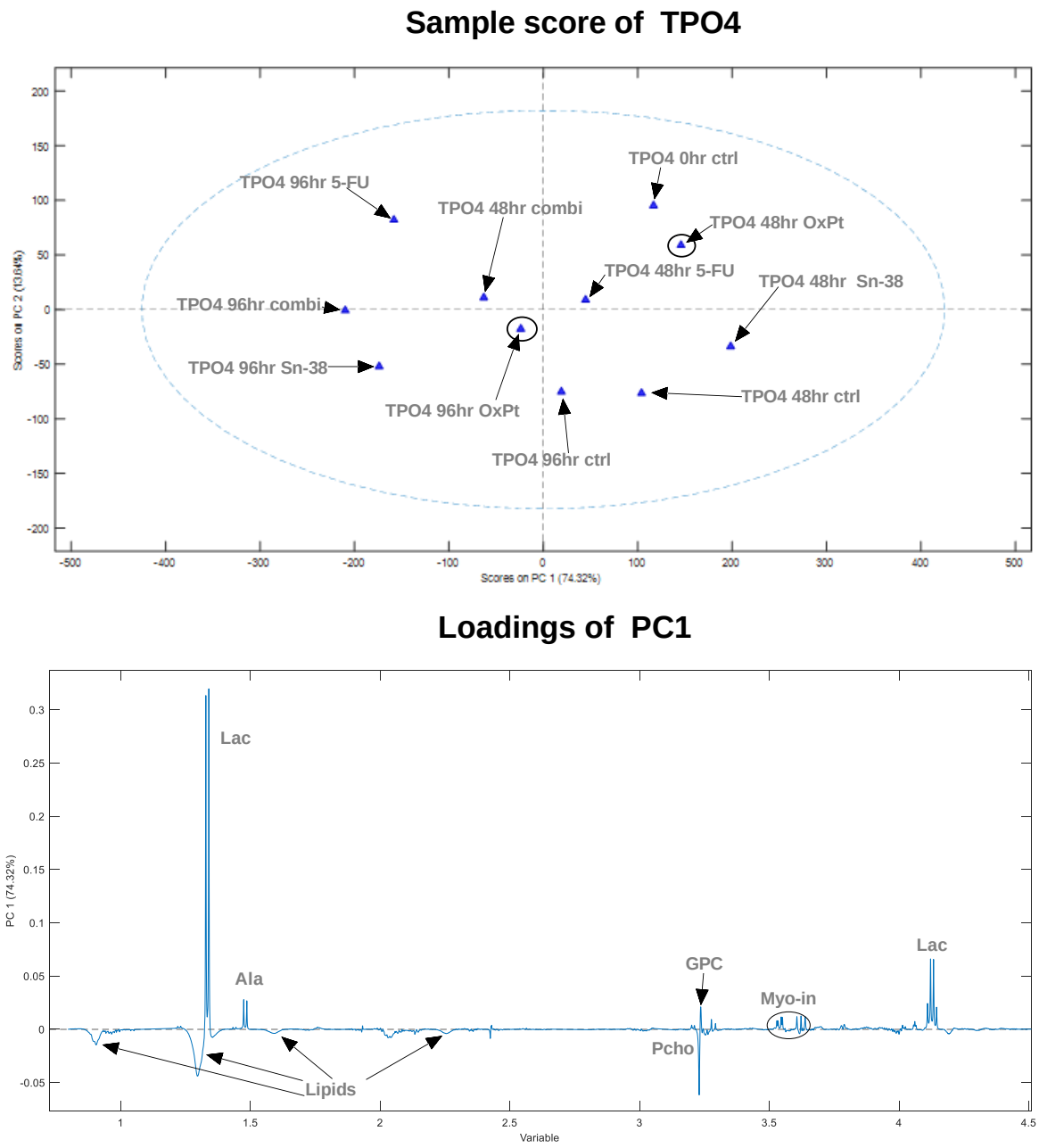

Figure 4.6.1 PCA of TPO4 *APC-KRAS-P53-SMAD4* samples.
The sample score show PC1 (74,32%) on the x-axis with the corresponding loadings of PC1. Circle in the sample score indicates non-responding organoids.

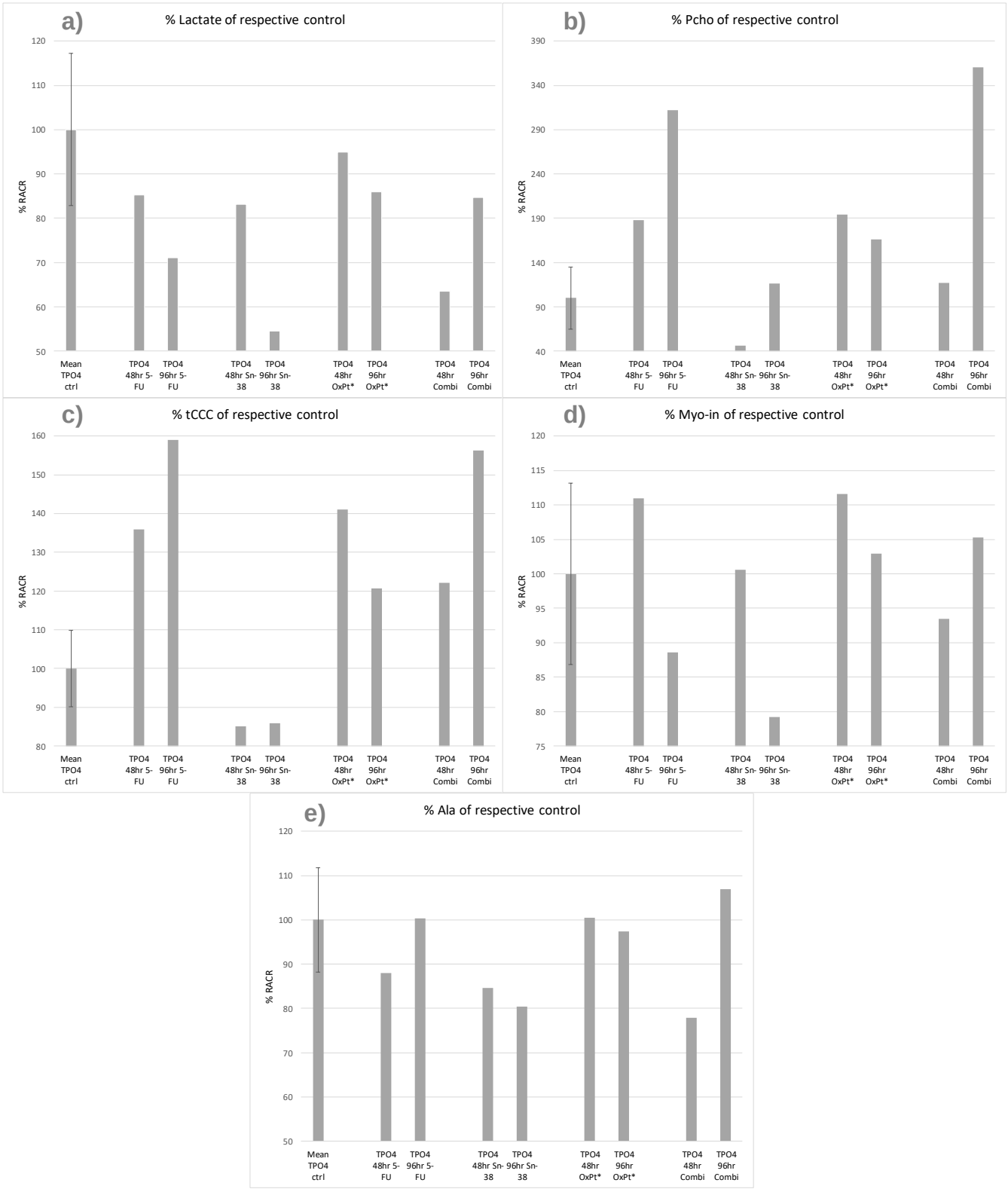

Figure 4.6.2 Metabolite content (relative area under the curve in untreated control) for organoids treated with 5-fluorouracil, oxaliplatin and Sn-38 a) lactate, b) phosphocholine, c) total choline containing compounds, d) myo inositol and e) alanine. Mean TPO4 ctrl includes 0hr, 48hr and 96hr ctrl. Error bars = standard deviation. * marks organoids that are non-responding to treatment.

4.7 Evaluation of metabolites as biomarkers for response to chemotherapy

All organoids treated with 5-FU showed response. It was observed that lactate (figure 4.7.0 a) decreases for all TPO's, while the amount of Pcho b) and tCCC c) increases from a minimum of 118% to a maximum of 310% and mimimum of 112% to a maximum of 186% respectively. Alanine d) decreases in TPO0, TPO2b and TPO2a. This trend is also displayed by TPO3 and TPO4 at the 48hr timepoint, but at 96hr timepoint alanine levels are unchanged for TPO3 and TPO4.

Organoids treated with Sn-38, lactate (figure 4.7.1 a) decreases except for TPO2a 48hr and TPO3 96hr with unchanged and increased amount respectively (responders). TPO2b also displayed a reduction in lactate (non-responsive). Pcho b) indicates a decrease in response to Sn-38 treatment for all organoids except for TPO2b (non-responsive) which is unchanged or higher. tCCC c) show a decrease for all responding TPO's except for TPO3 48hr (responder). The non-responding TPO2b show unchanged or increased amount of tCCC at both timepoints. Myo-in d) TPO2b treated organoids displayed an increase of 110% and 130% for 48hr and 96hr respectively (non-responsive). The rest of the Sn-38 treated responding TPO's show a decrease at either the 48hr or 96hr timepoint or both. Ala d) decreases for all TPO's when treated with Sn-38 treatment including TPO2b (non-responsive).

OxPt treatment decreases lac (figure 4.7.2 a) where this effect is less substantial for TPO3 at both timepoints (responders). TPO2b indicates a decrease at approximately 78% at both timepoints (non-responding). TPO4 OxPt treated organoids is observed to have a decrease of lactate at 95% and 87% for 48hr and 96hr respectively (non-responding). tCCC b) indicates an increase across all organoids except for TPO0 48hr. This observation includes both timepoints for the treated organoids TPO2b and TPO4 (non-responders). For myo-in c) the responsive samples TPO0, TPO2a and TPO3 indicates a decrease either at one or both timepoints. TPO2b and TPO4 treated organoids at both timepoints is relatively unchanged or increased (non-responders).

All organoids treated with combinational treatment are responders. A decreasing amount of lac a) were observed for all treated TPO's (figure 4.7.3). Pcho b) and tCCC c) increases where TPO4 96hr have the largest increase of Pcho of 360%. TPO2b show the largest increase in tCCC of 200% and 220% for the timepoints 48hr and 96hr respectively. The combi treated TPO3 at the 48hr timepoint show an increase of 143% and 106% for Pcho and tCCC respectively, while it is relatively unchanged at the 96hr timepoint. Difference in lipids is observed in the raw combinational spectra (figure 4.7.4) and from the PCA scores (figure 4.3.1, 4.5.1 and 4.6.1) especially at the 96hr timepoint.

All organoids treated with 5-FU and Combi were responsive to treatment. In Sn-38 treated organoids, TPO2b were non-responsive and Pcho, tCCC and myo-in discirminated responders from non-responders. In OxPt treated organoids, TPO2b and TPO4 were non-responders. Myo-in levels discriminated non-responders from responders for TPO2b and TPO4, while less decreasing lactate levels in TPO4 were observed compared to the responsive organoids.

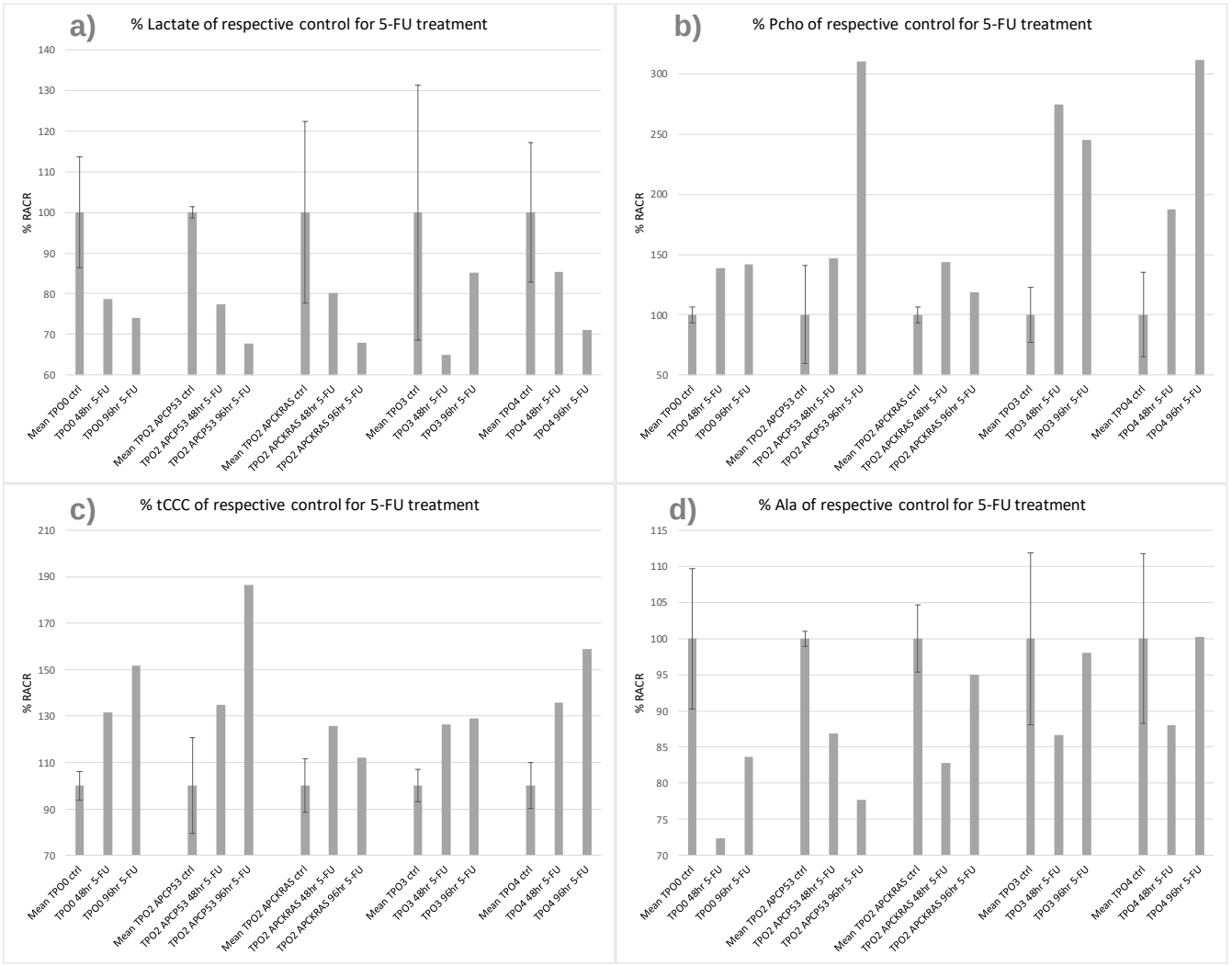

Figure 4.7.0 Metabolite content (relative area under the curve in untreated control) for organoids treated with 5-fluorouracil a) lactate, b) phosphocholine, c) total choline containing compounds and d) alanine. Mean TPO ctrl includes 0hr, 48hr and 96hr ctrl (0hr ctrl excluded for TPO2 *APC-P53*). Error bars = standard deviation.

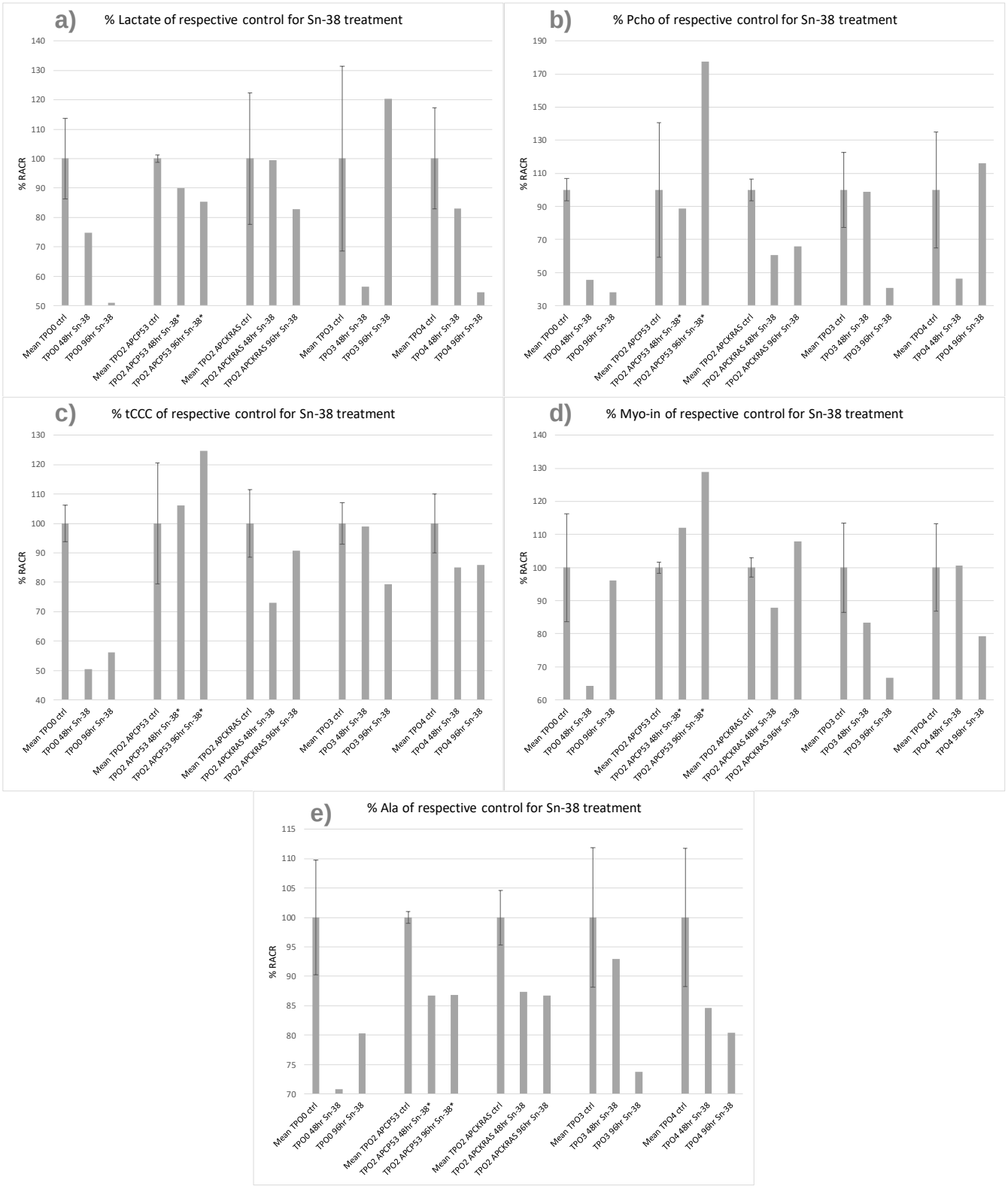

Figure 4.7.1 Metabolite content (relative area under the curve in untreated control) for organoids treated with Sn-38 a) lactate, b) phosphocholine, c) total choline containing compounds, d) myo inositol and e) alanine. Mean TPO ctrl includes 0hr, 48hr and 96hr ctrl (0hr ctrl excluded for TPO2 *APC-P53*).* marks organoids that are non-responding to treatment. Error bars = standard deviation.

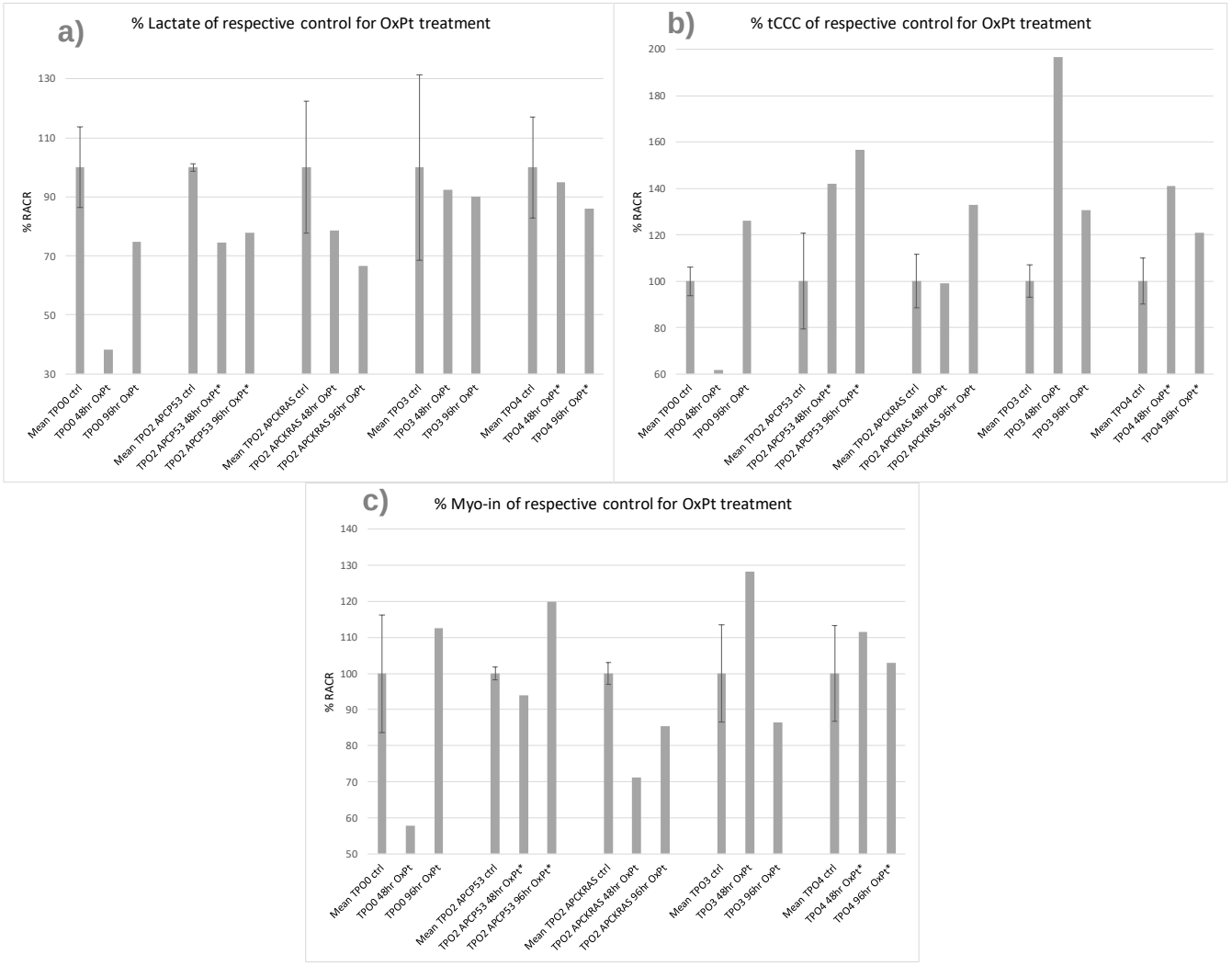

Figure 4.7.2 Metabolite content (relative area under the curve in untreated control) for organoids treated with oxaliplatin a) lactate, b) total choline containing compounds and c) myo inositol. Mean TPO ctrl includes 0hr, 48hr and 96hr ctrl (0hr ctrl excluded for TPO2 *APC-P53*).* marks organoids that are non-responding to treatment. Error bars = standard deviation.

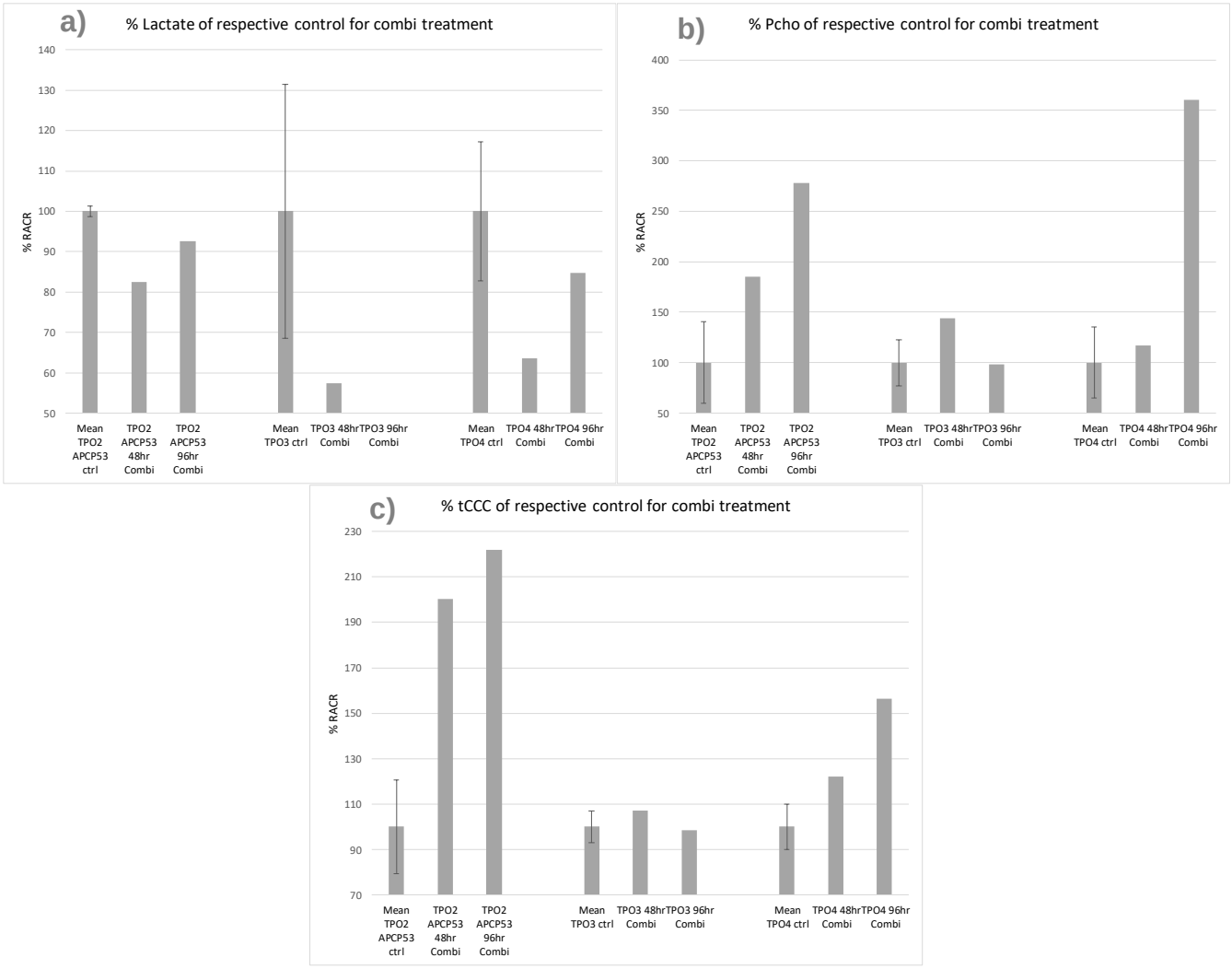

Figure 4.7.3 Metabolite content (relative area under the curve in untreated control) for organoids treated with combinational therapy a) lactate, b) phosphocholine and c) total choline containing compounds. Mean TPO ctrl includes 0hr, 48hr and 96hr ctrl (0hr ctrl excluded for TPO2 *APC-P53*). Error bars = standard deviation.

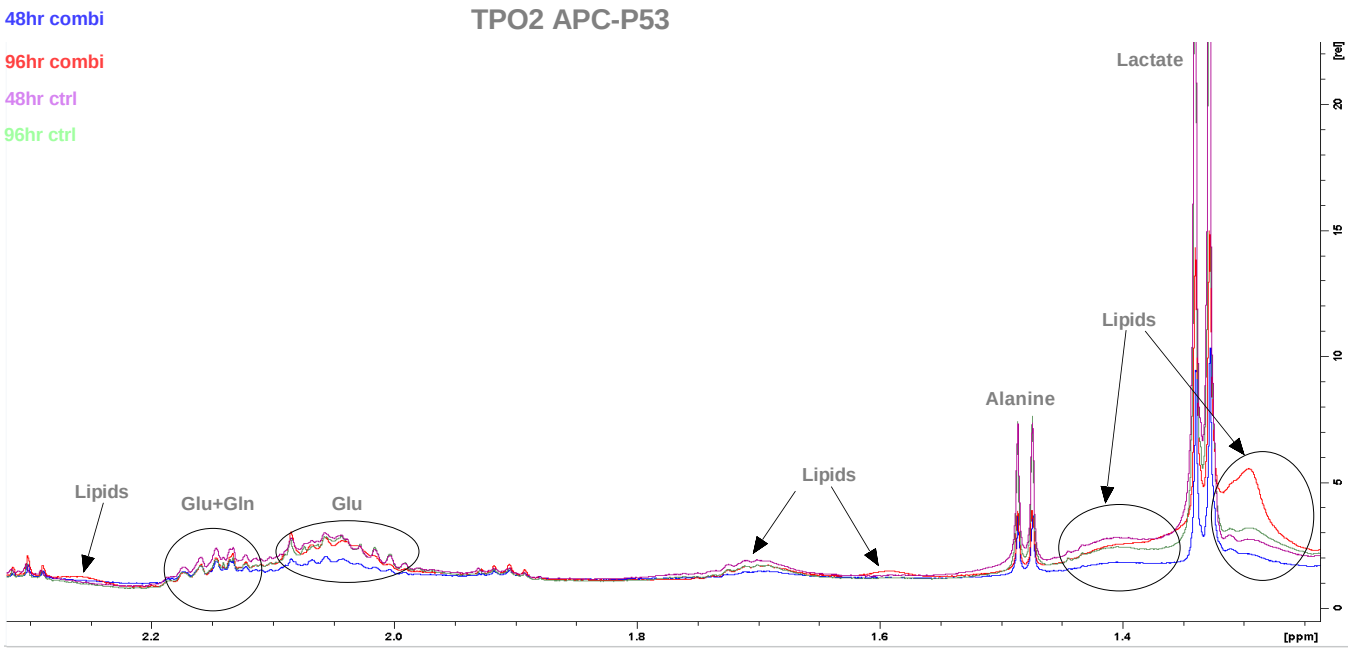
TPO2 APC-P53
48hr combi
96hr combi
48hr ctrl
96hr ctrl
Lactate
Lipids
Alanine
Lipids
Lipids
Glu+Gln
Glu
2.2
2.0
1.8
1.6
1.4
[ppm]
[rel]

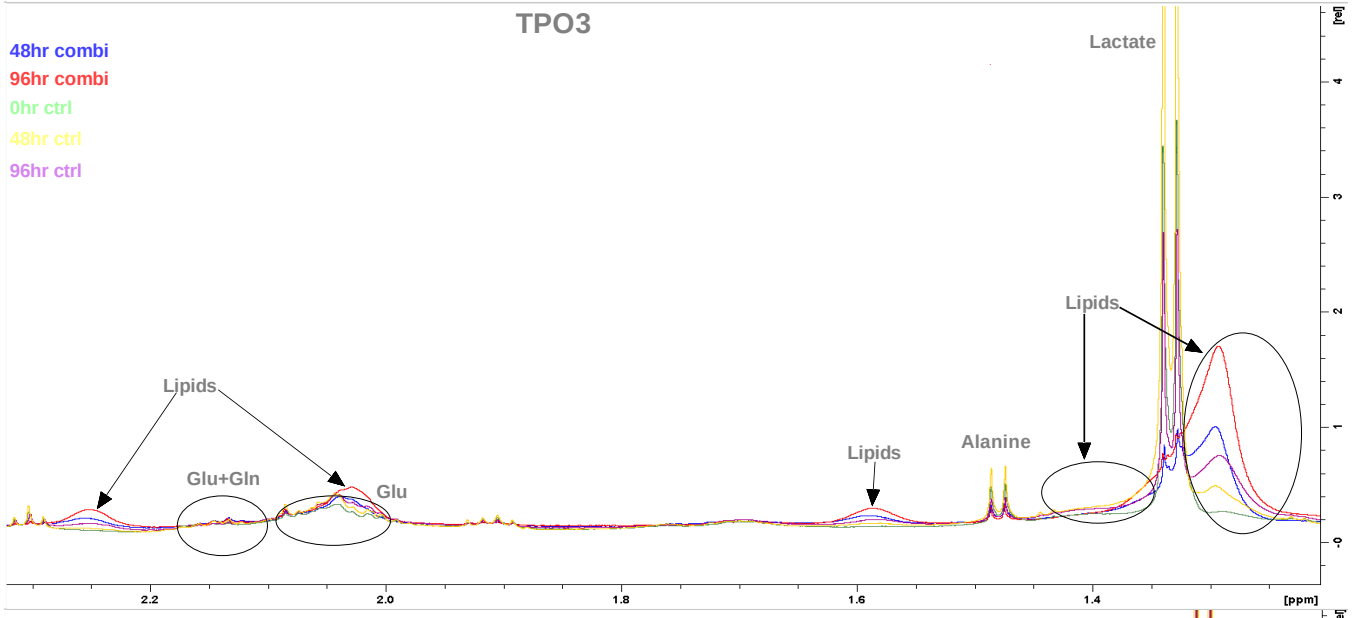
TPO3
48hr combi
96hr combi
0hr ctrl
48hr ctrl
96hr ctrl
Lactate
Lipids
Lipids
Alanine
Lipids
Glu+Gln
Glu
2.2
2.0
1.8
1.6
1.4
[ppm]
[rel]

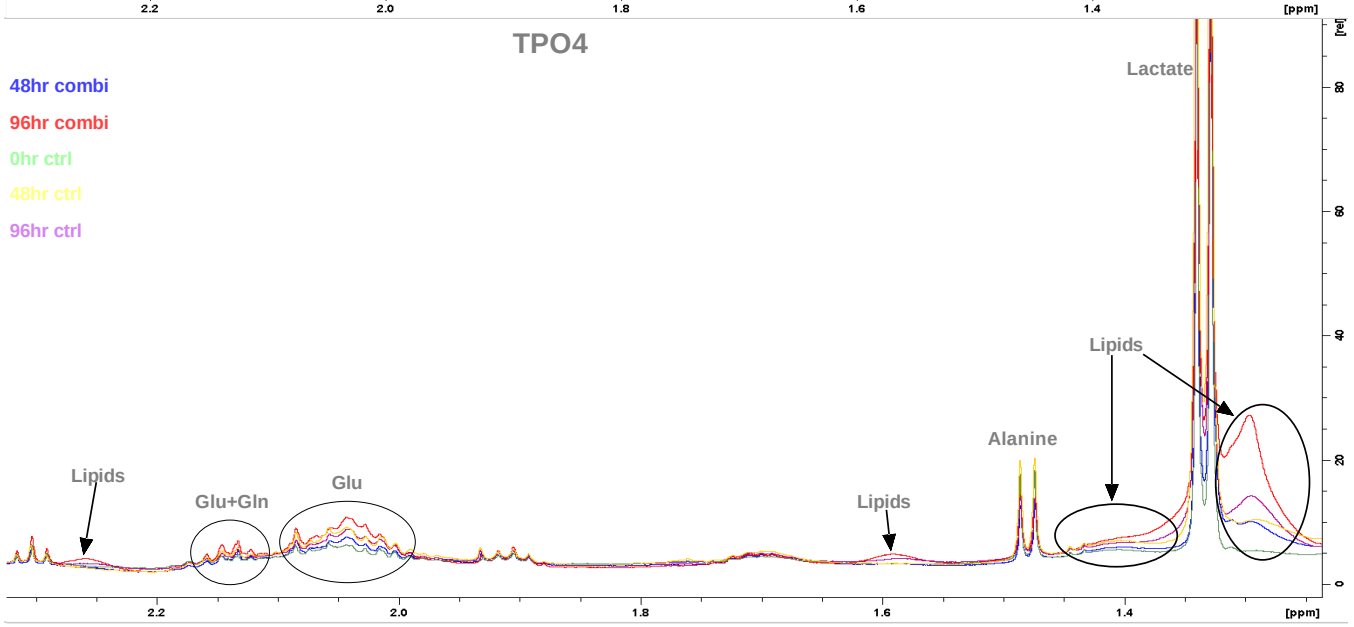
TPO4
48hr combi
96hr combi
0hr ctrl
48hr ctrl
96hr ctrl
Lactate
Lipids
Alanine
Lipids
Lipids
Glu+Gln
Glu
2.2
2.0
1.8
1.6
1.4
[ppm]
[rel]

Figure 4.7.4 Raw untreated and combinational treated organoids spectra of TPO2b, TPO3, and TPO4. Glu; glutamate, Gln; glutamine.

5.0 Discussion

The relationship between a cancer cells genetic background, its phenotype and its metabolic profile is poorly understood. In this study we used human colorectal tumor progression organoids with the four most common accumulating mutations *APC*, *KRAS*, *P53* and *SMAD4* using CRISPR/CAS9. We have obtained TPO's at timepoint 48hr and 96hr after treatment of oxaliplatin, 5-fluorouracil and the active metabolite of irinotecan Sn-38 and a combination of these. We have also obtained untreated control organoids at timepoint 0hr, 48hr and 96hr to evaluate the metabolic profile of tumor progression and metabolic response to chemotherapy using high resolution magic angle spinning nuclear magnetic ressonance spectroscopy. We have also quantified other metabolites including glutamine and glutamate, and calculated Pcho/GPC ratio with no apparent trends observed (results not shown).

5.1 Metabolic profiling of untreated tumor progression organoids

The tumor progression organoid model system is highly suitable for studies of how the metabolic profile is associated with genetic mutations. As the number of mutations increase, it is expected that organoids to an increasing degree acquire a cancer-like metabolic phenotype. From existing litterature, it would be expected that the most malignant organoid, TPO4, would display typical metabolic cancer traits such as increased lac, Pcho and choline and a decrease of myo-in as previously described by tissue samples from CRC patients (68, 69). However, the general direction of GPC is unclear with opposite findings. It has been reported that lac, Pcho and GPC is increased, while myo-in is decreased in all stages of human rectal cancer compared to normal rectal tissue. The amount of Myo-in, Pcho, GPC and lac were however unable to discriminate between the different stages of rectal cancer (68). A CRC lung metastatic xenograft model in mice reported increased Pcho, choline and lac levels (70). The CRC cell lines COLO 205, HCT 116, HT-29 and SW 620 xenografts has previously shown slight variation in metabolic profiles where GPC differ the most compared to human CRC tissue biopsies (71). It has previously been established increased choline kinase activity, Pcho, total choline and induction of the Warburg effect in multiple CRC cell lines (72-74). In general, the metabolic cancer phenotype of increased lac and Pcho seems to be somewhat universal between cancers (75). Increased lac, Pcho, cho and GPC levels in breast and prostate cancer has been described (76, 77), and overexpression of choline kinase accompanied by elevated Pcho in lung cancer (72). It has been demonstrated in tissue samples that increased GPC/Pcho ratio and choline levels were associated with tripple negative breast cancer, while decreasing GPC/Pcho ratio and choline levels were associated with estrogen+/progesterone+ breast cancer (42). These findings suggests that metabolic profiling can discriminate the more aggressive tumors associated with worse prognosis. However, it is less known how metabolic profiling can discriminate

between different stages from normal cells to carcinoma, which metabolites that can contribute, and the potential prognostic values it can offer.

Unxpectedly, we did not find significant increase of lactate when comparing TPO0 and TPO4 (p=0,0136) (fig. 4.1.2a). However, we observed a strong trend of increasing lactate with increasing mutations. The increase of lactate is thought to be a contribution from the warburg effect (78). From existing litterature, *APC* knockout may raise lactate levels via induction of pyruvate kinase M2 (PKM2) activity, representing the last step of glycolysis. PKM2 induction through β-catenin signaling for *APC* knockout has recently been demonstrated in human CRC cells (73). *KRAS* knockout is a known inducer of lactate production via increased PFK-1, hexokinase and lactate dehydrogenase A activity and glucose transport (32). *P53* knockout increases lactate production, possibly through loss of function of TIGAR and increased glucose influx (79). The linkage between SMAD4 knockout and increased glycolysis is not well understood. Panagiotis (80) suggests that SMAD4 inactivation on isogenic colon cancer cell lines exhibits more GLUT1 transporters, and therefore increased rate of glycolysis and lactate. Nevertheless, our results show a strong trend of increasing lactate with increasing mutations, but were not able to achieve significant lactate levels despite well-documented litterature. We do however believe that lactate show potential as a biomarker for tumor progression.

The suggestion of Pcho as a biomarker for malignant transformation in cancer has long been under investigation. Elevated choline kinase and Pcho has been previously described in resected human CRC tissue (81), increasing levels of Pcho, GPC and choline in human prostate cancer cell lines (77) and elevated choline kinase and choline transporter activity in human breast cancer cell lines, accompanied by an increase in Pcho levels (82). These observations are not in accordance with this study where Pcho and tCCC decreases with increasing mutations (figure 4.1.2b and c). The reason behind this might be in the difference in model systems where linear 2D culture is utilized in the breast cancer study whereas 3D culture is utilized in this study. Another study showed that CRC patient derived-tumors overexpressed choline kinase in 47% out of 30 tumors, which is closely tied to increased choline metabolism (72). These observations suggests that not all CRC express increased choline metabolism. Mori demonstrated the difference between two prostate and breast cancer cell lines compared to their corresponding xenografts in mice (35). The xenografts showed lower amount of Pcho, total choline containing compounds and choline kinase, but slightly higher amount of GPC compared to their respective 2D cell culture. The high Pcho/GPC ratio which is proposed as a biomarker for agressive cancer in cell cultures were not present in the tumor xenografts due to the low amount of Pcho. The author speculate that the difference arises from the microenvironment and the cancer cell-extracellular matrix (ECM) intrinsic to in-vivo tumors. The organoids in this study contains matrigel as an artificial ECM crucial for morphogenesis. This might make organoids resemble in-vivo tumors more than 2D cell cultures, based on lower levels of Pcho, tCCC (figure 4.1.2c) and the absence of a high Pcho/GPC ratio (data not shown) for the adenoma-like TPO3 and carcinoma-like TPO4 organoids. This does not explain why the amount of Pcho and tCCC decreases with progressive mutations when oncogenic activation of *RAS* and *P53* has been shown to elevate levels of Pcho and choline containing compounds (42, 43). However, our data show decreasing amount of Pcho and tCCC with accumulating mutations and therefore show potential as biomarkers for tumor progression. The decreasing amount of Pcho and tCCC is not in accordance with existing litterature. This means that Pcho and tCCC as

biomarkers for diagnostic purposes is not as obvious as originally thought. Observations on Pcho and tCCC indicate that genetic abnormalities and metabolic profiling is poorly understood, and that the model system used probably influences the results of choline metabolism.

Lastly, this study indicates decreasing myo-in with increasing mutations for untreated organoids (figure 4.1.2d). Myo-in is a known metabolic precursor for de-novo synthesis of phosphatidylinositol-phosphates (PIP), important molecules for anchoring proteins to the membrane and intracellular signaling especially in the PI3K signaling pathway (and other PIP-dependent signaling pathways) (83). A phosphorylated metabolic derivative of myo-in named inositol hexaphosphate (insP6) is prior shown to induce apoptosis and reduce growth and proliferation by inhibition of AKT in the PI3K signaling pathway and inhibition of the cell cycle through regulatory proteins such as P53 in the CRC cell line CaCo-2 (84). It might seem counterintuitive that a cancerous cell would produce metabolites which inhibits its own proliferation, however cancer does not mean that every metabolic nor signaling pathways are altered and might partly explain decreasing myo-in with increasing malignancy. Another momentum which remains to be investigated is if inhibition of cell cycle by insP6 applies to cancer with mutations in the *P53* gene. However, our method can not discriminate between increased or decreased cellular signaling in the PI3K pathway based on reduction of myo-in levels and this subject requires further elucidation. Recent findings suggests that myo-in plays a role in transforming a cell to lose cell-cell adhesion, thus enabling invasiveness and metastasis through epithelial-mesenchymal transition (EMT). Epidermal growth factor induced EMT in the breast cancer line MDA-MB-468 showed reduced myo-in levels after transition by ^{1}H NMR (Quinsgaard, E.M, unpublished data). In another study, the breast cancer cell line MDA-MB-231 showed characteristics of EMT whereby addition of pharmacological doses of myo-in nearly reversed EMT thus supressing motility and invasivness (85). TPO3 and TPO4 has been discovered to resemble cancer in immunodeficient mice where histological analysis of TPO3 resembled adenoma, while TPO4 were highly proliferative and displayed characteristics of invasive carcinoma (62). These observations might partly explain the sudden decrease of myo-in in untreated TPO3 and TPO4. This observation display myo inositol's potential as a biomarker for discriminating adenoma and carcinoma from normal cells.

5.2 Metabolic biomarkers for response to chemotherapy

Prior metabolic profiling studies of various cancers treated with chemotherapeutic agents with response has shown overall decrease of lac, myo-in, Pcho, GPC and tCCC. However, the difference in choline containing compounds varies the most between cancers, type of chemotherapeutic agents and their effect on cell signaling (74, 75, 86). An increase in lipids has also been observed in lymphoma, prostate, breast and neuroblastoma in apoptotic cancer cells treated with chemotherapeutic agents (87, 88). Evaluation of response on chemotherapeutic agents by metabolic profiling has prior been shown to be challenging. There has been reported that responding tripple negative breast cancer patient-derived xenografts to everolimus treatment showed increased glutamine, ala, GPC/Pcho and glucose influx while decreasing levels of Pcho and Lac/glucose. The non-

responding patient-derived xenografts showcased the same pattern. However, it was observed that the non-responding xenografts showcased the biomarkers to an overall lesser extent i.e less increase of GPC/Pcho (89).

We have demonstrated that treatment of 5-FU, OxPt, Sn-38 and a combination of these in TPO's indicate different metabolic profiles dependent upon treatment used (figure 4.7.0, 4,7.1, 4.7.2, 4.7.3 and 4.7.4). Increasing lactate have in a previous study shown to be correlated with metastatic spread and reduced overall survival rate compared to non-metastatic tumors in human cervical cancer patients and is therefore of interest (90). Lactate show an overall decrease regardless of mutations, treatment and response status in our data. This is in line with other observations made by comparing metabolic profiles before and after with a variety of chemotherapeutic agents (89, 91). This indicates that reduced lactate levels is observed across treatments, thus highlighting the potential of lactate as a universal biomarker for treatment response. However, OxPt treated TPO2b and TPO4 (figure 4.7.2 a) and Sn-38 treated TPO2b (figure 4.7.1 a) are non-responsive to the respective treatments but still show reduction in lactate levels. The study of tripple negative breast cancer patient-derived xenografts treated with everolimus were able to separate responders from non-responders partly by higher amount of lactate/glucose in non-responders (89). Our study show the same pattern with less of an decrease in lac levels in the non-responsive carcinoma-like TPO4 treated with OxPt. There has been suggestions that cisplatin, which oxaliplatin is derived from with the same mechanism of action by intra and inter-cross links of the DNA (92), resistant ovarian carcinoma cells evade apoptosis by upregulation of G6PDH, thus redirecting glucose to the oxidative PPP as a response mechanism (93). This redirection of glucose to the PPP might be an explanation for the reduction of lactate observed in the non-responding TPO2b and TPO4 organoids treated with OxPt. Resistance mechanism which alter metabolic pathways for Sn-38 treatment is not described by litterature and requires further investigation. However, if underlying resistant mechanisms rewire glucose metabolism, this might complicate the metabolic profile of cancer cells making it more challenging to predict response to treatment and should be further investigated. Glucose metabolism as a biomarker in clinical settings can be evaluated by two different modalities, MRS and positron emission tomography (PET). With ^{18}F-fluorodeoxyglucose (^{18}F-FDG), a radioactive glucose derivate, will accumulate in cancer tissues due to the Warburg effect and be a measurement of glucose influx, while clinical MRS scanners measures the end product of glucose metabolism lactate. The advantages with MRS is measurements of metabolites in vivo, non-invasive, spatial information with MRSI and allows acquisition of different NMR active nuclei's. However, the drawbacks are magnetic field inhomogenity causing signal broadening, low sensitivity, difficult quantification, not able to discriminate between different choline metabolites and long acquisition time especially for ^{31}P (86). Advantages with PET is dynamic imaging, high sensitivity and low detection limit, while the drawbacks are radiation dose, tracer kinetics and low spatial resolution (86).

It is believed that the anabolic metabolite Pcho important in phospholipid and second messenger biosynthesis decreases during apoptosis. The metabolite GPC, a catabolic product from the breakdown of ptd-cho (figure 2.3.2.0), is believed to increases during apoptosis because of lysis of the cell membrane (88). These observations have led to the

use of Pcho/GPC as a biomarker for cancer treatment response. The inverse relationship has also been established in everolimus treated breast cancer (89). We have shown that Pcho and tCCC decreases in responding Sn-38 treated organoids and is relatively unchanged in TPO2b (non-responding). The overall trend for OxPt, 5-FU and combi treated organoids increases Pcho and tCCC levels regardless of mutations and response status. In regards to Sn-38 treatment, this is in line with a study of neuroblastoma xenografts in mice (87). Interestingley, they observed a markedly decrease of choline compounds after 48hr and 72hr after treatment with irinotecan in sensitive xenografts, while the amount of choline compounds in insensitive xenografts were unchanged. The greater amount of Pcho and tCCC in OxPt, 5-FU and combi treated organoids is in contrast with the studies of breast cancer cell line MCF-7 treated with doxorubicin, tamoxifen and cisplatin and patient-derived tumor xenografts treated with everolimus. These studies observed decreasing Pcho, choline and GPC and an increase of GPC/Pcho (89, 94). There has been suggested that the cell membrane breaks during apoptosis induced by chemotherapeutic agents consequently realising choline containing compounds (95). With our method of intracellular detection, this hypothesis is not feasible and might suggest that apoptotic organoids upregulate choline metabolism to hinder lysis of the cell membrane regardless of response status when treated with OxPt, 5-FU and combi. It is known that cells exhibit different intracellular metabolic profiles dependent upon cell necrosis or cell apoptosis in HL60 leukemia cells (96). The HL60 induced apoptotic cells treated with the chemotherapeutic agent doxorubicin and radiation showed a decrease in choline containing metabolites, while heat treated necrotic cells showed an increase. This study is not able to distinguish primary apoptosis from a secondary necrosis thus rendering it a possible explanation. The different amount of Pcho and tCCC in Sn-38 treated organoids compared to other treatments and an upregulation of choline metabolism regardless of mutations and response status needs further investigations. One important point to emphasize is the different amount of Pcho and tCCC of Sn-38 treated organoids compared to OxPt and 5-FU treated organoids which indicates chemotherapeutic agents dependency of the metabolic profile thus complicating the picture when combining different chemotherapeutic agents.

An overall decrease of ala is observed in Sn-38 and 5-FU treated organoids regardless of mutations and response status (figure 4.7.0 d and figure 4.7.1 e). A study of human lung adenocarcinoma cell line A549 showed reduction in ala levels when treated with cisplatin (97). Furthermore, a study of human embroynic kidney and human hepatocellular carcinoma treated with 5-FU, etoposide and staurosporine demonstrated in contrast that increasing amount of ala corresponds to apoptosis regardless of treatment and propose ala as a potential biomarker for tumor apoptosis (98). The author suggest that the underlying mechanism is the metabolism of taurine to alanine. These findings are not observed in our study. However, our data supports the hypothesis that alanine levels are depleted by redirection to the glycolysis and oxidative phosphorylation as a defence mechanism when treated with chemotherapeutic agents regardless of response status and mutations (97). Why this is not observed in OxPt and combi treated organoids needs further investigation.

Decreasing myo-in in Sn-38 and OxPt treated organoids at either 48hr or 96hr indicates response. The level of myo-in in OxPt and Sn-38 treated TPO2b and OxPt treated TPO4 is

relatively unchanged or increased (non-responders) (figure 4.7.1 d and 4.2.7 c). Myo-in is not very elucidated by the litterature as a treatment response marker, but a study of human pancreatic cancer cell lines T3M4 and Capan-1 treated with gemcitabine showed an increase of myo-in, whereas gemcitabine resistant cells displayed decreased amount by ^{1}H NMR (99). The reason for this opposite trend is unclear. However myo-in is closely tied to oncogenic signaling especially through PI3K signaling pathway and it is therefore reasonable to presume that myo-in have potential as a biomarker for treatment response, but further investigations are needed (83).

Lastly, especially at the 96hr timepoint for combination treated organoids a marked increase of lipids are observed in the raw spectra (figure 4.7.4). The spectra are not normalized and can therefore be misleading. The lipid peaks are not quantified because of time issues, however PCA indicates that combi treated organoids contains more lipids (figure 4.3.1, 4.5.1 and 4.6.1). This observation has been seen in similar studies (87, 88). It is widely believed that mobile lipids resonating at 1.3 ppm from the methylene group increases during cell apoptosis or necrosis (100) and show potential as biomarker for treatment response.

From untreated organoids, increased organoid malignancy correlated with a strong trend of increasing lactate levels, while inverse levels were observed for Pcho, tCCC and myo-in. The carcinoma-like TPO4's metabolic profile showcased significant decreased levels of tCCC, Pcho and myo-in compared to TPO0 ($p \leq 0,05$), while a strong trend of increasing lactate was observed in TPO4 compared to TPO0 (not significant, $p=0,0136$). Furthermore, the adenoma-like TPO3 showed significant reduced tCCC, Pcho and myo-in levels compared to TPO0 ($p \leq 0,05$). TPO2a and TPO2b showed reduction in Pcho and tCCC levels compared to TPO0 ($p \leq 0,05$). From treated organoids, 5-FU treated responding organoids showed decreased level of lac and ala, and increased level of Pcho and tCCC. Sn-38 treated organoids showed decreased amount of lac, Pcho, tCCC, myo-in and ala, where Pcho, tCCC and myo-in were able to discriminate non-responders from responders. OxPt treated organoids showed increased amount of tCCC and overall decreasing level of lac and myo-in at 48hr or 96hr. The non-responding OxPt treated carcinoma-like TPO4 were discriminated from responders with less decreasing lac and increased myo-in levels at both timepoints. Discrimination of the non-responding TPO2b treated with OxPt had relativley unchanged or increased amount of myo-in. Combinational treated organoids showed decreased amount of lac and increased level of Pcho and tCCC. Furthermore, PCA indicated increased amount of lipids in the combinational treated organoids.

5.3 Limitations

The generally lack of multiple samples within treatments at the respective timepoints for statistical comparisons would have elucidated the results further. The lack of exact cell count at the start of the experiment when growing the organoids between the TPO lines which may affect metabolic contents during growth. This might affect comparisons of untreated TPO's. Quantification of Pcho was made difficult because of overlapping peaks with GPC and PE. Chenomx NMR suite provides an AUC approximation of Pcho when

simultaneously fitted with GPC and PE based on the height of the peaks to mitigate the issue. TPO1 *APC* mutant organoids were not grown in time, the response status of TPO0 on OxPt treatment is not evaluated and quantification of lipids were not feasible within time limits because of covid-19 situation.

6 Conclusion

By metabolic profiling of untreated TPO's at 0hr, 48hr and 96hr and treated TPO's at 48hr and 96hr we have demonstrated the TPO's gradually change their metabolic phenotype with increasing number of mutations. Unxpectedly, we did not observe significant increase of intracellular lactate levels with increasing degree of malignancy, but a strong trend was observed. However, we found an inverse relationship between the number of mutations and the levels of choline-containing compounds. This was unexpected, and further research is needed to clarify the significance of this. We also found significant reduction in myo-inositol levels in the two most malignant transforms. We identified several metabolites that are responsive to chemotherapy. However, the organoids displayed different metabolic responses to different chemotherapeutic agents, hence treatment used will be reflected in the metabolic profile. We have shown that lactate displayed the best potential as a universal biomarker, but further research is needed. We have shown that usage of cholines as a biomarker is not as obvious as originally thought and needs further research. We have also highlighted metabolites as potential biomarkers which can distinguish responders from non-responders. This method might be able to identify CRC patients who is non-responsive to treatment faster than todays measure. Further studies should be conducted on oncogenic choline metabolism, underlying resistance mechanisms and how they affect metabolism to deepen our understanding of cancer metabolomics.

References

1. kreftregisteret Oslo: kreftregisteret; 2020 [updated 03/02-2020; cited 2020 24/03]. Available from: https://www.kreftregisteret.no/Temasider/om-kreft/.
2. Valderrama-Trevino AI, Barrera-Mera B, Ceballos-Villalva JC, Montalvo-Jave EE. Hepatic Metastasis from Colorectal Cancer. Euroasian J Hepatogastroenterol. 2017;7(2):166-75.
3. Vander Heiden MG, Cantley LC, Thompson CB. Understanding the Warburg effect: the metabolic requirements of cell proliferation. Science. 2009;324(5930):1029-33.
4. Seierstad T, Roe K, Sitter B, Halgunset J, Flatmark K, Ree AH, et al. Principal component analysis for the comparison of metabolic profiles from human rectal cancer biopsies and colorectal xenografts using high-resolution magic angle spinning 1H magnetic resonance spectroscopy. Mol Cancer. 2008;7:33.
5. Righi V, Durante C, Cocchi M, Calabrese C, Di Febo G, Lecce F, et al. Discrimination of healthy and neoplastic human colon tissues by ex vivo HR-MAS NMR spectroscopy and chemometric analyses. J Proteome Res. 2009;8(4):1859-69.
6. Hanahan D, Weinberg RA. Hallmarks of cancer: the next generation. Cell. 2011;144(5):646-74.
7. cancer geneve, switzerland: world health organization; 2018 [updated 12/09-2018; cited 2020 26/03]. Available from: https://www.who.int/news-room/fact-sheets/detail/cancer.
8. Colorectal cancer Lyon, France: The global Cancer observatory; 2019 [updated 01.02.2019; cited 2020 17.08]. Available from: https://gco.iarc.fr/today/data/factsheets/cancers/10_8_9-Colorectum-fact-sheet.pdf.
9. Rawla P, Sunkara T, Barsouk A. Epidemiology of colorectal cancer: incidence, mortality, survival, and risk factors. Prz Gastroenterol. 2019;14(2):89-103.
10. Sameer AS. Colorectal cancer: molecular mutations and polymorphisms. Front Oncol. 2013;3:114.
11. Conteduca V, Sansonno D, Russi S, Dammacco F. Precancerous colorectal lesions (Review). Int J Oncol. 2013;43(4):973-84.
12. Fearon ER, Vogelstein B. A genetic model for colorectal tumorigenesis. Cell. 1990;61(5):759-67.
13. nasjonalt handlingsprogram med retningslinjer for diagnostikk, behandling og oppfølging av kreft i tykktarm og endetarm oslo: Helsedirektoratet; 2019 [updated 09/2019; cited 2020 30/03]. 6th edition:[Available from: https://helsedirektoratet.no/retningslinjer/nasjonalt-handlingsprogram-med-retningslinjer-for-diagnostikk-behandling-og-oppfolging-av-kreft-i-tykktarm-og-endetarm.
14. Rosen RD, Sapra A. TNM Classification. StatPearls. Treasure Island (FL)2020.
15. Thompson SL, Bakhoum SF, Compton DA. Mechanisms of chromosomal instability. Curr Biol. 2010;20(6):R285-95.
16. Sinicrope FA, Sargent DJ. Molecular pathways: microsatellite instability in colorectal cancer: prognostic, predictive, and therapeutic implications. Clin Cancer Res. 2012;18(6):1506-12.
17. Zhao M, Mishra L, Deng CX. The role of TGF-beta/SMAD4 signaling in cancer. Int J Biol Sci. 2018;14(2):111-23.
18. Zilfou JT, Lowe SW. Tumor suppressive functions of p53. Cold Spring Harb Perspect Biol. 2009;1(5):a001883.
19. Porru M, Pompili L, Caruso C, Biroccio A, Leonetti C. Targeting KRAS in metastatic colorectal cancer: current strategies and emerging opportunities. J Exp Clin Cancer Res. 2018;37(1):57.

20. Maik-Rachline G, Hacohen-Lev-Ran A, Seger R. Nuclear ERK: Mechanism of Translocation, Substrates, and Role in Cancer. Int J Mol Sci. 2019;20(5).
21. Hemmings BA, Restuccia DF. PI3K-PKB/Akt pathway. Cold Spring Harb Perspect Biol. 2012;4(9):a011189.
22. Jancik S, Drabek J, Radzioch D, Hajduch M. Clinical relevance of KRAS in human cancers. J Biomed Biotechnol. 2010;2010:150960.
23. Zhang L, Shay JW. Multiple Roles of APC and its Therapeutic Implications in Colorectal Cancer. J Natl Cancer Inst. 2017;109(8).
24. Qian J, Steigerwald K, Combs KA, Barton MC, Groden J. Caspase cleavage of the APC tumor suppressor and release of an amino-terminal domain is required for the transcription-independent function of APC in apoptosis. Oncogene. 2007;26(33):4872-6.
25. Massague J, Blain SW, Lo RS. TGFbeta signaling in growth control, cancer, and heritable disorders. Cell. 2000;103(2):295-309.
26. Phan LM, Yeung SC, Lee MH. Cancer metabolic reprogramming: importance, main features, and potentials for precise targeted anti-cancer therapies. Cancer Biol Med. 2014;11(1):1-19.
27. La Vecchia S, Sebastian C. Metabolic pathways regulating colorectal cancer initiation and progression. Semin Cell Dev Biol. 2020;98:63-70.
28. Pupo E, Avanzato D, Middonti E, Bussolino F, Lanzetti L. KRAS-Driven Metabolic Rewiring Reveals Novel Actionable Targets in Cancer. Front Oncol. 2019;9:848.
29. Patra KC, Hay N. The pentose phosphate pathway and cancer. Trends Biochem Sci. 2014;39(8):347-54.
30. Cho ES, Cha YH, Kim HS, Kim NH, Yook JI. The Pentose Phosphate Pathway as a Potential Target for Cancer Therapy. Biomol Ther (Seoul). 2018;26(1):29-38.
31. Jiang P, Du W, Wu M. Regulation of the pentose phosphate pathway in cancer. Protein Cell. 2014;5(8):592-602.
32. Ying H, Kimmelman AC, Lyssiotis CA, Hua S, Chu GC, Fletcher-Sananikone E, et al. Oncogenic Kras maintains pancreatic tumors through regulation of anabolic glucose metabolism. Cell. 2012;149(3):656-70.
33. Gibellini F, Smith TK. The Kennedy pathway--De novo synthesis of phosphatidylethanolamine and phosphatidylcholine. IUBMB Life. 2010;62(6):414-28.
34. Cheng M, Bhujwalla ZM, Glunde K. Targeting Phospholipid Metabolism in Cancer. Front Oncol. 2016;6:266.
35. Mori N, Wildes F, Takagi T, Glunde K, Bhujwalla ZM. The Tumor Microenvironment Modulates Choline and Lipid Metabolism. Front Oncol. 2016;6:262.
36. Morrish F, Isern N, Sadilek M, Jeffrey M, Hockenbery DM. c-Myc activates multiple metabolic networks to generate substrates for cell-cycle entry. Oncogene. 2009;28(27):2485-91.
37. Glunde K, Bhujwalla ZM, Ronen SM. Choline metabolism in malignant transformation. Nat Rev Cancer. 2011;11(12):835-48.
38. Glunde K, Shah T, Winnard PT, Jr., Raman V, Takagi T, Vesuna F, et al. Hypoxia regulates choline kinase expression through hypoxia-inducible factor-1 alpha signaling in a human prostate cancer model. Cancer Res. 2008;68(1):172-80.
39. Ramirez de Molina A, Gutierrez R, Ramos MA, Silva JM, Silva J, Bonilla F, et al. Increased choline kinase activity in human breast carcinomas: clinical evidence for a potential novel antitumor strategy. Oncogene. 2002;21(27):4317-22.
40. Trousil S, Kaliszczak M, Schug Z, Nguyen QD, Tomasi G, Favicchio R, et al. The novel choline kinase inhibitor ICL-CCIC-0019 reprograms cellular metabolism and inhibits cancer cell growth. Oncotarget. 2016;7(24):37103-20.
41. Glunde K, Penet MF, Jiang L, Jacobs MA, Bhujwalla ZM. Choline metabolism-based molecular diagnosis of cancer: an update. Expert Rev Mol Diagn. 2015;15(6):735-47.
42. Moestue SA, Borgan E, Huuse EM, Lindholm EM, Sitter B, Borresen-Dale AL, et al. Distinct choline metabolic profiles are associated with differences in gene expression for basal-like and luminal-like breast cancer xenograft models. BMC Cancer. 2010;10:433.
43. Mori N, Delsite R, Natarajan K, Kulawiec M, Bhujwalla ZM, Singh KK. Loss of p53 function in colon cancer cells results in increased phosphocholine and total choline. Mol Imaging. 2004;3(4):319-23.

44. Urban PL. Quantitative mass spectrometry: an overview. Philos Trans A Math Phys Eng Sci. 2016;374(2079).
45. Riekeberg E, Powers R. New frontiers in metabolomics: from measurement to insight. F1000Res. 2017;6:1148.
46. Zia K, Siddiqui T, Ali S, Farooq I, Zafar MS, Khurshid Z. Nuclear Magnetic Resonance Spectroscopy for Medical and Dental Applications: A Comprehensive Review. Eur J Dent. 2019;13(1):124-8.
47. van der Graaf M. In vivo magnetic resonance spectroscopy: basic methodology and clinical applications. Eur Biophys J. 2010;39(4):527-40.
48. Tognarelli JM, Dawood M, Shariff MI, Grover VP, Crossey MM, Cox IJ, et al. Magnetic Resonance Spectroscopy: Principles and Techniques: Lessons for Clinicians. J Clin Exp Hepatol. 2015;5(4):320-8.
49. Marion D. An introduction to biological NMR spectroscopy. Mol Cell Proteomics. 2013;12(11):3006-25.
50. Bingol K, Li DW, Zhang B, Bruschweiler R. Comprehensive Metabolite Identification Strategy Using Multiple Two-Dimensional NMR Spectra of a Complex Mixture Implemented in the COLMARm Web Server. Anal Chem. 2016;88(24):12411-8.
51. Oman T, Tessem MB, Bathen TF, Bertilsson H, Angelsen A, Hedenstrom M, et al. Identification of metabolites from 2D (1)H-(13)C HSQC NMR using peak correlation plots. BMC Bioinformatics. 2014;15:413.
52. Gogiashvili M, Nowacki J, Hergenroder R, Hengstler JG, Lambert J, Edlund K. HR-MAS NMR Based Quantitative Metabolomics in Breast Cancer. Metabolites. 2019;9(2).
53. Schanda P, Ernst M. Studying Dynamics by Magic-Angle Spinning Solid-State NMR Spectroscopy: Principles and Applications to Biomolecules. Prog Nucl Magn Reson Spectrosc. 2016;96:1-46.
54. Alia A, Ganapathy S, de Groot HJ. Magic Angle Spinning (MAS) NMR: a new tool to study the spatial and electronic structure of photosynthetic complexes. Photosynth Res. 2009;102(2-3):415-25.
55. Polenova T, Gupta R, Goldbourt A. Magic angle spinning NMR spectroscopy: a versatile technique for structural and dynamic analysis of solid-phase systems. Anal Chem. 2015;87(11):5458-69.
56. Kapalczynska M, Kolenda T, Przybyla W, Zajaczkowska M, Teresiak A, Filas V, et al. 2D and 3D cell cultures - a comparison of different types of cancer cell cultures. Arch Med Sci. 2018;14(4):910-9.
57. Lv D, Hu Z, Lu L, Lu H, Xu X. Three-dimensional cell culture: A powerful tool in tumor research and drug discovery. Oncol Lett. 2017;14(6):6999-7010.
58. Simian M, Bissell MJ. Organoids: A historical perspective of thinking in three dimensions. J Cell Biol. 2017;216(1):31-40.
59. Lehmann R, Lee CM, Shugart EC, Benedetti M, Charo RA, Gartner Z, et al. Human organoids: a new dimension in cell biology. Mol Biol Cell. 2019;30(10):1129-37.
60. Lancaster MA, Huch M. Disease modelling in human organoids. Dis Model Mech. 2019;12(7).
61. Xu H, Lyu X, Yi M, Zhao W, Song Y, Wu K. Organoid technology and applications in cancer research. J Hematol Oncol. 2018;11(1):116.
62. Drost J, van Jaarsveld RH, Ponsioen B, Zimberlin C, van Boxtel R, Buijs A, et al. Sequential cancer mutations in cultured human intestinal stem cells. Nature. 2015;521(7550):43-7.
63. Wallach TE, Bayrer JR. Intestinal Organoids: New Frontiers in the Study of Intestinal Disease and Physiology. J Pediatr Gastroenterol Nutr. 2017;64(2):180-5.
64. Lovitt CJ, Shelper TB, Avery VM. Advanced cell culture techniques for cancer drug discovery. Biology (Basel). 2014;3(2):345-67.
65. Sato T, Stange DE, Ferrante M, Vries RG, Van Es JH, Van den Brink S, et al. Long-term expansion of epithelial organoids from human colon, adenoma, adenocarcinoma, and Barrett's epithelium. Gastroenterology. 2011;141(5):1762-72.
66. Savorani F, Tomasi G, Engelsen SB. icoshift: A versatile tool for the rapid alignment of 1D NMR spectra. J Magn Reson. 2010;202(2):190-202.
67. Eilers PH. Parametric time warping. Anal Chem. 2004;76(2):404-11.

68. Wang H, Wang L, Zhang H, Deng P, Chen J, Zhou B, et al. (1)H NMR-based metabolic profiling of human rectal cancer tissue. Mol Cancer. 2013;12(1):121.
69. Tessem MB, Selnaes KM, Sjursen W, Trano G, Giskeodegard GF, Bathen TF, et al. Discrimination of patients with microsatellite instability colon cancer using 1H HR MAS MR spectroscopy and chemometric analysis. J Proteome Res. 2010;9(7):3664-70.
70. Li Y, Wang C, Li D, Deng P, Shao X, Hu J, et al. 1H-NMR-based metabolic profiling of a colorectal cancer CT-26 lung metastasis model in mice. Oncol Rep. 2017;38(5):3044-54.
71. Loftus NJ, Lai L, Wilkinson RW, Odedra R, Wilson ID, Barnes AJ. Global metabolite profiling of human colorectal cancer xenografts in mice using HPLC-MS/MS. J Proteome Res. 2013;12(6):2980-6.
72. Ramirez de Molina A, Rodriguez-Gonzalez A, Gutierrez R, Martinez-Pineiro L, Sanchez J, Bonilla F, et al. Overexpression of choline kinase is a frequent feature in human tumor-derived cell lines and in lung, prostate, and colorectal human cancers. Biochem Biophys Res Commun. 2002;296(3):580-3.
73. Cha PH, Hwang JH, Kwak DK, Koh E, Kim KS, Choi KY. APC loss induces Warburg effect via increased PKM2 transcription in colorectal cancer. Br J Cancer. 2020.
74. Podo F, Canevari S, Canese R, Pisanu ME, Ricci A, Iorio E. MR evaluation of response to targeted treatment in cancer cells. NMR Biomed. 2011;24(6):648-72.
75. Merz AL, Serkova NJ. Use of nuclear magnetic resonance-based metabolomics in detecting drug resistance in cancer. Biomark Med. 2009;3(3):289-306.
76. Cao MD, Lamichhane S, Lundgren S, Bofin A, Fjosne H, Giskeodegard GF, et al. Metabolic characterization of triple negative breast cancer. BMC Cancer. 2014;14:941.
77. Ackerstaff E, Pflug BR, Nelson JB, Bhujwalla ZM. Detection of increased choline compounds with proton nuclear magnetic resonance spectroscopy subsequent to malignant transformation of human prostatic epithelial cells. Cancer Res. 2001;61(9):3599-603.
78. Warburg O. On the origin of cancer cells. Science. 1956;123(3191):309-14.
79. Bensaad K, Tsuruta A, Selak MA, Vidal MN, Nakano K, Bartrons R, et al. TIGAR, a p53-inducible regulator of glycolysis and apoptosis. Cell. 2006;126(1):107-20.
80. Papageorgis P, Cheng K, Ozturk S, Gong Y, Lambert AW, Abdolmaleky HM, et al. Smad4 inactivation promotes malignancy and drug resistance of colon cancer. Cancer Res. 2011;71(3):998-1008.
81. Nakagami K, Uchida T, Ohwada S, Koibuchi Y, Suda Y, Sekine T, et al. Increased choline kinase activity and elevated phosphocholine levels in human colon cancer. Jpn J Cancer Res. 1999;90(4):419-24.
82. Eliyahu G, Kreizman T, Degani H. Phosphocholine as a biomarker of breast cancer: molecular and biochemical studies. Int J Cancer. 2007;120(8):1721-30.
83. Berridge MJ. Inositol trisphosphate and calcium signalling mechanisms. Biochim Biophys Acta. 2009;1793(6):933-40.
84. Kapral M, Wawszczyk J, Jesse K, Paul-Samojedny M, Kusmierz D, Weglarz L. Inositol Hexaphosphate Inhibits Proliferation and Induces Apoptosis of Colon Cancer Cells by Suppressing the AKT/mTOR Signaling Pathway. Molecules. 2017;22(10).
85. Dinicola S, Fabrizi G, Masiello MG, Proietti S, Palombo A, Minini M, et al. Inositol induces mesenchymal-epithelial reversion in breast cancer cells through cytoskeleton rearrangement. Exp Cell Res. 2016;345(1):37-50.
86. Moestue SA, Engebraaten O, Gribbestad IS. Metabolic effects of signal transduction inhibition in cancer assessed by magnetic resonance spectroscopy. Mol Oncol. 2011;5(3):224-41.
87. Lindskog M, Spenger C, Jarvet J, Graslund A, Kogner P. Predicting resistance or response to chemotherapy by proton magnetic resonance spectroscopy in neuroblastoma. J Natl Cancer Inst. 2004;96(19):1457-66.
88. Arlauckas SP, Browning EA, Poptani H, Delikatny EJ. Imaging of cancer lipid metabolism in response to therapy. NMR Biomed. 2019;32(10):e4070.
89. Euceda LR, Hill DK, Stokke E, Hatem R, El Botty R, Bieche I, et al. Metabolic Response to Everolimus in Patient-Derived Triple-Negative Breast Cancer Xenografts. J Proteome Res. 2017;16(5):1868-79.

90. Walenta S, Wetterling M, Lehrke M, Schwickert G, Sundfor K, Rofstad EK, et al. High lactate levels predict likelihood of metastases, tumor recurrence, and restricted patient survival in human cervical cancers. Cancer Res. 2000;60(4):916-21.
91. Gottschalk S, Anderson N, Hainz C, Eckhardt SG, Serkova NJ. Imatinib (STI571)-mediated changes in glucose metabolism in human leukemia BCR-ABL-positive cells. Clin Cancer Res. 2004;10(19):6661-8.
92. Faivre S, Chan D, Salinas R, Woynarowska B, Woynarowski JM. DNA strand breaks and apoptosis induced by oxaliplatin in cancer cells. Biochem Pharmacol. 2003;66(2):225-37.
93. Catanzaro D, Gaude E, Orso G, Giordano C, Guzzo G, Rasola A, et al. Inhibition of glucose-6-phosphate dehydrogenase sensitizes cisplatin-resistant cells to death. Oncotarget. 2015;6(30):30102-14.
94. Maria RM, Altei WF, Selistre-de-Araujo HS, Colnago LA. Effects of Doxorubicin, Cisplatin, and Tamoxifen on the Metabolic Profile of Human Breast Cancer MCF-7 Cells As Determined by (1)H High-Resolution Magic Angle Spinning Nuclear Magnetic Resonance. Biochemistry. 2017;56(16):2219-24.
95. Xu S, Zhou Y, Geng H, Song D, Tang J, Zhu X, et al. Serum Metabolic Profile Alteration Reveals Response to Platinum-Based Combination Chemotherapy for Lung Cancer: Sensitive Patients Distinguished from Insensitive ones. Sci Rep. 2017;7(1):17524.
96. Rainaldi G, Romano R, Indovina P, Ferrante A, Motta A, Indovina PL, et al. Metabolomics using 1H-NMR of apoptosis and Necrosis in HL60 leukemia cells: differences between the two types of cell death and independence from the stimulus of apoptosis used. Radiat Res. 2008;169(2):170-80.
97. Duarte IF, Ladeirinha AF, Lamego I, Gil AM, Carvalho L, Carreira IM, et al. Potential markers of cisplatin treatment response unveiled by NMR metabolomics of human lung cells. Mol Pharm. 2013;10(11):4242-51.
98. Halama A, Riesen N, Moller G, Hrabe de Angelis M, Adamski J. Identification of biomarkers for apoptosis in cancer cell lines using metabolomics: tools for individualized medicine. J Intern Med. 2013;274(5):425-39.
99. Gebregiworgis T, Bhinderwala F, Purohit V, Chaika NV, Singh PK, Powers R. Insights into gemcitabine resistance and the potential for therapeutic monitoring. Metabolomics. 2018;14(12):156.
100. Bezabeh T, Mowat MR, Jarolim L, Greenberg AH, Smith IC. Detection of drug-induced apoptosis and necrosis in human cervical carcinoma cells using 1H NMR spectroscopy. Cell Death Differ. 2001;8(3):219-24.

Supplementary materials

Table A.1 Contents of expansion medium for each of the TPO's. DMEM/F-12+: supplement, Wnt: growth factor, R-spondin: growth factor, Noggin: bone morphogenetic proteins inhibitor, b-27: supplement, n-AC: N-acetyl-L-cysteine (amino acid), nicotinamide: supplement, EGF: epidermal growth factor, A83: tumor growth factor beta inhibitor, SB: P38 MAP kinase inhibitor.

	DMEM/F-12+	Wnt	R-spondin	Noggin	B-27	n-AC	Nicotinamide	EGF	A83	SB
WT	2ml	5ml	2ml	1ml	200µl	25µl	100µl	1µl	1µl	3,3µl
APC-KRAS	9ml	-	-	1ml	200µl	25µl	100µl	-	1µl	3,3µl
APC-P53	9ml	-	-	1ml	200µl	25µl	100µl	1µl	1µl	3,3µl
APC-KRAS-P53	9ml	-	-	1ml	200µl	25µl	100µl	-	1µl	3,3µl
APC-KRAS-P53-SMAD4	10ml	-	-	-	200µl	25µl	100µl	-	1µl	3,3µl

Table A.2 Contents of differentiation medium for each of the TPO's. DMEM/F-12+: supplement, Wnt: growth factor, R-spondin: growth factor, Noggin:bone morphogenetic proteins inhibitor, b-27: supplement, n-AC: N-acetyl-L-cysteine (amino acid), nicotinamide: supplement, EGF: epidermal growth factor, A83: tumor growth factor beta inhibitor, SB: P38 MAP kinase inhibitor.

	DMEM/F-12+	Wnt	R-spondin	Noggin	B-27	n-AC	Nicotinamide	EGF	A83	SB
WT	5,5ml	2,5ml	1ml	1ml	200µl	25µl	-	1µl	1µl	-
APC-KRAS	9ml	-	-	1ml	200µl	25µl	-	-	1µl	-
APC-P53	9ml	-	-	1ml	200µl	25µl	-	1µl	1µl	-
APC-KRAS-P53	9ml	-	-	1ml	200µl	25µl	-	-	1µl	-
APC-KRAS-P53-SMAD4	10ml	-	-	-	200µl	25µl	-	-	1µl	-

To 500ml of DMEM/F12 medium (Thermofisher), 5 ml of gibco 100x glutamax (Thermofisher), 5 ml of hepes buffer (Thermofisher) and 5ml of penicillin-streptomycin (Thermofisher) were added. After addition the medium is called DMEM/F-12+

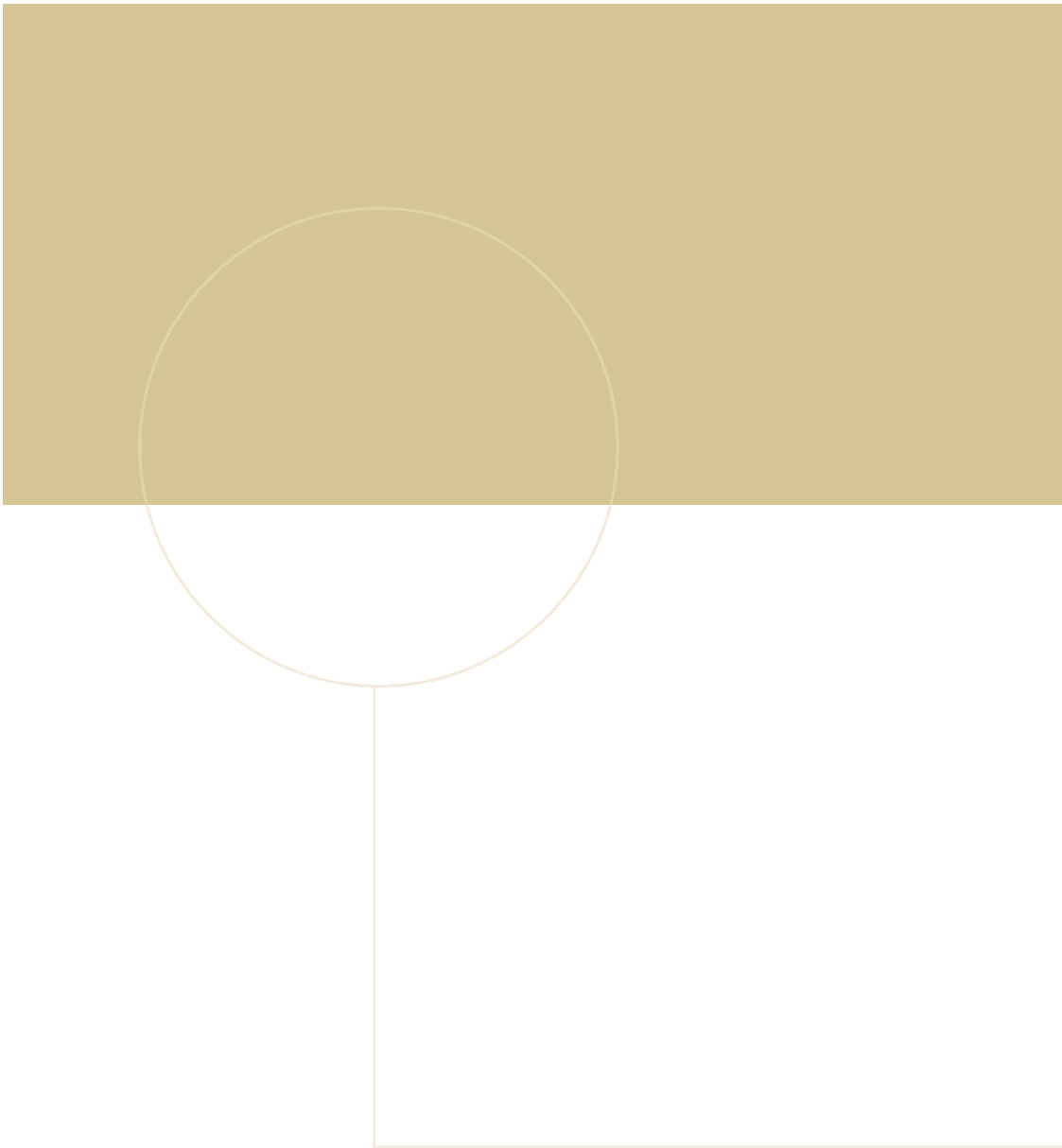

NTNU

Norwegian University of
Science and Technology